LCH Laboratoire de Constructions Hydrauliques
Laboratory of Hydraulic Constructions

ÉCOLE POLYTECHNIQUE
FÉDÉRALE DE LAUSANNE

Communication 64

Experimental study on the influence of abrupt slope changes on flow characteristics over stepped spillways

Mohammad J. Ostad Mirza

Editeur : Prof. Dr A. Schleiss

Lausanne, 2016

Communications du Laboratoire de Constructions Hydrauliques ISSN 1661-1179
Ecole Polytechnique Fédérale de Lausanne
Editeur: Prof. Dr A. Schleiss

Preface

Stepped spillways have been built since several decades in combination with roller compacted concrete dams. More recently stepped spillways are also excavated into rock along the abutments of embankment dams. According to the prevailing topography these stepped spillways are designed with variable step heights and slope changes along the channel.

In his research project Dr Mohammad Javad Ostad Mirza studied for the first time systematically with laboratory tests the influence of abrupt slope changes on the flow characteristics over stepped spillways. The air-water flow behaviour was studied in detail at several cross-sections along the chute, upstream and downstream of the slope change by measuring the evolution of water surface based on the equivalent clear water depth, flow bulking, flow velocities and air concentration profiles. Furthermore, dynamic pressures were measured on both vertical and horizontal faces at several steps in the vicinity and far downstream of the slope change.

The systematic experiments give new insights in the flow characteristics over stepped spillways in the vicinity of slope changes, which is helpful for practical applications.

We would like to thank the members of the jury, Prof. Dr. Alain Nussbaumer, EPF Lausanne, Switzerland, Prof. Daniel Bung from FH Aachen – University of Applied Sciences, Prof. João Teixeira Borges from IST, Universidade de Lisboa, Portugal and Dr. Stéphanie André from Stucky SA, Renens, Switzerland for their helpful suggestions. Finally, we also thank gratefully the Portuguese Foundation for Science and Technology (FCT) for their financial support under grant SFRH/BD/51527/2011.

Prof. Dr. Anton J. Schleiss Prof. Dr. Jorge Matos

Abstract

Numerous stepped spillways were built during the last decades, namely on the downstream face of roller compacted concrete (RCC) dams. Application of stepped spillways increases the energy dissipation rate along the spillway and may reduce the dimensions of the terminal energy dissipation structure. This pronounced energy dissipation makes stepped chutes attractive under various conditions, namely as service spillways on RCC gravity dams and on valley flanks near earth dams. For both, in some cases, an abrupt slope change may be required to be implemented on stepped chutes in order to follow the site topography and to minimize the needed excavations and hence respective costs. An abrupt slope change along stepped spillways can influence the flow properties such as the air entrainment, velocity and pressure distribution, and the energy dissipation. A quite limited number of stepped spillways have been built with an abrupt slope change, whereas no systematic scientific investigation for designing such type of configuration has been conducted to date. Accordingly, comprehensive information on the effect of an abrupt slope change on the flow features is missing.

Therefore, the present experimental research work aimed to examine the effect of an abrupt slope change (from steep to mild) on the skimming flow features, by analysing the air entrainment, flow bulking, velocity and dynamic pressure development and energy dissipation along the stepped chute. Physical modelling was conducted in a relatively large scale facility with slope changes from 50º to 18.6º ($\Delta\Theta$=31.4º) and 50º to 30º ($\Delta\Theta$=20º). Detailed air-water flow measurements were conducted at several cross-sections (step edges) along the chute, upstream and downstream of the slope change. In addition, dynamic pressure measurements were obtained on both vertical and horizontal faces of several steps in the vicinity and far downstream of slope change cross-section.

The results indicated a substantial influence of abrupt slope changes on the flow properties for the tested range of relative critical depths ($2.6 \leq d_c/h \leq 9.2$), particularly in comparison with typical results for constant sloping stepped spillway flows.

Four main local sub-regions have been found to describe the typical air-water flow patterns in the vicinity and further downstream of the slope change, namely with regard to the

mean (depth-averaged) air concentration, air concentration distribution, pseudo-bottom air concentration, air-phase frequency and characteristic flow depths.

The length of the reach under the influence of the slope change was found to depend mainly on the critical depth, regardless of the slope change and step height. Empirical formulae were developed for predicting the mean air concentration and characteristic flow depths along the reach under the influence of the slope change.

Velocity profiles and the specific energy are strongly affected, in the vicinity of the slope change. The relative head loss corresponding to the reach under the influence of the slope change was found to vary between 38% to 51%, for the tested range of relative critical depths ($2.6 \leq d_*/h \leq 4.6$) and slope change configurations.

Mean, 95^{th} and 5^{th} percentiles, probability distribution and spectral contents of the pressure signals were analysed. Mean pressures up to approximately 21 times the equivalent clear water depth (approximately 13 times the step height) were observed on the horizontal step faces in the vicinity of slope change cross-section for the tested range of relative critical depths ($2.6 \leq d_*/h \leq 4.6$). Negative values of the 5^{th} percentile of the pressure were found on the vertical step faces, particularly in vicinity of the slope change. However, they were not expected to be severe enough to cause cavitation.

In conclusion, for the first time, the influence of an abrupt slope change on skimming flow properties on stepped spillways was investigated with systematic experiments on two slope change configurations and for a wide range of relative critical flow depths. This thesis report describes and discusses the achieved results mainly on the air entrainment and flow bulking, velocity and dynamic pressure distributions, as well as the energy dissipation.

Keywords: Stepped spillways; Slope change; Skimming flow; Air entrainment; Air concentration distribution; Air-phase frequency; Characteristic flow depths; Flow bulking; Velocity distribution; Dynamic pressure distribution; Energy dissipation

چکیده

طی دهه های اخیر ، سریرز های پلکانی متعدد و متنوعی بر روی وجه پایین دست سدهای بتن غلتکی (RCC) ساخته شده اند . استفاده از سرریزهای پلکانی منجر به افزایش نرخ استهلاک انرژی در طول سرریز شده و می تواند باعث کاهش ابعاد ویا حذف سازه های پایانی گردد. افزایش چشمگیر نرخ استهلاک انرژی بر روی سرریزهای پلکانی، ضرورت طراحی و ساخت آنها بر روی سدهای وزنی بتن غلتکی و دره های جانبی سدهای خاکی را دوچندان نموده است. در طراحی و ساخت این سرریزها، ممکن است به منظور تبعیت از توپوگرافی و جنس بستر و در نتیجه کاهش هزینه های ساخت نیاز به تغییر شیب ناگهانی باشد. یک تغییر شیب ناگهانی بر روی سرریز پلکانی، عاملی است که ممکن است بر روی ویژگی های جریان مانند میزان هواگیری جریان، توزیع سرعت و فشار وهمچنین میزان استهلاک انرژی تاثیر به سزایی داشته باشد. تعداد کمی از سرریزهای پلکانی ساخته شده شامل تغییر شیب های ناگهانی هستند، در حالیکه هیچ مطالعه علمی نظام مندی نیز پیرامون طراحی این نوع از سرریزهای پلکانی انجام نگرفته است. بر این اساس، اطلاعات جامعی در مورد تاثیر این تغییر شیب های ناگهانی بر وِیژگی های جریان موجود نمی باشد.

از این رو، هدف از تحقیق آزمایشگاهی حاضر بررسی تاثیر تغییر شیب ناگهانی بر مشخصات جریان غیر ریزشی بر روی سرریزهای پلکانی می باشد. این بررسی با توجه به میزان هواگیری و افزایش حجم جریان، توزیع سرعت، فشار دینامیکی و استهلاک انرژی در طول سرریز پلکانی انجام گردیده است. مدلسازی فیزیکی بر روی مدلی نسبتا بزرگ مقیاس متشکل از تغییر شیب های 50^o به 18.6^o ($\Delta\Theta=31.4^o$) و50^o به 30^o ($\Delta\Theta=20^o$) انجام شده است. اندازه گیری های دقیق مشخصات جریان آب-هوا درمقاطع عرضی مختلف در طول سرریز(عمود بر لبه پله ها) صورت گرفته است. همچنین، فشار دینامیکی بر روی سطوح عمودی و افقی پله ها در مجاورت مقطع عرضی تغییر شیب و انتهای پایین دست سرریزانجام شده است.

نتایج به دست آمده نشان دهنده تاثیر به سزای تغییر شیب ناگهانی برمشخصات جریان در مقایسه با نتایج معمول بر روی سرریزهای پلکانی با شیب ثابت میباشد. با بررسی و تحلیل پارامترهایی همچون غلظت هوای متوسط، توزیع غلظت هوا، غلظت هوای کف ،فرکانس فاز گازی (هوا)، و عمق معادل جریان، چهار محدوده برای تشریح الگوی جریان در مجاورت و پایین دست تغییر شیب ناگهانی مشخص گردید.

بررسی ناحیه تحت تاثیر تغییر شیب ناگهانی نشان داد اساسا طول این ناحیه فقط به عمق بحرانی جریان (مستقل از شیب سرریز و ارتفاع پله) وابسته است . با استفاده از داده های آزمایشگاهی روابطی تجربی برای تخمین تغییرات غلظت هوای متوسط و عمق های مشخصه جریان درامتداد ناحیه تحت تاثیر تغییر شیب های ناگهانی ارائه گردید. آزمایش ها نشان داد که پروفایل های توزیع سرعت و انرژی مخصوص به شدت تحت تاثیر تغییر شیب های ناگهانی قرار می گیرند. محدوده افت نسبی انرژی تحت تاثیر تغییر شیب های مختلف آزمایش شده بین 38% تا 51% بدست آمد.

مقادیر متوسط، و صدک های 5 و 95 فشار دینامیکی، به همراه توزیع احتمال و طیف سیگنال های فشارتحلیل گردید. در مجاورت تغیر شیب، مقادیر فشار متوسط بر روی سطوح افقی پله ها تا 21 برابر عمق معادل جریان (13 برابر ارتفاع

پله) بدست آمد. همچنین مقادیر منفی صدک 5 فشار دینامیکی بر روی وجوه عمودی پله ها (خصوصا در محدوده تحت تاثیرتغییر شیب) مشاهده گردید. با این حال، این مقادیر فشار منفی، از شدت کافی جهت بروز کاویتاسیون برخوردار نبود. در مجموع، برای اولین بار تاثیر تغییر شیب های ناگهانی بر مشخصات جریان غیر ریزشی بر روی سرریزهای پلکانی با انجام آزمایشهای نظام مند برروی دو نوع تغییر شیب و به ازای طیف گسترده ای از دبی ها مورد مطالعه قرارگرفت. پایان نامه حاضر، به تشریح و بحث پیرامون نتایج به دست آمده به خصوص هواگیری، افزایش حجم جریان، توزیع سرعت و فشاردینامیکی ونیز استهلاک انرژی می پردازد.

کلمات کلیدی: سرریزهای پلکانی، تغییر شیب، جریان غیر ریزشی، هواگیری، توزیع غلظت هوا ، فرکانس فاز گازی (هوا)، عمق مشخصه جریان، افزایش حجم جریان، توزیع سرعت، توزیع فشار دینامیکی، استهلاک انرژی.

Résumé

De nombreux coursier en marches d'escalier ont été construits au cours des dernières décennies, à savoir sur la face l'aval de barrages en béton compacté au rouleau (BCR). L'application de coursier en marches d'escalier augmente le taux de dissipation d'énergie sur de l'évacuateur de crues et peut réduire les dimensions du dissipateur d'énergie aval. Cette dissipation d'énergie prononcée rend les coursiers en marches d'escalier attrayants sous diverses conditions, à savoir en tant que déversoirs sur les barrages-poids en BCR et sur les flancs de vallée pour des digues en remblai. Pour ces deux situations, dans certains cas, un changement de pente abrupte peut être nécessaire pour suivre la topographie du site et minimiser les excavations nécessaires et donc des coûts respectifs. Le changement de pente abrupte sur les coursiers en marches d'escalier peut influencer les propriétés d'écoulement tel que l'entraînement d'air, la distribution de vitesses et de pressions, et la dissipation d'énergie. Un nombre limité de coursiers en marches d'escalier ont été construits avec un changement de pente abrupte, alors qu'aucune étude scientifique systématique pour la conception de ce type de configuration n'a été réalisée à ce jour. Ainsi, des informations complètes sur l'effet d'un changement de pente abrupte sur les caractéristiques d'écoulement sont manquantes.

Par conséquent, la présente recherche vise à examiner l'effet d'un changement de pente abrupt sur les caractéristiques d'écoulement en mousse, en analysant l'entraînement d'air, le gonflement de l'écoulement, le développement de la vitesse et de la pression dynamique ainsi que de la dissipation de l'énergie sur une rampe en gradin. La modélisation physique a été réalisée dans un canal à relativement grand échelle avec des changements de pente de 50º à 18.6º ($\Delta\Theta$ = 31.4º) et 50º à 30º ($\Delta\Theta$ = 20º). Des mesures détaillées du débit air-eau ont été effectuées à plusieurs sections transversales (au bord extérieur des marches) de la rampe, en amont et en aval de la variation de pente. En outre, des mesures de pression dynamiques ont été obtenues sur les faces verticales et horizontales de plusieurs marches dans le voisinage et loin en aval du changement de pente.

Les résultats indiquent une influence substantielle des changements de pente abrupts sur les propriétés de l'écoulement pour la gamme de profondeurs critiques relatives testée (2.6

$\leq d_o/h \leq 9.2$), en particulier en comparaison avec les résultats typiques d'écoulement sur coursiers en marches d'escalier à pente constante.

Quatre principales sous-régions ont été définies pour décrire les régions d'écoulement air-eau typiques à proximité et plus en aval de la variation de la pente, à savoir en ce qui concerne la concentration d'air moyenne (moyenne sur la profondeur), la distribution de la concentration de l'air, la concentration d'air au pseudo-fond, la fréquence de la phase d'air et les profondeurs d'écoulement caractéristiques.

La longueur du tronçon sous l'influence du changement de pente a été trouvée comme dépendant principalement de la profondeur critique, quel que soit le changement de pente et de la hauteur des marches. Des formules empiriques ont également été développées pour prédire la concentration moyenne d'air et des profondeurs d'écoulement caractéristiques le long du tronçon sous l'influence de la variation de la pente.

Les profils de vitesse et l'énergie spécifique sont fortement affectés au voisinage de la variation de pente. La perte de charge relative du tronçon sous l'influence de la variation de la pente s'avère varier entre 38% à 51%, pour la gamme de profondeurs critiques relatives testée ($2.6 \leq d_o/h \leq 4.6$) et les changements de pente testés.

La distribution de probabilité de la moyenne, des 95^e et 5^e centiles, et le contenu spectral des signaux de pression ont été analysés. Des pressions moyennes jusqu'à approximativement 21 fois la profondeur équivalente de l'eau claire (approximativement 13 fois la hauteur de marche) ont été observées sur les faces horizontales des marche à proximité du changement de pente pour la gamme de profondeurs critiques relatives testée ($2.6 \leq d_o/h \leq 4.6$). Des valeurs négatives du 5^e centile de la pression ont été trouvées sur les faces verticales des marches, en particulier dans le voisinage du changement de pente. Cependant, ils ne devraient pas être suffisamment importants pour provoquer de la cavitation.

En conclusion, pour la première fois, l'influence d'un changement de pente abrupte sur les propriétés de l'écoulement en mousse sur coursiers en marches d'escalier a été étudiée avec des expériences systématiques sur deux configurations de changement de pente et pour une large gamme de profondeurs critiques relatives. Ce rapport de thèse décrit et analyse les résultats obtenus principalement sur l'entraînement d'air et le gonflement de l'écoulement, la vitesse et les distributions de pression dynamiques, ainsi que la dissipation d'énergie.

Mots-clés: Coursiers en marches d'escalier; Changement de pente; Écoulement en mousse; Entraînement d'air; Distribution de la concentration d'air; Fréquence de la phase d'air; Profondeur caractéristique d'écoulement; Gonflement de l'écoulement; Distribution de vitesse; Distribution des pressions dynamiques; Dissipation d'énergie

Resumo

Nas últimas décadas foram construídos inúmeros descarregadores de cheias em degraus, nomeadamente no paramento de jusante de barragens de betão compactado com cilindros (BCC). A aplicação de descarregadores de cheias em degraus permite aumentar a dissipação de energia ao longo do descarregador e, desta forma, reduzir as dimensões da estrutura de dissipação de energia localizada a jusante. A elevada dissipação de energia torna este tipo de descarregadores de cheia atrativo em diversas condições, como sejam em barragens de BCC ou associados a barragens de aterro. Em alguns casos pode afigurar-se necessário implementar uma variação do declive do descarregador, por forma a acompanhar a topografia local e minimizar o volume a escavar e, assim, reduzir o custo da obra. Uma variação do declive do descarregador em degraus conduz à alteração das características do escoamento, como sejam o emulsionamento de ar, a distribuição de velocidades, o campo de pressões hidrodinâmicas nos degraus, assim como a dissipação de energia. Embora em número limitado, foram já contruídos alguns descarregadores de cheias em degraus com variação brusca de declive. Contudo, não se conhecem trabalhos de investigação sistemáticos que permitam estimar as grandezas características do escoamento ao longo do descarregador, assim como o dimensionamento hidráulico de descarregadores de cheias em degraus com mudança de declive.

O presente trabalho de investigação experimental tem como principal objetivo o estudo do efeito de uma variação brusca (redução) do declive nas principais grandezas do escoamento deslizante sobre turbilhões, como a distribuição da concentração de ar, a distribuição de velocidades, o campo de pressões hidrodinâmicas nos degraus, as alturas características do escoamento e o empolamento da veia líquida, bem como a dissipação de energia.

A modelação física foi conduzida numa instalação experimental de relativamente grande dimensão, com variações de ângulo com a horizontal de 50° para 18.6° ($\Delta\Theta$=31.4°), ou de 50° para 30° ($\Delta\Theta$=20°). Foram efetuadas medições da concentração de ar, velocidade do escoamento, e alturas características do escoamento de emulsão ar-água nas verticais de diversas secções transversais a partir das extremidades dos degraus, a montante e a jusante do local de variação do declive. Foram igualmente efetuadas medições de pressão hidrodinâmica

nas faces horizontais e verticais de vários degraus na vizinhança da secção de mudança de declive, bem como em alguns degraus localizados a jusante daquela secção.

Os resultados mostram que uma mudança brusca do declive do descarregador conduz a uma alteração significativa das grandezas principais do escoamento, no intervalo de alturas críticas adimensionalizadas que foram objeto de estudo ($2.6 \leq d_c/h \leq 9.2$), comparativamente com as que seriam expectáveis em descarregadores de cheias em degraus com declive constante.

A partir de dados de distribuição da concentração de ar, concentração média de ar, concentração de ar junto da soleira fictícia, frequência da fase gasosa, e alturas características do escoamento, identificaram-se quatro trechos que permitem descrever padrões típicos do escoamento bifásico na proximidade e a jusante do trecho influenciado pela mudança de declive.

Observou-se que o comprimento do trecho no qual se manifestam os efeitos da mudança de declive depende principalmente da altura crítica, independentemente da magnitude de variação de declive e da altura dos degraus. Foram desenvolvidas expressões empíricas para estimar a concentração média de ar, a altura equivalente de água e a altura característica do escoamento ao longo do trecho em que se manifestam os efeitos da mudança de declive.

O perfil de velocidades e a energia específica do escoamento são fortemente modificados na proximidade do local de mudança de declive. A perda de carga no trecho em que os efeitos da mudança de declive se manifestam ficou compreendida entre 38% e 51%, para a gama de alturas críticas adimensionalizadas ($2.6 \leq d_c/h \leq 4.6$) e configurações analisadas.

Relativamente às séries de pressão hidrodinâmica, analisaram-se os seus valores médios, os percentis 95 e 5, a distribuição de probabilidades e o seu conteúdo espectral. Nas faces horizontais dos degraus, na proximidade da secção de mudança de declive, obtiveram-se valores médios de pressão até 21 vezes superiores à altura equivalente de água (aproximadamente 13 vezes a altura dos degraus), para o intervalo de alturas críticas adimensionalizadas estudadas ($2.6 \leq d_c/h \leq 4.6$). Registaram-se valores negativos do percentil 5 nas faces verticais dos degraus, na vizinhança da secção de mudança de declive. Contudo, não é expectável que tais valores conduzam à ocorrência de cavitação.

Em conclusão, a presente dissertação inclui um estudo sistemático original dedicado ao efeito de uma variação brusca do declive de um descarregador de cheias em degraus (para duas configurações e uma para gama alargada de alturas críticas adimensionalizadas) nas principais grandezas do escoamento deslizante sobre turbilhões, como emulsionamento de ar, empolamento da veia líquida, distribuição de velocidades, distribuição de pressões hidrodinâmicas e dissipação de energia.

Palavras-chave: Descarregador de cheia em degraus; Variação de declive; Escoamento deslizante sobre turbilhões; Emulsionamento de ar; Distribuição da concentração de ar; frequência da fase de ar; alturas características do escoamento; empolamento da veia líquida; distribuição de velocidades; distribuição de pressões dinâmicas; dissipação de energia.

با نام و یاد دادار هستی بخش

خداوندی که نوآوری سنت اوست*

پیشکش به محضر

بانوی عالمین فاطمه زهرا (سلام الله علیها)،

همو که خلقت کائنات بهانه ای بود برای خلق او،

بانوی عظیم الشانی که این رساله و همه رساله های علمی تنها حرفی است از مصحفش.

و

تقدیم به

جگر گوشه اش **آخرین حجت حق (عجل الله تعالی فرجه الشریف)**، صاحب مصحف فاطمیه که بدون استمداد عنایتش انجام این تحقیق ناممکن می نمود.

*برگرفته از شعر "بیایید از عشق صحبت کنیم"، قیصر ملک شعر، مرحوم قیصر امین پور

با سپاس و قدردانی فراوان از خانواده ام،

بزرگترین حامیانی که بی شائبه موفقیت من را موفقیت خود دانسته اند.

پدر و مادر عزیز و گرانقدرم که همه زندگی ام را مرهون آنها و در عین حال ناتوان از قدرشناسی الطاف بی دریغشان هستم

و

برادر عزیزم "علیرضا"، که در سراسر زندگی برادرانه همراه و یاورم بوده است

و

مادربزرگ ها و پدربزرگ های مهربانم، که همواره دعای خیرشان بدرقه راهم بوده است.

بزرگوارانی که بعد از نعمت وجود، بزرگترین نعمت زندگی ام هستند و خداوند را به سبب چنین نعماتی از صمیم قلب شاکرم.

Great appreciation to my beloved family,

the greatest constant supporters who knew my achievements as their own selflessly.

My dear parents, to whom I am indebted all my life and incapable to show my gratitude for their kindness,

And ***My beloved younger brother "Ali Reza"*** who accompanied me in all stages of my life,

And ***My tender grandparents***, whom their prayers have been a source of encouragement and help.

You, my dear ones who are my greatest gifts after the blessing of being, and I thank GOD for such great blessings wholeheartedly.

Contents

List of Figures

List of Tables

List of Symbols

a	*Coefficient (-)*
b	*Coefficient (-)*
c	*Coefficient (-)*
B	Chute width (m)
C	Air concentration defined as the volume of air per unit volume (%)
C_b	Pseudo-bottom air concentration, air concentration at vicinity of step edge (%)
C_{mean}	Mean (depth-averaged) air concentration (%)
$C_{mean\ ups}$	Mean (depth-averaged) air concentration upstream of, but not influenced by, the slope change (%)
d_0	Jetbox opening, inflow depth (m)
d_c	Critical flow depth (m)
d_w	Equivalent clear water depth (m)
$d_{w\ up}$	Equivalent clear water depth upstream of, but not influenced by, the slope change (m)
E	Specific energy at any cross-section of the spillway (m)
E_{usc}	Specific energy immediately at the first step edge upstream of the reach under the influence of slope change (m)
f	Time-averaged air-phase frequency (s^{-1}) / Frequency (Hz)
F	Probability of pressure occurrence (%)
f_{max}	Maximum air-phase frequency in a cross-section (s^{-1})
F_{r0}	Inflow Froude number (-)
g	Gravitational acceleration (ms^{-2})
h	Step height (m)
H_{max}	Maximum upstream head above the downstream step edge (m)
H_{res}	Specific energy obtained at the downstream last step (m)
H_{usc}	Total head immediately (at the first step edge) upstream of the reach under the influence of slope change above the datum cross-section defined at the downstream end of such region (m)
H_{dsc}	Total head at the downstream end of the region influenced by the slope change (m)

ΔH_{sc}	Head loss corresponding to the reach under the influence of the slope change (m)
k_s	Normal step height (m)
k_u	kurtosis (-)
l	Step length (m)
L_t	Total length of the chute under the influence of the slope change (m)
N	Exponent of velocity power law distribution (-)
P	Dynamic pressure (pa)
P_{xx}	Power spectral densities (PSD) of the pressure signals (bar^2Hz^{-1})
q_w	Water discharge per unit width (m^2s^{-1})
r	Cross-correlation coefficient associated to the velocity measurement (-)
R_e	Reynolds number (-)
S_k	Skewness (-)
t_{acq}	Acquisition time (s)
t_A	Time-averaged air-phase time (s)
t_W	Time-averaged water-phase time (s)
v	Flow velocity (ms^{-1})
v_c	Critical flow velocity (ms^{-1})
V_{m0}	Inflow mean flow velocity at the exit of the jetbox (ms^{-1})
V_{mean}	Mean flow velocity (ms^{-1})
V_{90}	Characteristic flow velocity at Y_{90} (ms^{-1})
W_{e0}	Inflow Weber number at the exit of the jetbox (-)
x	Streamwise distance downstream of the jetbox (m) / Distance from the step edge along the horizontal step face (m)
x_{sc}	Streamwise distance between the jetbox and the slope change cross-section (m)
X	Dimensionless distance from the slope change cross-section, measured along the chute, $X=(x-x_{sc})/d_c$ (-)
y	Transverse coordinate originating at the pseudo-bottom (m)
Y_{90}	Characteristic flow depth where the air concentration is 90% (m)
Y_{95}	Characteristic flow depth where the air concentration is 95% (m)
Y_{99}	Characteristic flow depth where the air oncentration is 99% (m)
Y_{ψ}	Characteristic flow depth where the air concentration is ψ% (m)
z	Distance from the step edge along the vertical step face (m)
ΔZ_0	Dam height above the spillway toe (m)
ΔZ_{sc}	Elevation above the datum cross-section (m)
α	kinetic energy correction coefficient (-)
Θ	Chute slope (˚)

$\Delta\Theta$	Slope change angle (º)
σ	Interfacial surface tension (Nm^{-1})
ρ	Water density (Kgm^{-3})
υ	kinematic viscosity of water (m^2s^{-1})
γ	Water specific weight (Nm^{-3})

Part (I)

1 Introduction

Several stepped spillways were built to date in particular linked to the application of the roller compacted concrete (RCC) dam construction as a cheaper, quicker and easier technique of construction (Chanson, 2002; Felder and Chanson, 2011b). A significant number of hydraulic physical modelling research has been conducted to investigate the flow features on stepped spillways.

For a given stepped chute geometry, the general behaviour of the flow may be characterized by three different regimes, namely nappe, transition and skimming flow (e.g., Ohtsu and Yasuda, 1997; Chanson, 2002). For typical hydraulic design of dam stepped spillways, the skimming flow regime is relevant (e.g., Chanson, 1994, 2002; Matos, 2000; Boes and Hager, 2003a).

1.1. Conventional stepped spillways

So far, most of the design and associated physical modelling studies were conducted on a conventional constant sloping stepped chute (e.g., Sorenson, 1985; Chanson, 1994, 2002; Chamani and Rajaratnam, 1999; Pegram et al., 1999; Matos et al., 1999; Boes, 2000a,b; Matos, 2000; Sánchez-Juny et al., 2000, 2007; Chanson and Toombes, 2002; Boes and Hager, 2003a,b; Sánchez-Juny and Dolz, 2005; Takahashi et al., 2005; Frizell, 2006; Pfister et al., 2006a,b; André and Schleiss, 2008; Gonzalez and Chanson, 2008; Kavianpour and Masoumi, 2008; Amador et al., 2009; Felder and Chanson, 2009a,b; Schleiss, 2009; Bung and Schlenkhoff, 2010; Pfister and Hager, 2011; Bung, 2011; Meireles et al., 2012; Zhang et al., 2012; Felder, 2013; Frizell, et al., 2013, 2015; Hunt and Kadavy, 2013; Matos and Meireles, 2014; Felder and Chanson, 2015).

1.2. Non-conventional stepped spillways

1.2.1. Constant slope

In addition to the hydraulics of conventional stepped spillways, a variety of experimental studies have also been carried out on non-conventional geometries, such as stepped spillways with macro-roughness (e.g., André, 2004; André et al., 2004; Gonzalez et al., 2008; Bung and Schlenkhoff, 2010), with non-uniform step heights (e.g., Felder and Chanson, 2011b), with rounded step edges (e.g., Zare and Doering, 2012a), with converging sidewalls (e.g., Frizell, 1990; André et al., 2005; Hunt et al., 2008; Hakoishi & Sumi, 2000; Willey et al., 2010), or without sidewalls (e.g., Estrella et al., 2012).

1.2.2. Varying slope

Stepped spillways may be integrated economically into the downstream face of a RCC gravity dam. They have also been built on valley flanks adjacent to embankment or rockfill dams, where the possibility of slope change may allow for a more efficient design, particularly if the spillway follows the topography of a valley flank. Only a few prototypes incorporate a stepped spillway with an abrupt slope change, such as the Upper Stillwater Dam (Houston, 1987), New Victoria Dam (Chanson, 2002) and the Lower Siah-Bishe Dam (Baumann et al. 2006), and no systematic scientific investigation for designing such type of configuration has been conducted so far. Thus, there is presently insufficient information available on the flow behaviour on an abrupt slope change on stepped spillways.

To fill this gap of knowledge, the effect of an abrupt slope change on the main skimming flow properties were investigated in the present study. Various sets of measurements was conducted in 9 model test runs over 50º-18.6º ($\Delta\Theta$=31.4º) and 50º-30º ($\Delta\Theta$=20º) slope change configurations with a uniform step height of 0.03m and 0.06 m for a wide range of discharges ($2.6 \leq d_c/h \leq 9.2$). The results of this systematic experimental study on air entrainment, flow bulking, velocity and dynamic pressure distribution, as well as the energy dissipation are presented and discussed, particularly in the vicinity of the slope change.

1.3. Structure of the thesis report

This thesis report is organized in three parts with a total of eight chapters (Figure 1.1):

- **Part (I)** includes 3 chapters that review previous studies on stepped spillways, describes the present research objectives and introduces the experimental set-up, as explained below:
  - **Chapter 1** presents an introduction on stepped spillways and relevant issues, emphasizing on an abrupt slope changes, and what was conducted and achieved in the present study.
  - **Chapter 2** summarizes the state of the art on the air-water flow properties on stepped spillways, e.g. air entrainment and velocity distribution, pressure fluctuation, as well as the energy dissipation on constant sloping stepped chutes. Then it gives a brief literature review on very limited findings on stepped spillways incorporating abrupt slope changes.
  - **Chapter 3** outlines the experimental installation, measurement equipment and test procedure.

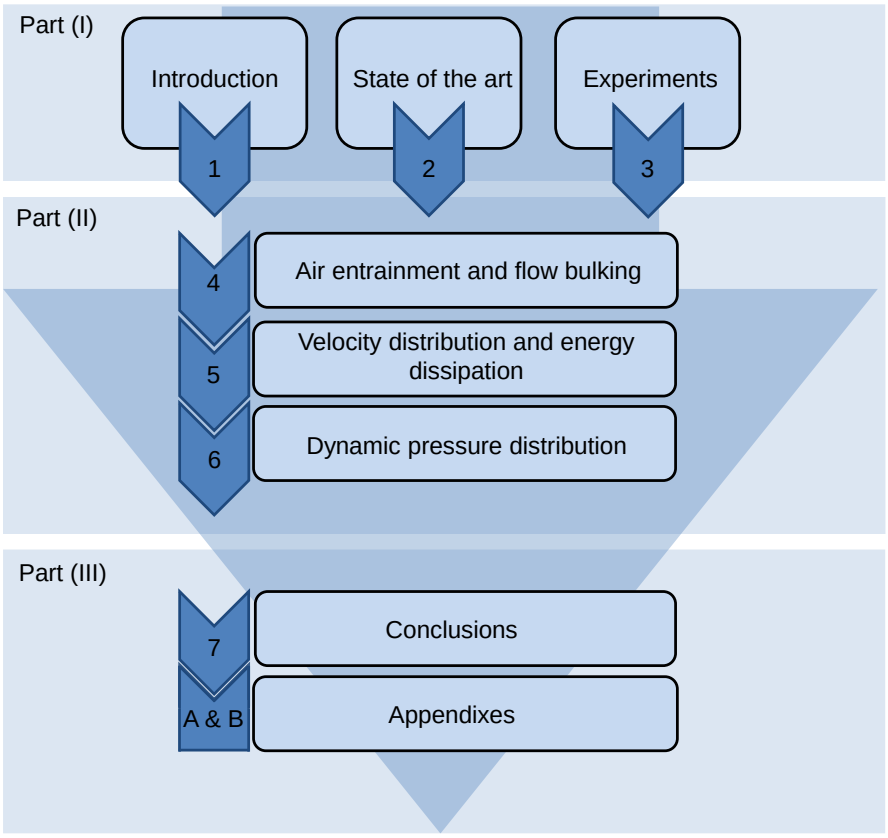

Figure 1.1 Outline of thesis report.

- **Part (II)** presents the findings in three chapters which have been prepared as journal papers:

- **Chapter 4** shows the effect of an abrupt slope change on air entrainment and flow bulking, with different step heights and flow rates.
- **Chapter 5** describes the effect of an abrupt slope change on the velocity distribution and energy dissipation with constant step heights and different flow rates.
- **Chapter 6** addresses the effect of an abrupt slope change on the pressure development on the vertical and horizontal step faces in vicinity and far downstream of the slope change, with constant step heights and different flow rates.

➢ **Part (III)** presents the conclusions of the results obtained in the present research work, and recommends some suggestions for future research work.

- **Chapter 7** explains the conclusions in three main sub-chapters on air entrainment and flow depth, velocity and energy dissipation as well as pressure development. Some recommendations for future research work on an abrupt slope change on stepped spillways are provided.
- **Appendixes A and B** provide the results associated to the influence of acquisition time on air concentration and velocity profiles, as well as the supplementary experimental data obtained from nine model test runs. They are also available on request at the Laboratory of Hydraulic Constructions of the Ecole Polytechnique Fédérale de Lausanne (LCH-EPFL).

2

State of the art

2.1. Introduction

A significant number of stepped spillways were built during the last decades, in particular linked to the application of the roller compacted concrete (RCC) dam construction technique. Stepped spillways are easy to construct and increase the energy dissipation rate which may reduce cavitation risk potential, as well as the needed dimensions of the terminal energy dissipator structure (Boes and Hager, 2003b). These pronounced advantages make stepped spillways attractive under various conditions, namely as service spillway on downstream face of RCC dams (Fig.2.1a), and on valley flanks besides embankment or rockfill dams (Fig. 2.1b).

(a) (b)

Figure 2.1 Stepped spillways: a) Pedrógão RCC dam stepped spillway, Portugal (courtesy of Prof. Jorge Matos), b) Upper Siah-Bishe dam stepped spillway, Iran (http://www.iwpco.ir),

Initial physical model studies on stepped spillways were initiated roughly in the 1980s (Hager and Pfister, 2013). Parallel to the increasing number of constructed stepped spillways, the number of related studies also augmented and research on the hydraulics of stepped spillways has been active (Chanson, 1994; Chanson and Toombes, 2002). These studies have focused mainly on studying the inception of air entrainment, air concentration, velocity and pressure distributions as well as energy dissipation. They characterized two-phase flow features along stepped spillways, in order to provide better design guidelines (Sorensen, 1985; Houston, 1987; Rajaratnam, 1990; Christodoulou, 1993; Chanson, 1994; Rice and Kadavy, 1996; Matos, 2000; Chanson, 2002; Boes and Hager, 2003a,b; Ohtsu et al., 2004; André, 2004; Gonzalez, 2005; Frizell, 2006; Pfister et al., 2006a,b, 2011). This chapter gives a summary of studies and associated findings of flow properties over stepped spillways, including:

- Flow regimes
- Air entrainment
- Velocity and pressure distribution
- Energy dissipation and residual energy
- Scale effects
- Slope changes on smooth and stepped spillways

2.2. Flow regimes

The general behaviour of the flow on stepped spillways may be characterized by three different regimes, namely nappe, transition and skimming flow (e.g., Ohtsu and Yasuda, 1997; Chanson, 2002).

Nappe flow occurs at low flow rates and can be defined as a succession of free-falling nappes. In skimming flow, the water (or air-water) flows as a coherent stream over the pseudo-bottom formed by the outer step edges (Fig. 2.2a). It is also evident that beneath the main stream flow three-dimensional recirculating vortices occur (e.g., Matos et al., 1999; Chanson, 2002; Gonzalez and Chanson, 2008), contributing to energy dissipation (Carosi and Chanson, 2008). It is shown that near the step edge, the direction of the flow is practically aligned with the pseudo-bottom; however, the effect of the vorticity is noticeable in between the step edges (Fig. 2.2b, Boes and Hager, 2003a). According to Takahashi and Ohtsu (2012), flow impacts near the step edge of the horizontal step face, in skimming flow, and the area of the impact region increases with decreasing the chute slope for a given flow rate.

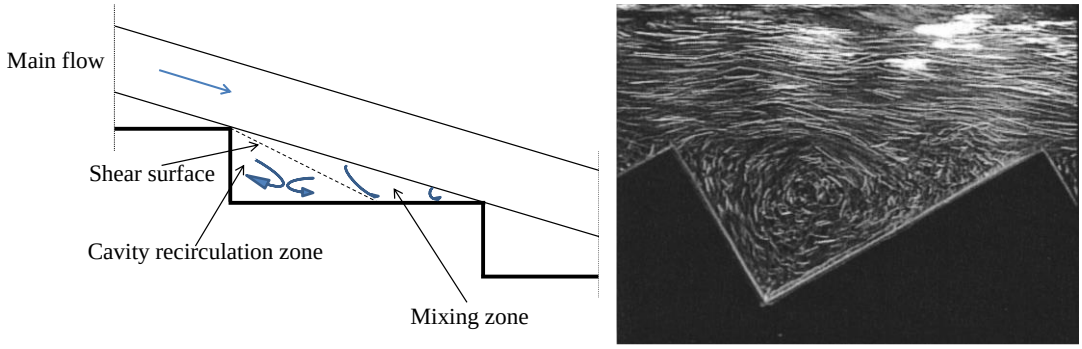

(a) (b)

Figure 2.2 Skimming flow over stepped spillway: a) sketches of the flow pattern (adapted from Zare and Doering, 2012a); b) flow pattern on 30º sloping chute with 0.092 m step height (Boes and Hager, 2003a), flow direction is from left to the right.

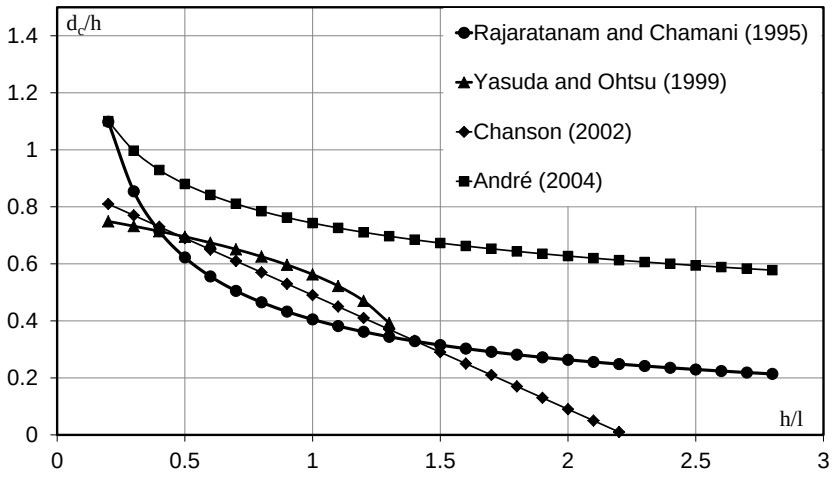

(a)

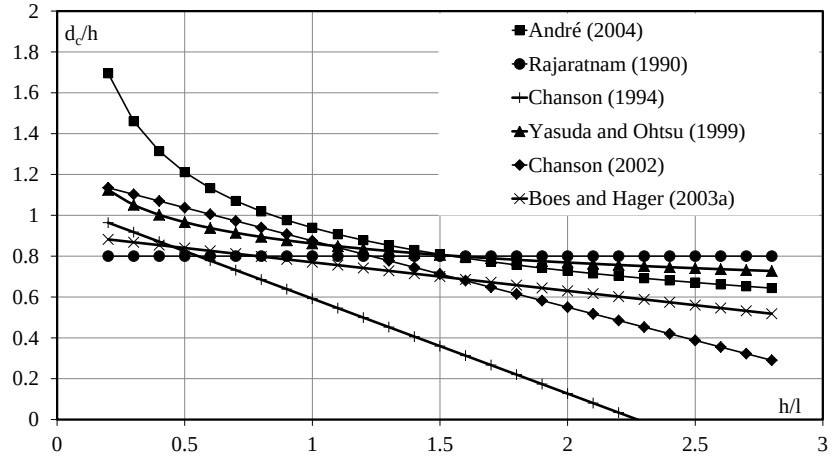

(b)

Figure 2.3 Comparison of proposed empirical relationship to estimate the onset of (a) transition and (b) skimming flow regimes.

Between the upper limit of nappe flow and the lower limit of skimming flow, a gradual and continuous transition flow regime takes place. For typical hydraulic design of dam stepped spillways, the skimming flow regime is relevant (e.g., Chanson, 1994, 2002; Matos, 2000; Boes and Hager, 2003a). Numerous laboratory studies were conducted to define the criteria for evaluating the onset of flow regimes based on the relative critical depth (d_c/h) and chute geometry (h/l), where d_c is the critical flow depth, h and l are the step height and step length, respectively. Most of the studies evaluated the flow regimes by means of visual observation. Thus, large scatter of the empirical criteria may be found in literature as shown in Fig. 2.3 for onset of transition and skimming flow. As it can be seen, the required discharge for obtaining the skimming flow regime decreases with increasing the ratio of h/l.

Similar to high-velocity flows on smooth spillways (e.g. Wood, 1985; 1991 and Chanson, 1997), skimming flow down stepped spillways can be divided into four main regions (Fig. 2.4):

1) Clear-water flow region close to the spillway crest (upstream of the inception point of air entrainment)
2) Partially aerated flow region (shortly downstream of the inception point)
3) Fully aerated flow region (downstream of the inception point)
4) Uniform or gradually varied flow region (far downstream of the inception point)

Quasi-uniform flow condition is generally assumed to be attained if the time-averaged air content and the flow velocity remain unvaried in the flow direction (Bung, 2011). Several studies were conducted to estimate the distance of the quasi-uniform flow region as a function of the chute geometry and flow rate such as Christodoulou (1999) and Boes and Minor (2000). It was revealed by Pfister & Hager (2011) and Bung (2011) that the development of quasi-uniform flow requires a flow distance of around 2 to 3 times the inception point length.

(a)

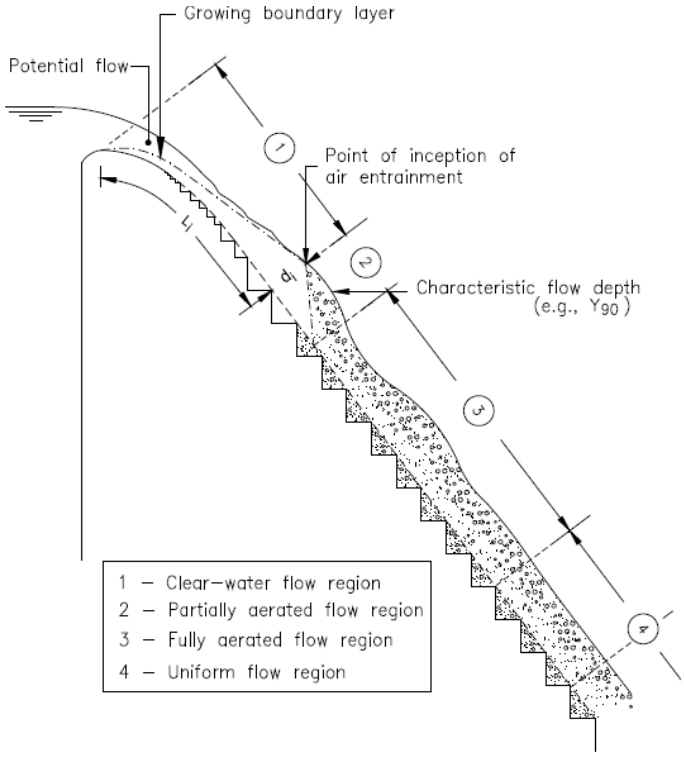

(b)

Figure 2.4 Skimming flow over a steeply sloping chute a) side view of Θ =50º sloping stepped chute assembled at LCH-EPFL; b) sketch of the flow regions (Matos and Meireles, 2014)

2.3. Air entrainment and flow depths in skimming flow

2.3.1. Air inception point

Flow accelerates down stepped spillways and at a location defined as the inception point the turbulent boundary layer will reach the free surface. Then air will be entrained into the flow because of the weakness of the surface tension in comparison with turbulence forces. A significant number of studies were conducted to define the location and flow properties of the inception point on uncontrolled and gated stepped spillways in order to determine the type of the flow region for a given stepped geometry and flow rate. A short summary could be given as follows:

- Uncontrolled intake spillways:
  - $14 \leq \Theta$ (º) ≤ 59: Mateos & Elviro (1997), Chamani (2000), Matos (2000), Amador et al. (2009), Hunt and Kadavy (2011), Meireles et al. (2012) and Hunt & Kadavy (2013)

- Gated spillways or pressurized intakes :
  - $3.4 \leq \Theta$ (º) ≤ 50: Boes & Hager (2003b), André (2004), Chanson (2006)

Chanson (2006) analysed previous study results with a wide range of inflow conditions. His findings indicated that with a pressurized intake, the outer edge of the boundary layer reaches the free-surface earlier than on an uncontrolled chute, due to the thinner and faster out flow of pressurized intake (jetbox). Therefore, using a pressurized intake shorten the length of the developing flow region for an identical flow rate and stepped geometry.

Due to the diversity of methods that have been used, there are several definitions for estimating the location and flow properties of the inception point on skimming flow over stepped spillways. The definition and methods can be categorized as (Meireles et al., 2012, 2014):

- visual observation of the cross-section where there is a continuous presence of air within the flow surface, cavity recirculation zones and at sidewalls (e.g., Sorensen, 1985; Chanson, 1994, 2002; Bung, 2009)

- observation of the cross-section where the pseudo-bottom air concentration (C_b) is 1% (e.g., Boes and Hager, 2003b; Pfister and Hager, 2011);

- determination of the intersection between the flow free surface and the outer edge of the developing boundary layer (e.g. Amador et al., 2009; Meireles and Matos 2009; Meireles et al., 2012)

- observation of the cross-section where the mean (depth averaged) air concentration, equals 0.20 (e.g., Bung, 2011).

Basic findings indicated that the steps provoke a higher and earlier flow self-aeration if compared to smooth sloping chutes. It is also revealed that the air inception length increase with the flow rate and decrease with the chute slope (e.g. Boes and Hager, 2003b; Matos and Meireles, 2014).

2.3.2. Air transport mechanism

Along the upstream portion of the clear-water region (region 1, Fig. 2.4b), the boundary layer grows from the chute invert (Chanson, 2002). The air concentration is equal to zero in the lower part of the profile and close to the pseudo-bottom, however a significant increase in the air concentration is observed along the upper part of the profile close to the free surface, due to the entrapped air (e.g. Meireles at al., 2012; Matos and Meireles, 2014).

At the downstream portion of the clear-water region (close to the inception point), larger values of the air concentration are found within the wavy zone. The latter is judged to be due to the air-bubble entrainment caused by the unsteadiness of the inception point location (Meireles at al., 2012; Matos and Meireles, 2014). In addition, the air concentration immediately below the wavy zone departs from zero (Meireles at al., 2012; Pfister & Hager, 2011; Matos and Meireles 2014).

Near the inception point, highly macro-roughness induced turbulence causes a rapidly varied air-water flow (Matos and Meireles, 2014). According to the visual observations with a high-speed camera and air concentration measurements conducted by Pfister & Hager (2011), in the vicinity of the pseudo-bottom air inception point, the rough and highly turbulent flow surface includes significant surface waves with water crests and air troughs combined with bubbly flow.

Although the air concentration increases downstream of the rapidly varied flow region, it follows a wavy pattern and a decrease in the air concentration with distance may occur as

well (Matos and Meireles, 2014). Nevertheless, quasi-uniform flow may be reached far downstream from the point of inception, and the main flow properties such as the mean air concentration and flow velocity, equivalent clear water depth and specific energy will practically remain constant along the spillway (Matos and Meireles, 2014).

2.3.3. Local air concentration and air-phase frequency

The local air concentration *C*, and the air-phase frequency *f*, are defined as time-averaged values over the entire acquisition period. The values of *C* and *f* are independent, whereas the time-averaged air-phase (t_A) and water-phase (t_W) are related as $C = t_A/(t_W + t_A)$ (Pfister and Hager, 2011). Several studies were conducted to obtain the air concentration profiles perpendicular to the pseudo-bottom). Chanson (1997) proposed S-shape distribution based on the advection-diffusion model for air bubbles in turbulent self-aerated flows.

$$C = 1 - \tanh^2\left(k' - \frac{y/\mathrm{Y}_{90}}{2D'}\right) \tag{2.1}$$

where *y* is measured perpendicular to the pseudo-bottom formed by the step edges, and Y_{90} defined as the distance from the pseudo-bottom to the location where the air concentration is 90%, $k' = \tanh^{-1}(0.1)^{1/2} + 1/(2D')$ and $D' = (0.848\, C_{mean} - 0.00302)/(1 + 1.1375\, C_{mean} - 2.2925\, {C_{mean}}^2)$, where the C_{mean} is the depth-averaged air concentration. Chanson and Toombes (2002) also developed an improved model to better describe the S-shape profiles.

$$C = 1 - \tanh^2\left(k' - \frac{\frac{y}{\mathrm{Y}_{90}}}{2\mathrm{D}_0} + \frac{\left(\frac{y}{\mathrm{Y}_{90}} - \frac{1}{3}\right)^3}{3\mathrm{D}_0}\right) \tag{2.2}$$

where $k' = \tanh^{-1}(0.1)^{1/2} + 1/(2\mathrm{D}_0) - 8/(81\mathrm{D}_0)$ and

$\mathrm{D}_0 = -\log\,(1.0434 - C_{mean}/0.7622)/3.614$.

The dimensionless air-phase frequency fd_c/V_c can be expressed as a function of y/Y_{90}, where *f* is the average number of detected air bubbles per second, d_c the critical flow depth and $V_c = \sqrt{g d_c}$ the critical flow velocity. Felder and Chanson (2009b, 2011a) and Pfister & Hager (2011) revealed that the number of entrained air bubbles increases in the streamwise direction, for a given y/Y_{90}. In Pfister & Hager (2011) it is also shown that close to the inception point of air entrainment, the maximum value of fd_c/V_c is located near the flow surface, while it is located close to the pseudo-bottom far downstream of the inception point. According to Chanson (2002), the relationship between local air concentration and dimensionless air-phase frequency presents some self-similarity

$$\frac{f}{f_{max}} = 4\,C(1-C) \tag{2.3}$$

where f_{max} is the maximum air-phase frequency in a given cross-section.

Toombes (2002) observed that the maximum dimensionless air-phase frequency occurs for an air concentration slightly lower than C = 0.50; Bung (2011) found maximum dimensionless air-phase frequency for C = 0.45 and 0.43 (for 18.4º and 26.6º sloping chutes), and the results of Felder and Chanson (2011a, on a 26.6º sloping chute), indicated a maximum for $0.35 \leq C \leq 0.65$.

2.3.4. Mean air concentration

The mean (depth-averaged) air concentration is defined as (Fig 2.5):

$$C_{mean} = \frac{1}{Y_{90}} \int_0^{Y_{90}} C\,dy \tag{2.4}$$

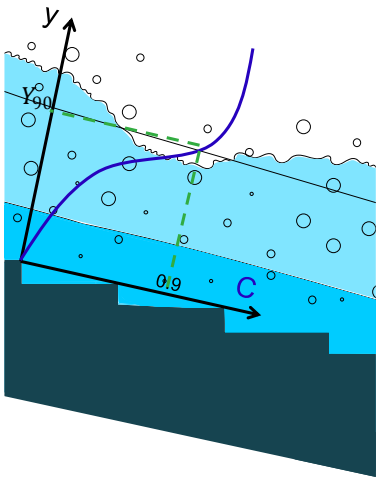

Figure 2.5 Definition of mean air concentration obtained from the integration of air concentration profile from pseudo-bottom up to Y_{90} .

2.3.5. Characteristic and equivalent clear water depths

It is difficult to determine the flow surface along turbulent aerated flow over stepped spillways. Therefore, different flow depths were defined to characterize the flow behaviour (André, 2004), such as

- Characteristic flow depth Y_{ψ}, where the air concentration is ψ%

- Equivalent clear water depth d_w

$$d_w = \int_0^{Y_{90}} (1 - C) dy = (1 - C_{mean})\, Y_{90} \quad (2.5)$$

where the C_{mean} is the depth-averaged air concentration (Fig. 2.5). Boes and Hager (2003a) stated that in the quasi-uniform flow, the normalized equivalent clear water depth (d_w/d_c) varies only with the chute slope independently of the step height and the discharge and proposed the following formula

$$\frac{d_w}{d_c} = 0.215(\sin\theta)^{-\frac{1}{3}} \quad (2.6)$$

On a long, constant sloping stepped chute, for a given flow rate, the mean air concentration tends to increase in the streamwise direction, until quasi-uniform flow conditions are attained, (e.g., Pfister and Hager, 2011; Takahashi and Ohtsu, 2012; Matos and Meireles, 2014).

In the literature, there are several proposed formulas for predicting the mean air concentration in quasi-uniform flow condition. Boes (2000a) and André (2004) developed the following equations as a function of the chute geometry and flow rates:

Boes (2000a):

$$c_{mean} = 0.60 - 6.11 \times 10^{-3} \times F^* \quad for\ \theta = 50° \quad (2.7)$$

$$c_{mean} = 0.43 - 2.34 \times 10^{-3} \times F^* \quad for\ \theta = 30° \quad (2.8)$$

André (2004):

$$c_{mean} = 0.55(sin\,\theta)^{-0.12} \quad for\ \theta = 30° \quad F^* < 4 \quad (2.9)$$

$$c_{mean} = 0.81(sin\,\theta)^{0.81} \quad for\ \theta = 30° \quad F^* > 4 \quad (2.10)$$

$$F^* = \frac{q_w}{\left(g\ {k_s}^3\ sin\,\theta\right)^{0.5}} \quad (2.11)$$

where q_w is flow discharge and k_s is normal step height. Takahashi and Ohtsu (2012) developed an equation as a function of the chute slope and relative critical depth for a wide range of chute slopes ($19 \leq \Theta^o \leq 55$)

$$C_{mean} = \left(\frac{6.9}{\Theta} - 0.12\right)\frac{h}{d_c} + 0.656\left\{1 - e^{-0.0356(\Theta - 10.9)}\right\} + 0.073 \quad (\Theta\ in\ \text{degrees}) \quad (2.12)$$

They indicated that mean air concentration increases with the chute slope and decreases with the relative critical depth.

2.4. Velocity distribution in skimming flow

Dimensionless time-averaged interfacial velocity distribution on stepped chutes may be approximated by a power law (Chanson, 1994; Felder and Chanson, 2015), in which the maximum velocity V_{90} occurs at the Y_{90} where the air concentration is 90%.

$$\frac{v}{V_{90}} = \left(\frac{y}{Y_{90}}\right)^{\frac{1}{N}} \tag{2.13}$$

Assuming the power law distribution for velocity as Eq. (2.13), *N* exponent could be estimated as (Bung, 2011)

$$N = \frac{V_{mean}}{V_{90} - V_{mean}} \tag{2.14}$$

where the mean flow velocity may be defined as (Chanson, 1997; Matos, 1999)

$$V_{mean} = \frac{q_w}{d_w} = \frac{\int_0^{Y_{90}} (1 - C) v \, dy}{\int_0^{Y_{90}} (1 - C) dy} \tag{2.15}$$

Considering the results presented by Pfister & Hager (2011) for a 50º sloping stepped chute, Bung (2011) proposed the following formula for estimating the *N* exponent as a function of chute slope

$$N = \frac{(\cos\Theta)^{0.984} (\sin\Theta)^{0.078}}{0.947 - (\cos\Theta)^{0.984} (\sin\Theta)^{0.078}} \tag{2.16}$$

Takahashi and Ohtsu (2012) proposed *N* exponent as a function of chute slope and relative critical flow depth

$$N = 14(\Theta)^{-0.65} \frac{h}{d_c} \left(\frac{100h}{\Theta d_c} - 1\right) - 0.041\Theta + 6.27 \quad (\Theta \; in \; \text{degrees}) \tag{2.17}$$

The *N* exponent decreases with the increase of chute slope (Θ) and may vary from one step edge to the next one for a given flow rate, due to some interference between adjacent shear layers and cavity flows, (Felder and Chanson, 2009a,b; 2011a; 2015). Bung (2011) obtained *N*=11 and *N*=8 respectively on 18.4º and 26.6º sloping chute. Gonzalez and Chanson (2004) obtained

N values between 5 and 12 on 15.9º sloping chute. Meireles et al. (2012) obtained *N*=3.4 on 50º sloping chute. In general, it can be concluded that the proposed range of *N* values for different slopes and flow rates are roughly limited in between 3 and 14, as shown in Fig. 2.6. The lower and upper reported limits (*N*≈3 and *N*≈14) belong to Takahashi and Ohtsu (2012) respectively on 55º and 19º sloping stepped chutes.

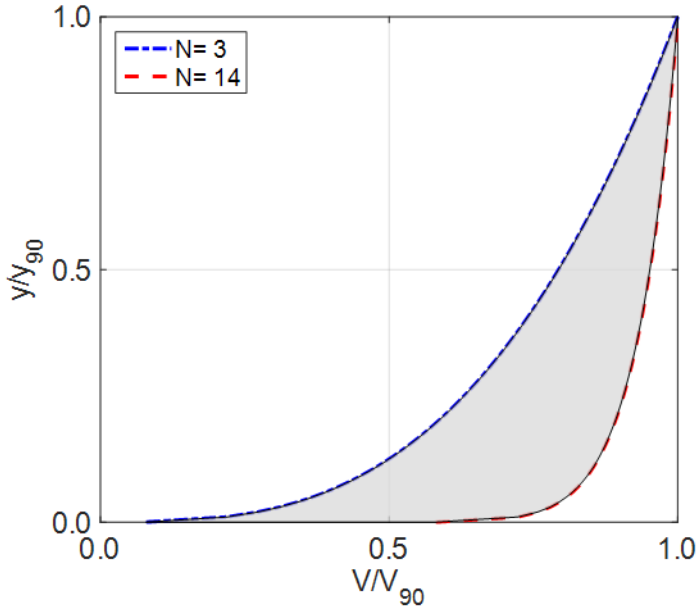

Figure 2.6 Lower and upper limits of the velocity distribution in air-water skimming flow, obtained by Takahashi and Ohtsu (2012) on 55º and 19º sloping stepped chutes respectively.

2.5. Pressure distribution in skimming flow

According to Sánchez-Juny and Dolz (2005) and Khatsuria (2008), the flow pressure shows the hydrodynamic distribution in skimming flow over stepped spillways. The hydrodynamic pressure distribution and its prediction play an important role in structural analysis of stepped chutes and were investigated extensively (e.g., Matos et al., 2000; Sánchez-Juny et al., 2000, 2007, 2008; André, 2004; Sánchez-Juny and Dolz, 2005; André and Schleiss, 2008; Amador et al., 2009; Zhang et al., 2012; Takahashi and Ohtsu, 2012; Frizell et al., 2013, 2015; Chanson, 2015). Studies showed that pressure distribution on stepped spillways drawn attention in two main aspects (Frizell, 2006):

- likely damages on step invert in presence of high pressures (horizontal step faces)
- probable cavitation damage corresponding to the low pressure (vertical step faces)

2.5.1. Horizontal step faces

According to previous studies, the maximum positive pressure occurs on the horizontal step faces (e.g. Sánchez-Juny et al., 2000). Sánchez-Juny et al. (2007), Zhang et al. (2012) and Takahashi and Ohtsu (2012) observed S-shape pressure distribution on horizontal step faces. The minimum pressure values were observed along the upstream portion of horizontal step faces, ($x/l > 0.5$), whereas the maximum values are observed along the portion closer to the step edges ($x/l < 0.5$), where x is the distance from the step edge, along the horizontal face, and l is the step length. This is in agreement with the other findings, illustrating that the downstream portion of the horizontal step face is subjected by the jet impact whereas the upstream portion involves a boundary layer separation due to step vorticity and recirculating internal eddies (Sánchez-Juny et al., 2000; André and Schleiss, 2008; Amador et. al, 2009).

Sánchez-Juny et al. (2000, 2007, 2008), André (2004), André and Schleiss (2008), Amador et al. (2009), Takahashi and Ohtsu (2012) stated that the outer step edge is under the flow impact and the inner step edge is under the influence of flow recirculation, and the highest absolute pressures occurs at flow separation in between these two regions ($x/l \approx 0.2$). Takahashi and Ohtsu (2012) revealed that the impact region increases with decreasing relative critical depth (d_c/h) and the highest pressure location moves toward the inner step edge (x/l increases), on a given sloping chute. However, Sánchez-Juny et al. (2007) and André (2004) concluded that the pressure distribution on the step faces is entirely conditioned by the chute slope. They also observed the maximum pressures up to ≈7 and 5.5 times the step height on horizontal step faces of respectively 51.2º and 30º sloping stepped chutes for d_c/h=2.25 and 2.65.

Sánchez-Juny et al. (2008) analyzed the pressure distribution obtained from model tests on a 51.2° stepped sloping chute and proposed empirical equations to estimate the pressures acting on the vertical and horizontal step faces in the fully-developed zone of the skimming flow.

Amador et al. (2009) also investigated the probability distribution of dynamic pressures along the horizontal step faces and compared them with the Normal (Gaussian) distribution. Their results indicate that the normal probability plots obtained along the upstream portion of the horizontal step faces (x/l>0.5) differed from those obtained along the downstream portion (x/l<0.5). For x/l<0.5, a higher and positive skewness was found, showing that large negative pressure values are not as frequent as large positive values; hence a Gaussian model will underestimate the maximum pressures on the step edges. Close to the outer step edge, negative pressures with very low probability were found.

Smaller pressure fluctuations were found along $x/l>0.5$, by comparison with the downstream portion of the steps ($x/l<0.5$) and negative skewness was observed. The minimum pressure of larger magnitude was observed near to the step inner edges. Along the inner region of the steps, the pressure distribution found to be more in agreement with the Gaussian distribution, if compared to the downstream portion of steps.

The variation of the mean pressure values with different discharges has been investigated by André (2004) and Sánchez-Juny et al. (2007) on horizontal step faces of 30° and 50° sloping chutes. The greater the discharge, the greater the pressure values were. Results obtained by Sánchez-Juny et al. (2007) fitted well with linear expressions.

2.5.2. Vertical step faces

Recent studies have indicated that the most important negative pressures occur on the vertical step faces, in particular near the edge of the steps, where the step experiences a separation of the flow (Sánchez-Juny et al., 2000, 2007, 2008; André, 2004; Sánchez-Juny and Dolz 2005; Amador et al. 2005; Gomes et al. 2006; Amador et al., 2009; Zhang et al., 2012). Therefore, this area might be sensitive regarding cavitation attack due to low negative pressure occurrence. It is relevant to measure pressures to determine whether they are high enough to avoid cavitation (Falvey, 1990), as the hydraulic performance of stepped spillways at high velocities may compromise its use due to the concern with safety against cavitation damage.

Amador et al. (2009) found that the probability plots of dynamic pressures on the vertical step faces are different from those observed on the horizontal step faces. In the direction of the outer step edge, the skewness decreases and negative values were found. These results indicate that large negative pressure values are much frequent than large positive values. In this case, a Gaussian model underestimates the extreme minimum pressures, as expected close to the step edge on the vertical step faces (Amador et al., 2009). Their findings have also shown that pressure sensors located closer to the outer step edge presented higher negative pressures. Towards the inner step edge skewness increased.

Amador et al. (2005) investigated the probability of attaining low pressures corresponding to cavitation inception close to the inception point on a stepped spillway. The vertical face near the outer step edge close to the inception point is identified as a critical region for predicting cavitation (Matos et al., 2001; Amador et al., 2009). For increasing discharges, the non-aerated region of the spillway will increase and larger velocities will be reached supporting the generation of extreme negative pressure (Amador et al., 2009). Therefore, high steps may be prone to cavitation damage under high head flow with a large unit discharge and high velocity. So, it could be concluded that the steps upstream of the inception point might be particularly prone to damage (Pfister et al., 2006a,b).

Frizell et al. (2013) investigated the critical cavitation index to provide enhanced design criteria for stepped chutes. They obtained critical cavitation indices of 0.3-0.4 for a mild slope and 0.6 for a steep slope. Their findings are higher than the critical value (0.2) found for smooth chutes (Falvey, 1990). In literature there is a lack of consensus on the maximum specific discharge to avoid cavitation damage (Amador et al., 2009). Gomes et al. (2006) and Amador et al. (2009) analysed the negative pressure in the vicinity of the inception point on vertical step faces. Amador et al. (2009) proposed limiting the mean velocity up to ≈15 m/s, corresponding to ≈15m^2/s unit discharge on 51.3º stepped sloping chute.

As observed by Peterka (1953), presence of an adequate percentage of air near the solid surfaces can prevent cavitation damage. Therefore forced aeration should be considered along non-aerated flow region for unit discharges higher than these thresholds (Amador et al., 2009). For example, Pfister et al. (2006a), Zamora et al. (2008) and Terrier et al. (2015) studied and compared the effects of forced aeration on stepped and smooth chutes.

2.6. Energy dissipation

The energy dissipation rate is a basic parameter to be considered for the design of spillways. Studies demonstrated that stepped spillways are effective in kinetic energy dissipation, thereby reducing the required size of the stilling basin at the toe of the dam. For example, approximately 75% greater energy dissipation was achieved on Upper Stillwater Dam stepped spillway if compared to a conventional smooth spillway of the same height (Houston, 1987). This reduction in energy required the length of stilling basin to be shortened from 61 to 9 meters.

In skimming flow, energy dissipation is caused by the momentum exchanges between the mainstream flow and cavity zones (Felder and Chanson, 2011b), as well as the jet impact on the step surface. The specific energy at any cross-section of the spillway can be expressed similarly as for air-water flows on smooth chutes as (Wood, 1991; Chanson, 1997, 2002; Matos, 1999)

$$E = d_w \cos\theta + \alpha \frac{q_w^2}{(2g)d_w^2} = d_w \cos\theta + \alpha \frac{V_{mean}^2}{(2g)} \quad (2.18)$$

where α is the kinetic energy correction coefficient as (Matos, 1999)

$$\alpha = \frac{1}{V_{mean}{}^2} \frac{\int_0^{Y_{90}} (1-C)v^3 dy}{\int_0^{Y_{90}} (1-C)v dy} \quad (2.19)$$

Based on the air concentration and velocity profiles, the kinetic energy correction coefficient and the specific energy may be computed along the sloping chute. Further, the rate of the energy dissipation ($\Delta H/H_{max}$) and dimensionless residual energy (H_{res}/d_c) may be introduced as basic parameters for design of stepped spillways (Felder and Chanson, 2011b), where the H_{max} is the maximum upstream head above the downstream step edge: $H_{max} = \Delta z_0 + \frac{3}{2} d_c$ in which Δz_0 is the dam height above the spillway toe and $\Delta H = (H_{max} - H_{res})$ is total head loss, and H_{res} is the specific energy obtained at the downstream last step (residual head).

Chanson (1994), Matos (2000), Felder and Chanson (2011b) indicated that the rate of energy dissipation decrease with increasing flow rate. Felder and Chanson (2011b) showed that the residual head decreased with increasing discharge for the smaller flow rates, while it was about constant for the largest flow rates.

Stephenson (1988) observed 10% increase in energy dissipation on stepped spillways incorporating nonuniform step heights. In contrast, Felder and Chanson (2011b) indicated that the rate of energy dissipation is not significantly influenced by nonuniform stepped configurations and remains almost identical as with using uniform steps. Therefore, nonuniform step heights do not enhance the energy dissipation at the downstream end of the chutes. Some authors (e.g. Meireles and Matos, 2009; Hunt and Kadavy, 2011) presented simple equations for determining the relative energy lost upstream of the inception point on typical embankment dam slope. However, there are still some design challenges as pointed out by Hunt and Kadavy (2011).

2.7. Scale effects

Highly turbulent self-aerated flow can be precisely represented in the scale model if Froude, Reynolds and Weber similarity laws are fulfilled simultaneously. This condition cannot be fully satisfied at the scale model due to the experimental setup limitations; therefore model tests are conducted under the Froude similarity due the dominant effect of gravity forces (André, 2004). Applying the Froude similitude scaling, the viscous force represented by the Reynolds number ($R_e = q_w/\upsilon$) is underestimated and the surface tension force represented by the Weber number ($W_e = V_{mean}/(\sigma \sin\Theta/\rho h)^{1/2}$ $\mathrm{w_e} = \frac{\mathrm{V_m}}{\sqrt{))))\frac{\sin\Phi}{\rho \mathrm{h}}}}$) is overestimated, where υ is the kinematic viscosity of water, V_m is the mean flow velocity ($V_{mean} = q_w/d_w$), σ is the interfacial surface tension, and ρ is the water density.

To date, some studies have been conducted to evaluate the scale effects, particularly with regard to air concentration (void fraction), bubble count rate, interfacial velocity as well

as the turbulence flow properties (e.g., Boes, 2000b, Chanson and Toombes, 2002, Boes and Hager, 2003a; Chanson & Gonzalez, 2005, Takahashi et al., 2005, 2006; Felder & Chanson 2009b, Felder, 2013).

Pfister & Chanson (2014) gives a general review and proposed a range of Reynolds and Weber numbers (or Reynolds and Froude numbers), emphasizing the importance of the selection of the criteria to evaluate scale effects on two-phase air-water flows. They indicated that scale effects are expected to be negligible, in particular with regard to air concentration, if the Reynolds and Weber numbers are respectively greater than $2\text{-}3\times10^5$ and 140. They addressed the need for full-scale prototype measurements data as well. André (2004) assumed that the scale effects are mitigated on the velocity and air concentration, thus it may be judged that they are also negligible on the pressures as well.

2.8. Slope Changes

An abrupt change in bottom slope may occur in open channel hydraulic structures such as aerators, ski jumps and at the toe of spillways (Fig. 2.7). The profile of the open channels follows the topographic and geologic site conditions (USBR, 1965). Therefore, the channel profile is consisted of straight reaches which are connected by vertical curves (USBR, 1965). On the other hand, abrupt slope changes may increase the risk of unsatisfactory flow condition, such as jet deflection (on steep to mild slope change, Chanson 2002), or generating a free jet (on mild to steep slope change, Pfister, 2009).

There is some design criteria presented to be fulfilled on smooth spillways with convex or concave slope changes (e.g. USBR 1965), to minimize or avoid the unsatisfactory flow condition. In presence of an abrupt slope change, however, prediction of pressure development is necessary for structural analysis of the chute invert and walls (Zarrati et al., 2004). Flow bulking and splashing is also necessary to be analyzed in order to find an adequate sidewall height, further including a sufficient freeboard. Therefore, the flow over an abrupt slope change is interesting to be investigated, particularly in terms of air entrainment and flow bulking, as well as the pressure field.

(a) (b) (c) (d)

Figure 2.7 A few examples of slope changes over spillways: a) Llyn Brianne dam, United Kingdom; b) Alqueva dam, Portugal; c) Cleveland Dam, Canada; d) Kárahnjúkar dam, Iceland (www.en.wikipedia.org, www.google.com, www.ethz.ch).

2.8.1. Smooth spillways

Few numerical investigations have been conducted in order to simulate the flow behaviour over sudden mild to steep changes on smooth spillways (e.g. Montes, 1994; 1997) in which the conformal transformation technique has been applied to locate the free surface in order to analyse the flow features in slope change zone.

Zarrati et al. (2004) conducted a numerical and experimental investigation on the flow over steep to mild abrupt slope changes of $\Delta\Theta$ = 6.22°, 10°, and 15° associated to a bottom aerator. The pressure distribution in the vicinity of abrupt slope change was a particular focus in their study.

According to Zarrati et al. (2004), a sudden change in pressure and velocity distribution occurs as the flow passes over an abrupt change in smooth sloping chutes. They indicated that the slope change of $\Delta\Theta$=15º may lead to an increase of the pressure in vicinity (up and downstream) of the slope change cross-section. They measured pressures up to 25 times the hydrostatic pressure near the point of abrupt change in slope. Their findings indicated that the dynamic pressures fall rapidly with increasing distance from the point of slope change. They observed that the modification in pressure and velocity initiates slightly upstream of slope change, despite of supercritical flow. The latter is judged to be due to the back internal pressure waves, corresponding to the non-hydrostatic pressure distribution upstream of the slope change, which leads to influence the flow properties upstream of the slope change, even in the supercritical flows. They found that separation may occur in a very small zone near the stagnation point where the flow boundary direction suddenly changes, due to boundary layer

effects. They also concluded that separation intensifies with higher flow discharges and the slope change angle.

2.8.2. Stepped spillways

Abrupt slope changes over stepped spillways have not been deeply investigated to date and the number of research studies and built prototypes are limited. However, the possibility to vary the slope along the stepped spillway may be an interesting feature to implement on valley flanks or to gain flexibility for the section of a RCC gravity dam (Ostad Mirza et al., 2015a,b). Given the rare application of slope changes, only limited information on its effect is available.

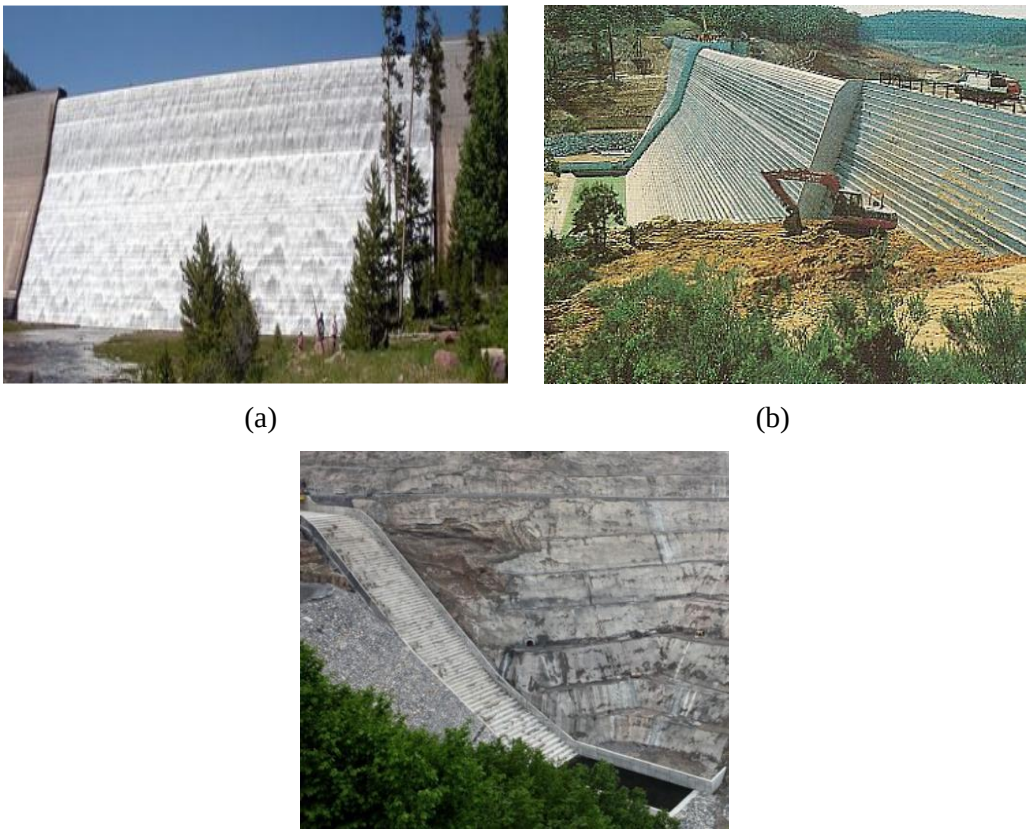

(a) (b)

(c)

Figure 2.8 Stepped spillways with an abrupt slope change (a) Upper Stillwater dam spillway, USA (http://www.google.com); (b) New Victoria Dam, Australia (http://www.pickeringbrookheritagegroup.com/infrastructure8.html); (c) Siah-Bishe lower Dam, Iran (http://www.iwpco.ir).

Only singular projects as well as the associated physical model studies included a stepped spillway with an abrupt slope change, such as the Upper Stillwater Dam in USA (Houston, 1987), New Victoria Dam in Australia (Chanson, 2002), and the Lower Siah-Bishe Dam in Iran (Baumann et al., 2006), as shown in Fig. 2.8. Houston (1987) found the highest pressure values at abrupt slope change from 72º to 59º, for all the tested discharges. Minimum pressures were also measured near the slope change. However, Houston (1987) did not evaluate minimum and maximum pressure severe enough to cause impact or cavitation damage. Chanson (2002) stated that the break in slope of New Victoria dam has increased the risks of jet deflection at the transition between crest and chute.

3

Experimental installation and test procedure

3.1. Experimental facility

The data presented below were collected on a steep channel with variable slope, equipped with steps of constant height, assembled at the Laboratory of Hydraulic Constructions (LCH), of the Ecole Polytechnique Fédérale de Lausanne (EPFL). The channel consisted of two 4 m long modules with a 0.6 m high transparent sidewall to allow for flow observation. The channel width was B=0.5 m. The upstream chute slope (i.e. pseudo-bottom angle) was set to Θ_1 = 50º (1V:0.84H), while the downstream chute slope was set to Θ_2 = 30º (1V:1.7H), or 18.6º (1V:3H) (Fig. 3.1).

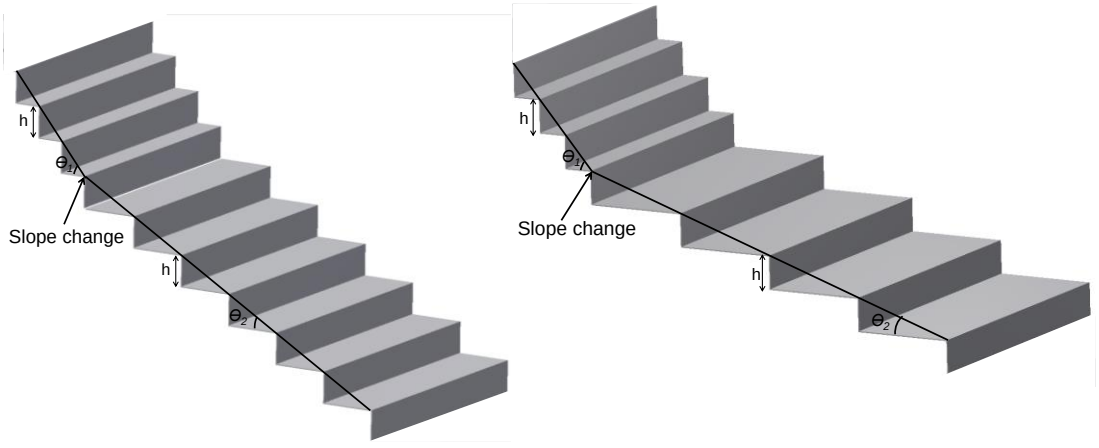

(a) (b)

Figure 3.1 Sketch of slope change configurations: a) 50º-30º and b) 50º-18.6º configuration.

The maximum tested chute slope was 50°, which is typical of RCC gravity dams. Step heights of h = 0.06 m and 0.03 m, constant on both parts of the chute, were tested. The total number of 0.06 m high steps included 41 steps along the 50º chute and 34 steps on the 30º chute, or 20 steps on the 18.6º chute. The number of 0.03 m high steps doubled those adopted for the first series of tests (h = 0.06 m).

To allow for an independent variation of the inflow depth (d_0) and Froude number ($F_{r0} = q_w/(gd_0^3)^{1/2}$, where q_w is unit discharge and g is gravitational acceleration), the flume inflow device consisted of a jetbox with a maximum opening of 0.12 m, designed for passing the maximum unit discharge of 0.48 m^2s^{-1}. By using the jetbox, the pressurized pipe approach flow was transformed into a free surface flow (Fig. 3.2); the location of the inception of air entrainment was shifted upstream and the developing region of the flow was shorten, in comparison to the typical situation corresponding to an un-gated crest, for identical chute slope, step height and discharge (Chanson, 2006). Hence, gradually varied or quasi-uniform air-water flow conditions were reached on the upstream slope, for the tested range of step geometries and discharges.

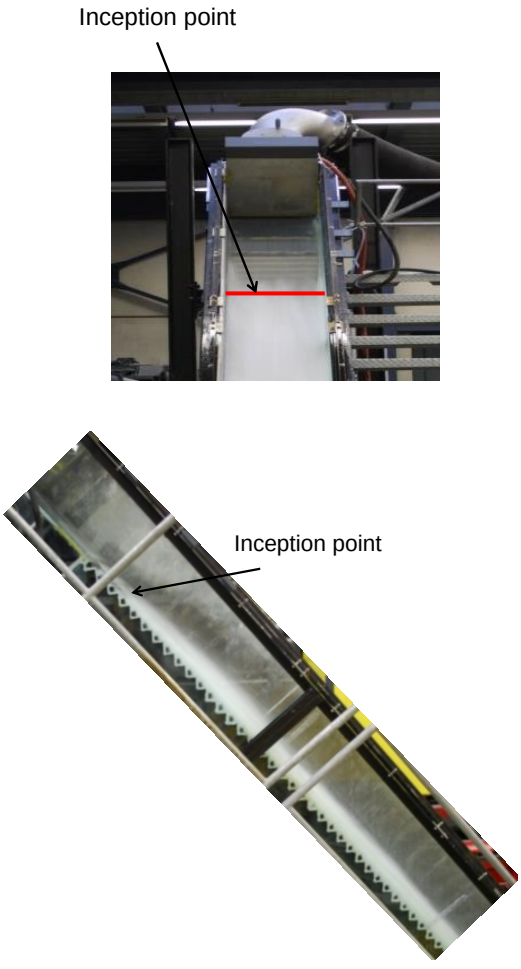

Figure 3.2 Frontal view (a), and side view (b) of configuration associated to test number 1, as per Table 3.1 (Θ_i= 50º; d_c/h = 2.6; R_e = 1.9×10^5).

An electromagnetic flow meter was used to measure the discharge with an accuracy of 1% full span, corresponding to a discharge of 3 l/s. The test program included observations and measurements in the skimming flow regime (see Fig. 2.3b), for unit discharges (q_w) ranging between 0.20 m^2s^{-1} (d_c/h = 2.6, for h = 0.06 m) and 0.47 m^2s^{-1} (d_c/h = 4.6, for h = 0.06 m; d_c/h = 9.2, for h = 0.03 m), where $d_c = \sqrt[3]{\frac{q_w^2}{g}}$ is the critical flow depth and h is the step height. Skimming flow conditions were chosen since the design discharge of a prototype is typically in that regime. Bottom pressures at the slope change, as well as the local flow aeration and de-aeration, are then dominant, what is relevant for the concrete load and cavitation issues. Transition flow occurs in the present channel at around $d_c/h < 0.8$ for Θ_1=50º, $d_c/h < 1.0$ for Θ_2=30º for $d_c/h < 1.1$ for Θ_2=18.6º according to Chanson and Toombes (2004).

Skimming flow over stepped spillways can be characterised by a number of different parameters which cannot be modelled completely unless measuring at full scale prototype. A dimensional analysis can identify the most relevant air-water flow parameters as conducted by many other authors such as Carosi and Chanson (2006) and Felder (2013). They found that, with Froude similitude, the most relevant parameters in skimming flow on stepped spillways are

$$C, \frac{v}{\sqrt{g\,h}}, \ldots = F\left(\frac{x}{d_c}, \frac{y}{d_c}, \frac{d_c}{h}, R_e\right) \tag{3.1}$$

where C is the local air concentration and v is the local velocity.

Based on the jetbox performance, and among possible hydraulic inflow condition choices, three combination of discharges and inflow depths coresponding to inflow Froude number range of $3.9 \leq F_{r0} \leq 6.7$ have been selected, as shown in Fig. 3.3.

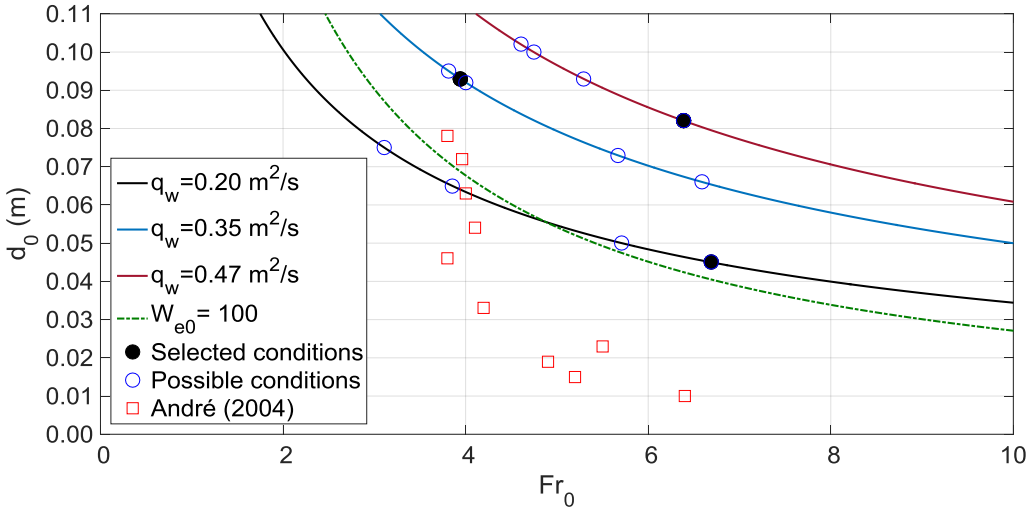

Figure 3.3 Selected inflow hydraulic conditions: jetbox opening (inflow depth) as a function of inflow Froude number (F_{r0}).

For such range of flow rates, the Reynolds number ($R_e = q_w/\upsilon$) varied between 2.0×10^5 and 4.6×10^5; the minimum inflow Weber number at the exit of the jetbox W_{e0} varied between 111 and 193. Therein $W_{e0} = V_{m0}/(\sigma / \rho d_0)^{1/2}$ $\mathrm{w_e} = \frac{\mathrm{V_m}}{\sqrt{\frac{\sin\Phi}{\rho h}}}$, where υ is the kinematic viscosity of water, V_{m0} is the inflow mean velocity at the exit of the jetbox ($V_{m0} = q_w/d_0$), σ is the interfacial surface tension, and ρ is the water density (Table 3.1).

Table 3.1 Test program.

Test no.	Θ_1 (°)	Θ_2 (°)	h (m)	d_0 (m)	q_w (m^2s^{-1})	d_c/h (-)	R_e (-)×10^5	F_{r0} (-)	W_{e0} (-)
1	50	18.6	0.06	0.045	0.20	2.6	2.0	6.7	111
2	50	18.6	0.06	0.093	0.35	3.8	3.4	3.9	135
3	50	18.6	0.06	0.082	0.47	4.6	4.6	6.4	193
4	50	18.6	0.03	0.093	0.35	7.6	3.4	3.9	135
5	50	18.6	0.03	0.082	0.47	9.2	4.6	6.4	193
6	50	30.0	0.06	0.045	0.20	2.6	2.0	6.7	111
7	50	30.0	0.06	0.093	0.35	3.8	3.4	3.9	135
8	50	30.0	0.06	0.082	0.47	4.6	4.6	6.4	193
9	50	30.0	0.03	0.082	0.47	9.2	4.6	6.4	193

In light of the findings of Boes and Hager (2003b) and Pfister and Chanson (2014), for such range of R_e and W_e numbers (or R_e and F_r), scale effects are expected to be negligible, in particular with regard to the main flow properties such as the mean air concentration and characteristic flow depths. Other parameters related to the bubble characteristics dominated by turbulence, as for instance the air-phase frequency, are affected by scale effects (Felder and Chanson 2009b). Note that the flow further accelerates along the chute, so that the streamwise values of W_e is going to even increase. Also the reader may note that according to the range of $5.5 \leq B/d_w \leq 22$, the step chute is considered wide (Takahashi et al. 2005; Takahashi and Ohtsu, 2012). Thus, the bottom shear stress is judged to be predominant if compared to the side-wall shear stress, and the flow may be assumed as two-dimensional (Takahashi and Ohtsu, 2012). Figure 3.4 shows the typical flow pattern as observed and induced by a slope change. Details are discussed subsequently in next chapters.

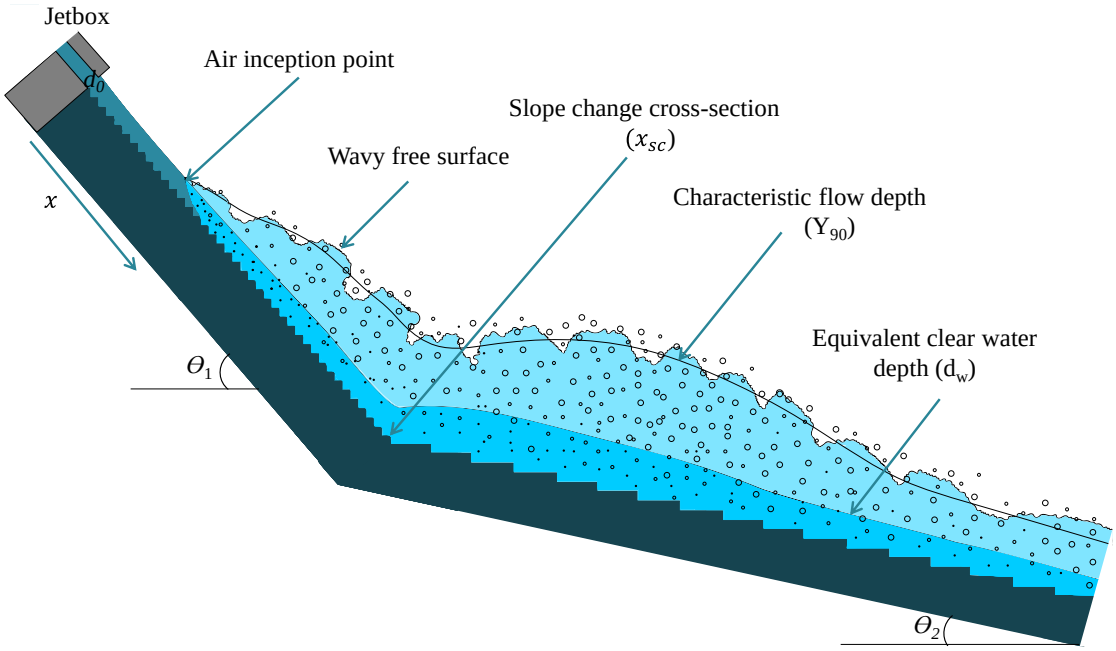

(a)

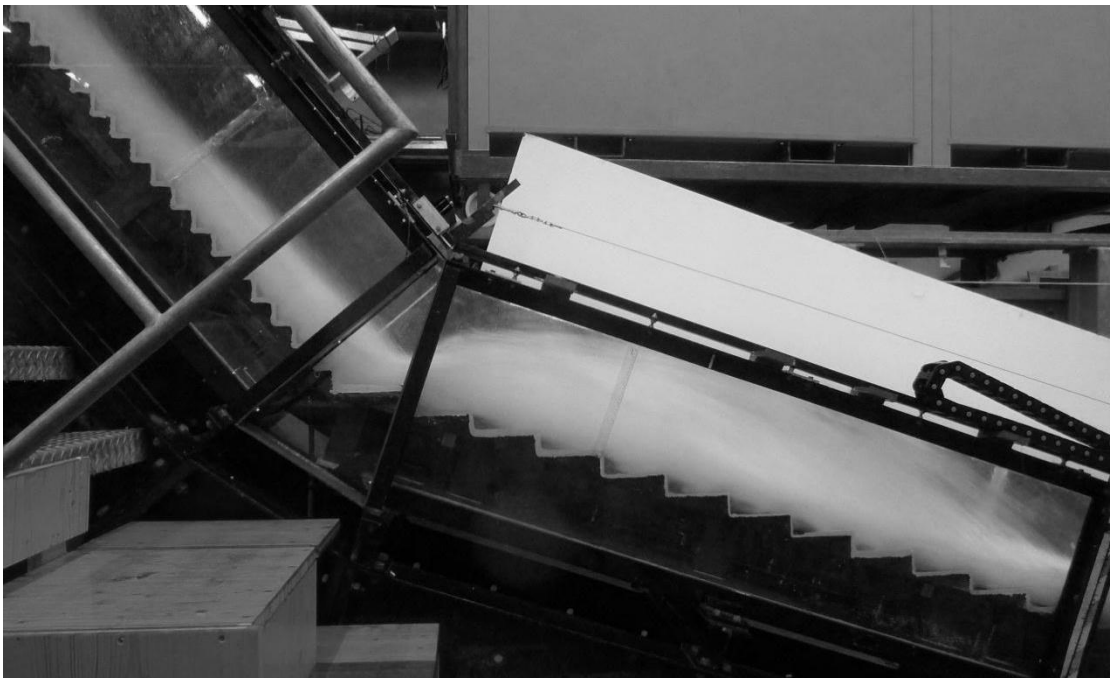

(b)

Figure 3.4 a) Sketch of the typical flow pattern on the stepped chute assembled at LCH-EPFL, with an abrupt slope change, b) Flow over 50˚-18.6 ˚ slope change configuration, (Test run 1).

3.2. Measuring parameters and instrumentation

The present study is focused on an experimental investigation of the air entrainment, flow velocity and dynamic pressure distributions on skimming flow on stepped spillways, in the vicinity of an abrupt slope change. Physical modelling was conducted in a relatively large scale facility, where detailed air-water flow measurements were gathered upstream and downstream of a 50˚-30˚ and 50º-18.6º slope changes. In addition, dynamic pressure measurements were obtained on both vertical and horizontal faces of several steps in the vicinity and far downstream of the slope change. The experimental facility comprises three main parts as shown on Fig. 3.5:

(i)- stepped channel incorporating the slope change

(ii)- double fiber-optical probe, RBI, mounted on an automatic positioning system on the downstream chute slope

(iii)- associated electronics of double fiber-optical probe, RBI, and automatic positioning system

Figure 3.5 General view of experimental facility at LCH-EPFL, (i) stepped channel incorporating the slope change, (ii) double fiber-optical probe, RBI, mounted on an automatic positioning system, (iii) associated electronics of double fiber-optical probe, RBI, and automatic positioning system

3.2.1. Air entrainment and velocity distribution

A dual fiber-optical probe including two sapphire tips of 30 µm diameter with a streamwise distance of 2 mm and a sampling rate of 1 MHz developed by RBI Instrumentation, France, was mounted on an automatic positioning system for measuring the air concentration and velocity. This probe measures the totally conveyed air concentration, without any distinction between entrapped and entrained air (Pfister and Hager, 2011).

The measurement principle is based on the Snell's law of optics. According to different refraction indices between the sapphire tips and the surrounding air–water phase, an infrared light supplied from an opto-electronic device to the tip is reflected and detected if the tip is positioned in the air-phase, while it is refracted and lost in the water-phase (Fig. 3.6). After amplification, the signal is passed through a threshold level in the opto-electronic module to be transformed into a digital Transistor-Transistor-Logic (TTL) signal with 0 Volts for the water phase and 5 Volts for the gas phase. In fact, this system transforms the analog signal and delivers crenel type voltage outputs, in which high and low parts correspond to air and water-phase respectively (Chaumat et al., 2007). Based on the recommendation of the RBI, the threshold signals were fixed at 1 and 3 Volts in present study. A software, ISO, developed by RBI was used to provide the air concentration C, velocity v and the corresponding correlation factor r as well as the time-averaged air-phase frequency f, defined as number of detected air-phases per second.

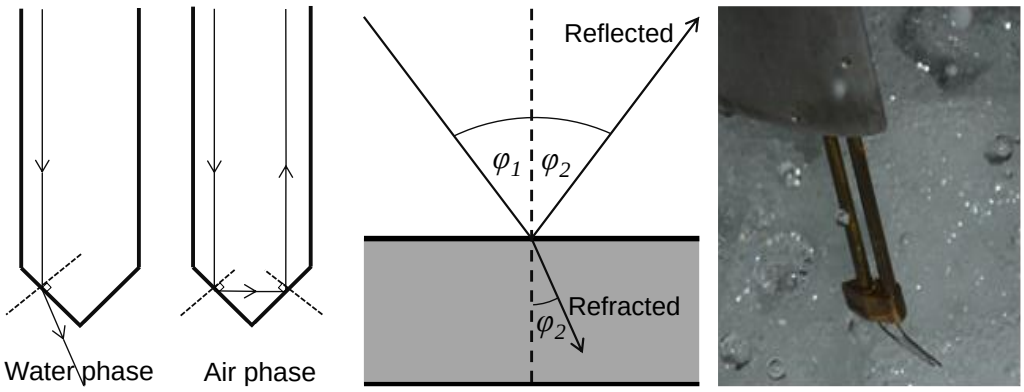

Figure 3.6 Schematic of the measurement principle and photograph of the double fiber-optical probe, RBI, used at LCH-EPFL.

Regarding to the acquisition time, Kramer (2004) has examined different time steps of 20, 40 and 60 seconds for measuring the air concentration and velocity profiles. He also compared the mean air concentration and mean velocity values obtained for different acquisition time. He found that the acquisition time t_{acq} greater than 20 s has almost no influence on the results.

Analyzing the present air concentration *C* and velocity *V* profiles which were obtained in high and low spray zones, indicated very low scatter and fairly high accordance of all profiles for acquisition times between 20 s and 60 s (see Appendix A.1). Therefore, the local air concentration *C* and interfacial velocity *V* of the two-phase air–water flow resulted from an acquisition period of 25 s in present study.

With regards to the mixture flow velocity, RBI suggests that the signals are well correlated for cross-correlation coefficient (*r*) values greater than 0.7. As shown exemplary for test run 3, in Fig. 3.7, the cross-correlation profiles corresponding to the velocity measurements obtained on the step edges are mostly higher than 0.7 (particularly in the upper flow zone) for steps located far from the slope change. However, for some steps in vicinity of the slope change (steps number -2 to +2), (*r*) values lower than 0.7 can be observed even in the upper flow region, which is judged to be due to the flow curvature and non-alignment between the flow direction and the probe tips.

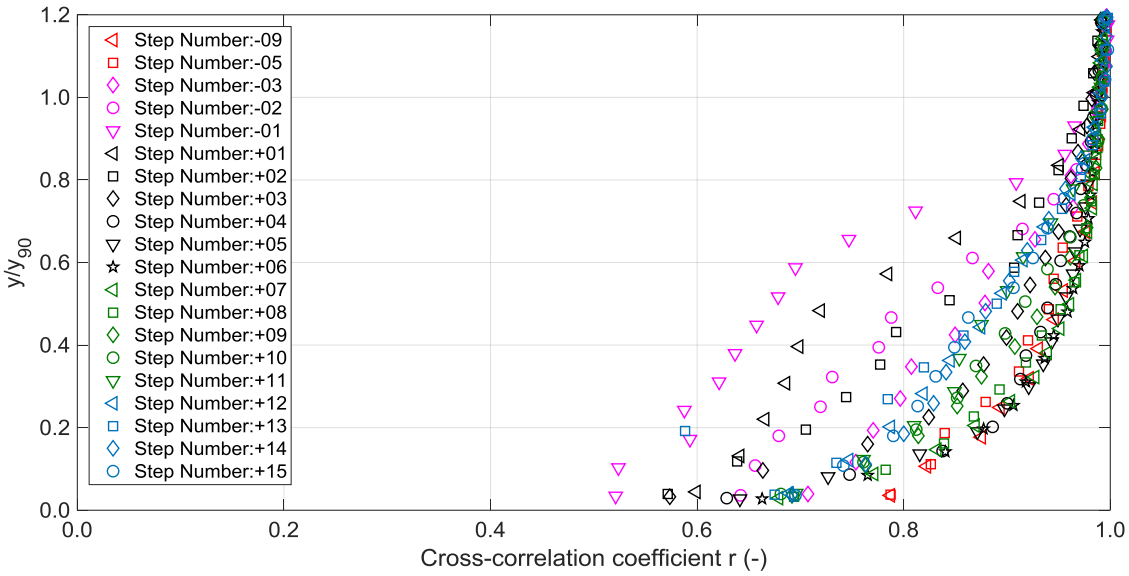

Figure 3.7 Cross-correlation coefficient distribution associated to the velocity measurements with the double fiber-optical probe signal, for test run 3.

The measurements of the air–water flow properties (i.e. *C*, *f*, and *V*) were conducted perpendicular to the pseudo-bottom (Fig. 3.8) at the centreline of 20 streamwise cross-sections along the chute, namely at 5 steps upstream of the slope change and 15 steps downstream of that location, from step number -09 to +23 (on 50º-30º), or from -09 to +15 (on 50º-18.6º), respectively (Fig. 3.9).

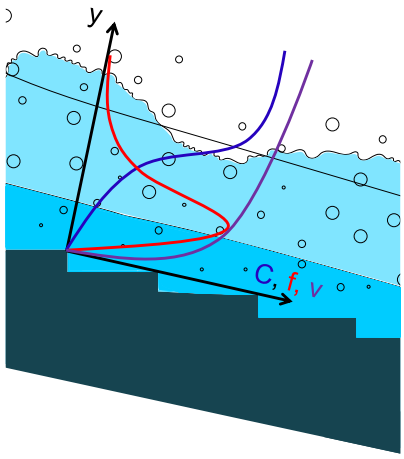

Figure 3.8 Sketch of the typical air concentration C, air-phase frequency f and velocity v profiles measured perpendicular to the pseudo-bottom

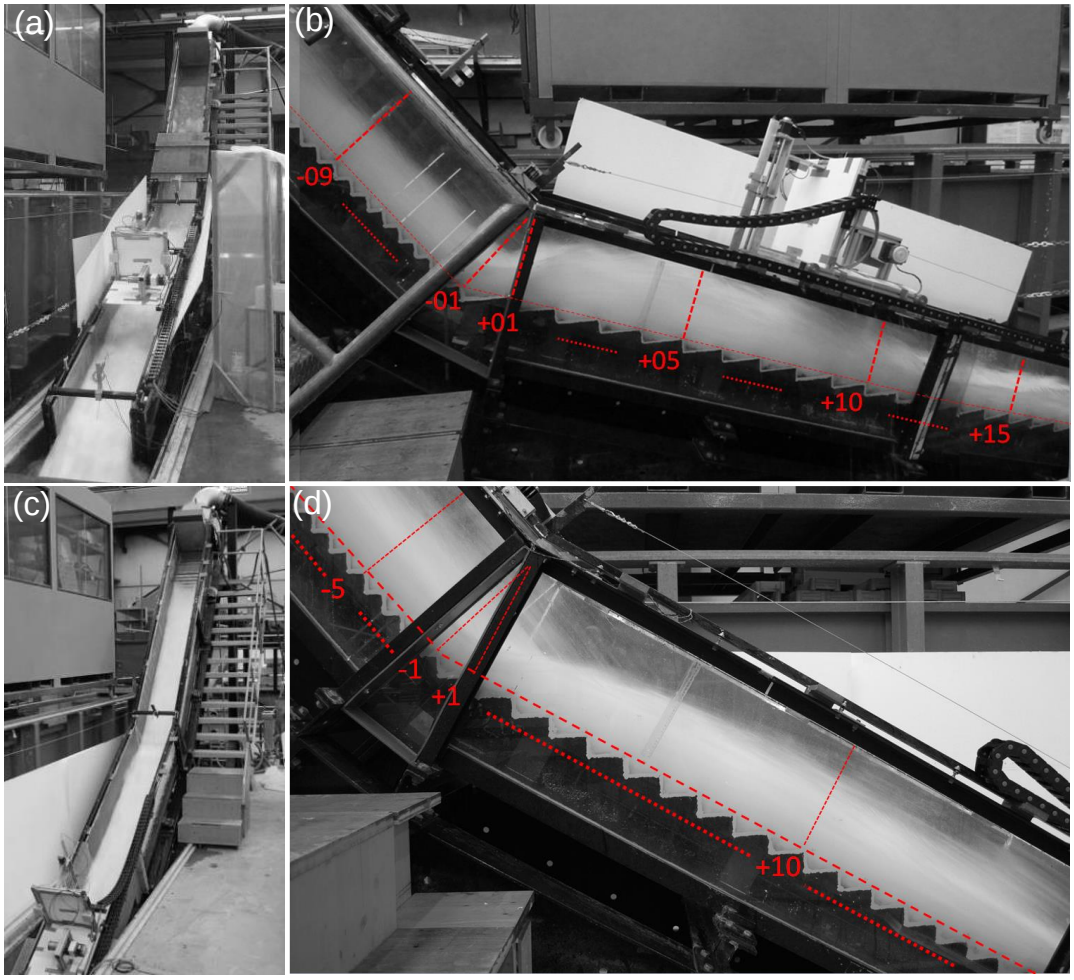

Figure 3.9 Physical model of the stepped spillway with an abrupt slope change assembled at LCH-EPFL: a,c) General view; b,d) Side view of configuration associated to test number 3 and 8, as per Table 3.1 (Θ_1 = 50°; Θ_2 = 30° and 18.6°; d_c/h = 4.6; R_e = 4.6×10^5); the dual fiber-optical probe is mounted on the automatic positioning system (step numbers used in the following are indicated).

As mentioned already, precise measurements on the downstream chute slope were conducted by using an automatic positioning system (Fig. 3.10a) with the possibility of movement in 2D direction, parallel and perpendicular to the pseudo-bottom, with less than 0.001m of error in each direction. In preliminary phase of experimental campaign, a laser beam was installed on the automatic positioning system and the step edge locations were detained very precisely. Then, the automatic positioning system has been programmed in a way that the air concentration, velocity and air-phase frequency profiles were measured perpendicular to the pseudo-bottom, including 30 points from about 5 mm distance to the step edge up to the flow surface, with 0.01 m point spacing (Fig. 3.10b).

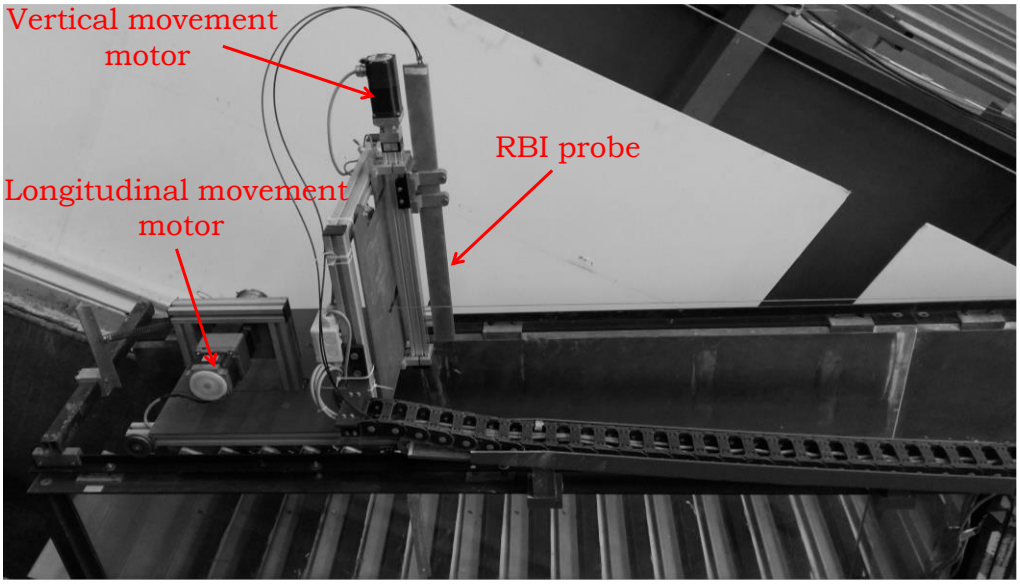

(a)

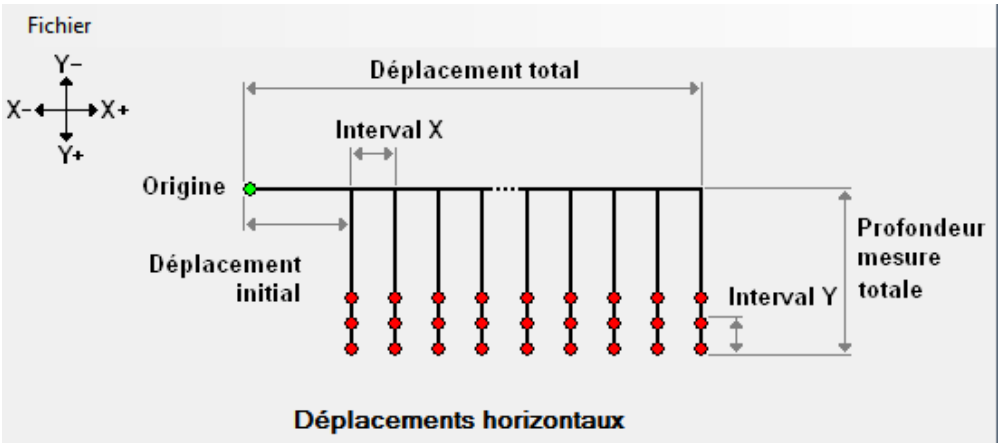

(b)

Figure 3.10 a) side view of the automatic positioning system, b) exemplary output of the code generator software for programming the automatic positioning system.

3.2.2. Dynamic pressures

The pressure measurements were collected by means of piezoresistive pressure transmitters (Keller-druck PR-23/8465.2) with measuring cell at the step face with 2mm diameter. The sensors were designed to work in high humid and dusty environment (IP 68). The range of measurements was from -0.1 to 0.2 bar and have been carried out along the vertical and horizontal face of steps in vicinity and far downstream of the slope change cross-section (Fig. 3.11). For each measurement position, three runs with t_{acq} = 70 s with 1 kHz frequency were performed to ensure repeatability of the results.

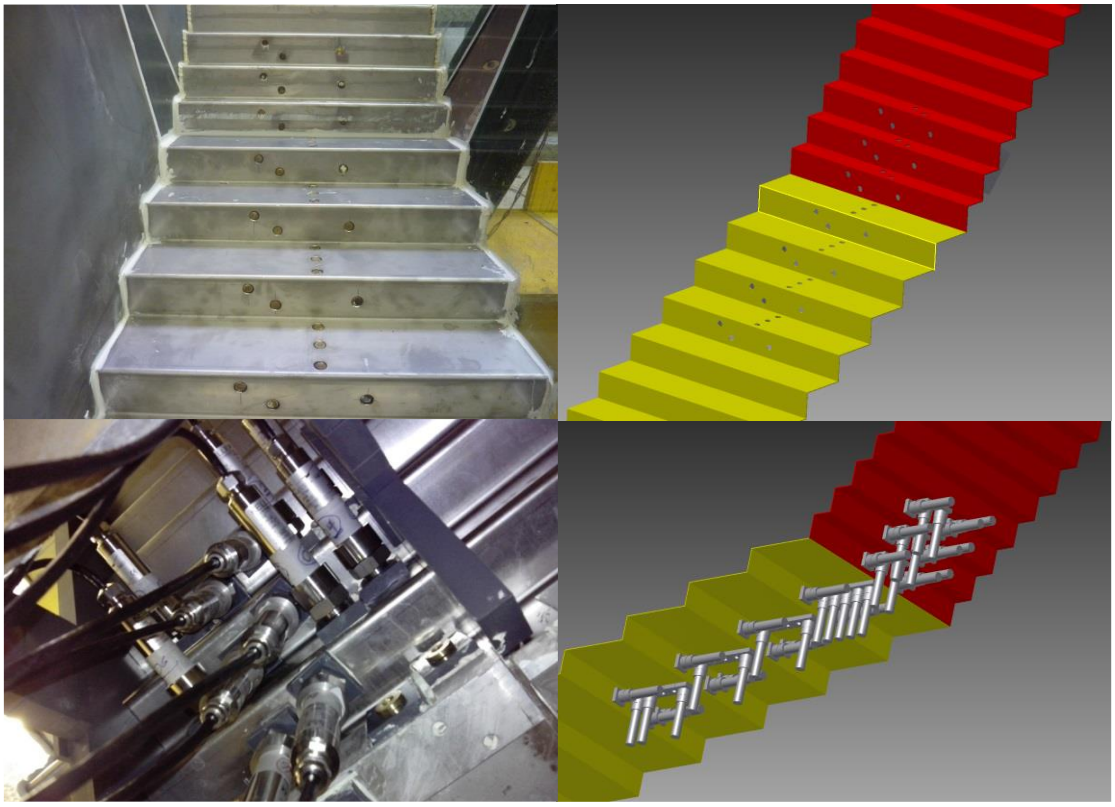

Figure 3.11 Pressure transducers installed in the vicinity of the slope change: photographs (left side) and schematics (right side) of the 50º-30º slope change equipped with pressure transducers.

The linearity error including the hysteresis and repeatability was less than ±0.5% of full scale, with the error of ±1.5 mbar for the water temperature range between 0º *C* and 50º *C*. The range of measurements have been chosen, considering the present step height of 0.06 m, due to the results obtained by Sánchez-Juny et al. (2007) and André (2004) indicating that the extreme maximum and minimum pressures are limited respectively to ≈7 and ≈-3 times of the step height on 51.2º and 30º sloping stepped chutes for d_c/h=2.25 and 2.65.

Each of the 12 sensors was connected to a 16 bit high-speed multifunction data acquisition card (NI 6259) with the capacity of 32 analog entries. This card, was optimised for superior accuracy at fast sampling rates (up to 32 MHz), (Figure 3.12)

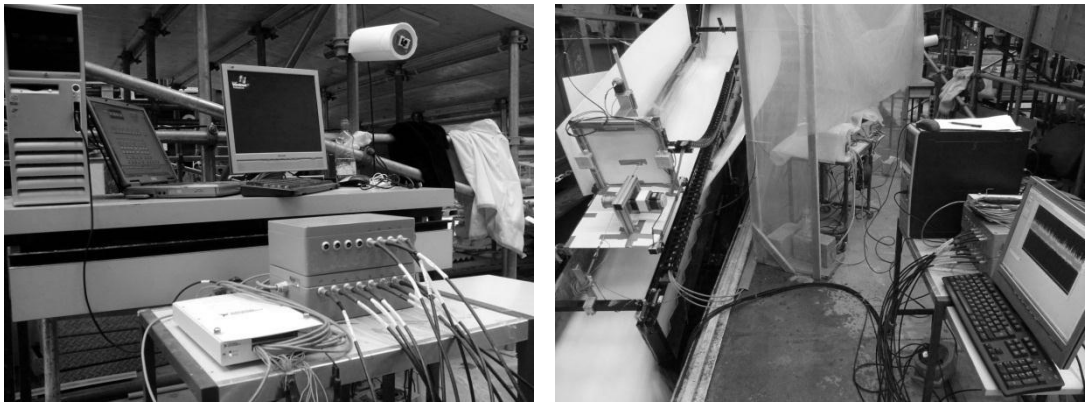

Figure 3.12 Electronics associated to the pressure measurement including the 16 bit high-speed multifunction data acquisition card (NI 6259) with the capacity of 32 analog entries.

The pressure transducers arrangement is shown in Fig. 3.13. Therein the values of *z/h* are equal to 0.30, 0.55 and 0.70, irrespective of the chute slope (*z* is the distance from the step edge, along the vertical face, and *h* is the step height; *h*=0.06 m). The *x/l* values for different sloping chutes are presented in Table 3.2, where *x* is the distance from the step edge, along the horizontal face, and *l* is the step length.

Table 3.2 Location of acquisition points for pressure sensors on horizontal step faces of tested sloping chutes, upstream and downstream of slope change cross-section.

Θ (°)	*l (m)*	*x/l* (-)				
50.0	0.050	0.35	0.64	-	-	-
30.0	0.104	0.17	0.50	0.84	-	-
18.6	0.178	0.10	0.30	0.50	0.70	0.88

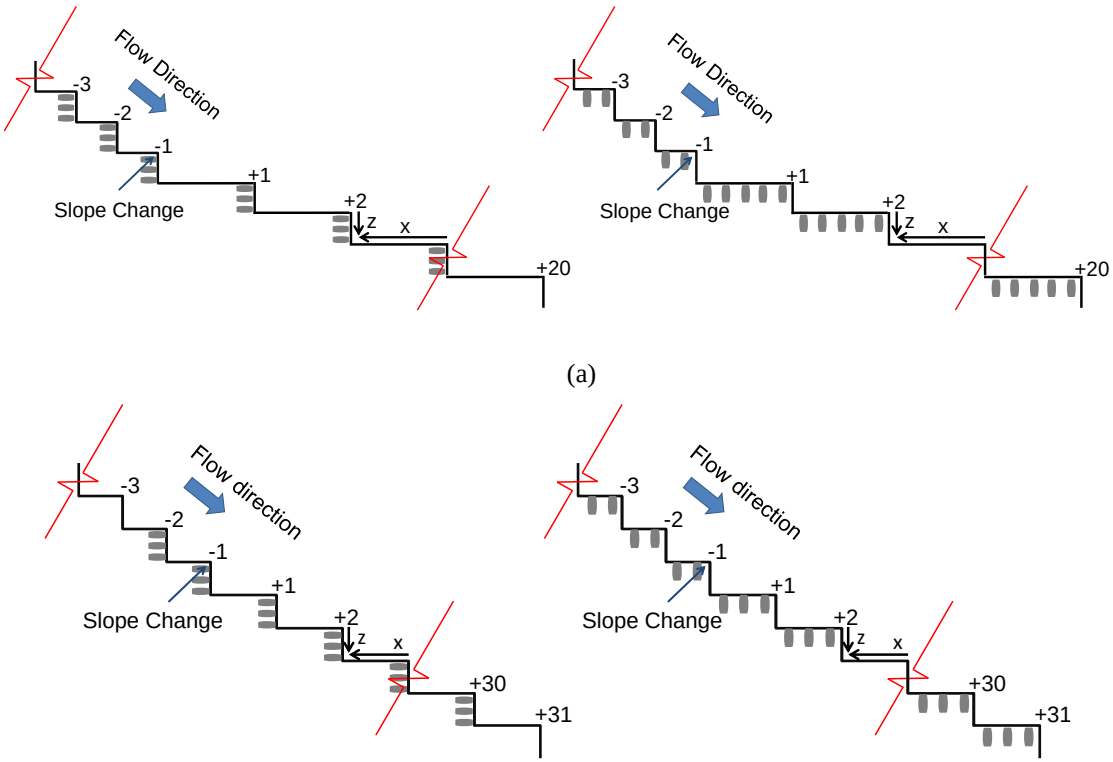

(a)

(b)

Figure 3. 13 Schematic of the pressure transducers installed on the horizontal and vertical step faces in the vicinity and far downstream of a) 50º-18.6º and b) 50º-30º slope change cross-sections.

Part (II)

4

Air entrainment and flow bulking

4.1. Introduction

A significant number of stepped spillways were built during the last decades, in particular linked to the application of the roller compacted concrete (RCC) dam construction technique. Stepped spillways may be integrated economically into the downstream face of a RCC gravity dam. They have also been built on valley flanks adjacent to embankment or rockfill dams, where slope changes may be implemented due to topography and economic reasons.

For a given stepped chute geometry, the general behaviour of the flow may be characterized by three different regimes, namely nappe, transition and skimming flow (e.g., Ohtsu and Yasuda, 1997; Chanson, 2002). Nappe flow occurs at low flows and can be defined as a succession of free-falling nappes. In skimming flow, the water (or air-water) flows as a coherent stream over the pseudo-bottom formed by the outer step edges; beneath it three-dimensional vortices occur (e.g., Matos et al., 1999; Chanson, 2002; Gonzalez and Chanson, 2008). Between the upper limit of nappe flow and the lower limit of skimming flow, a transition flow takes place. For typical hydraulic design of dam stepped spillways, the skimming flow regime is of relevance (e.g., Chanson, 1994, 2002; Matos, 2000; Boes and Hager, 2003a).

In the last couple of decades, a significant number of physical model studies were conducted on the hydraulics of skimming flow over constant sloping stepped spillways (e.g., Chanson, 1994, 2002; Chamani and Rajaratnam, 1999; Pegram et al., 1999; Sánchez-Juny et al., 2000, 2007; Matos, 2000; Boes and Hager, 2003a,b; Frizell, 2006; Amador et al., 2009; Meireles et al., 2012; Pfister and Hager, 2011; Bung, 2011; Felder and Chanson, 2009a,b; Felder, 2013; Matos and Meireles, 2014). In addition to the hydraulics of conventional stepped spillways, a variety of experimental studies have also been carried out on non-conventional

geometries, such as stepped spillways with macro-roughness (e.g., André, 2004; André et al., 2004; Gonzalez et al., 2008; Bung and Schlenkhoff, 2010), or with non-uniform step heights (e.g., Felder and Chanson, 2011b).

Despite some few exceptions, such as the Upper Stillwater dam in the USA (Houston, 1987) and lower Siah-Bishe dam in Iran (Baumann et al., 2006), most stepped spillways have been designed for a constant chute slope. Hence there is presently insufficient information available on the flow behaviour on slope changes on stepped spillways. The purpose of the present research is to study and describe the effect of an abrupt slope change on the main skimming flow properties. Various sets of measurements were conducted under different geometric and flow conditions. The experimental results on air entrainment and flow bulking, namely in the vicinity of the slope change, are presented and discussed in this chapter.

4.2. Mean air concentration

On a long, constant sloping stepped chute, for a given flow rate, the mean air concentration tends to increase in the streamwise direction, until quasi-uniform flow conditions are attained, (e.g., Pfister and Hager, 2011; Takahashi and Ohtsu, 2012; Matos and Meireles, 2014).

The development of the mean air concentration (C_{mean}) along the chute, for slope changes of 50º-18.6º and 50º-30º, is plotted in Figs. 4.1a and 4.1b, respectively. In the following, open symbols represent experimental data measured on the 50˚-18.6˚ slope change configuration, whereas filled symbols are applied to the 50˚-30˚ slope change configuration. Four main sub-regions may be identified: *sub-region (I)*, characterized by a decrease in the mean air concentration when approaching the slope change cross-section (Fig. 4.1, $-0.5 \leq X \leq 0$, where $X = (x-x_{sc})/d_c$, and x_{sc} is the distance of the slope change cross-section to the jetbox, measured along the chute); *sub-region (II)*, mainly characterized by a markedly increase in the mean air concentration shortly downstream the slope change cross-section, reaching a peak (Fig. 4.1, $0 < X \leq 5$); *sub-region (III)*, where the mean air concentration decreases considerably (Fig. 4.1, $5 < X \leq 9$); and *sub-region (IV)*, where the mean air concentration exhibits a gradually varied, quasi-constant trend down the chute (Fig. 4.1 , $X > 9$).

The dimensionless distance $X=(x-x_{sc})/d_c$ defining the boundaries of the above sub-regions (I) to (III) was found to be virtually independent of the slope change (50º-18.6º and 50º-30º) and relative critical depth (d_c/h), as illustrated in Fig. 4.2. The dimensionless distance for the onset of region (IV) was also practically constant, regardless of the chute slope and relative critical depth, except for its lowest values ($d_c/h = 2.6$), for which a moderate increase occurs. An average value of $X = 9$ was obtained for $3.8 \leq d_c/h \leq 9.2$, representing fairly well most of the data for the onset of sub-region (IV). Hence, the total length of the chute under the influence

of the slope change (L_t) is approximately equal to $9.5d_c$, for the studied range of slope changes and relative critical depths ($-0.5 \leq X \leq 9$).

Even though most of the mean air concentration data ($3.8 \leq d_c/h \leq 9.2$) would be fairly well fitted by a unique function (Fig. 4.1), larger values were obtained for d_c/h = 2.6, corresponding to the smallest jetbox opening, hence to the smallest flow depth at the upstream end of the chute. Consequently, relatively larger extents of the self-aerated region were obtained in comparison with the other test runs, implying that flow conditions upstream of the slope change were likely closer to uniform flow. This reasoning seems to be strengthen by the analysis of Fig. 4.3, where the mean air concentration upstream of the slope change compares well with the uniform mean air concentration estimated from Takahashi and Ohtsu (2012), for identical chute slope (50º) and relative critical depth, namely for $d_c/h \leq 4.6$. For the highest values of the relative critical depth (d_c/h = 7.6, 9.2) on the 50º sloping chute, the mean air concentration is slightly lower than the uniform mean air concentration calculated from Takahashi and Ohtsu (2012). On the other hand, Fig. 4.3 shows that the mean air concentration at the downstream end of the 18.6º sloping chute remains considerably larger than that expected for uniform flow (regardless of d_c/h), which is judged to be due to the limited length of this measuring reach.

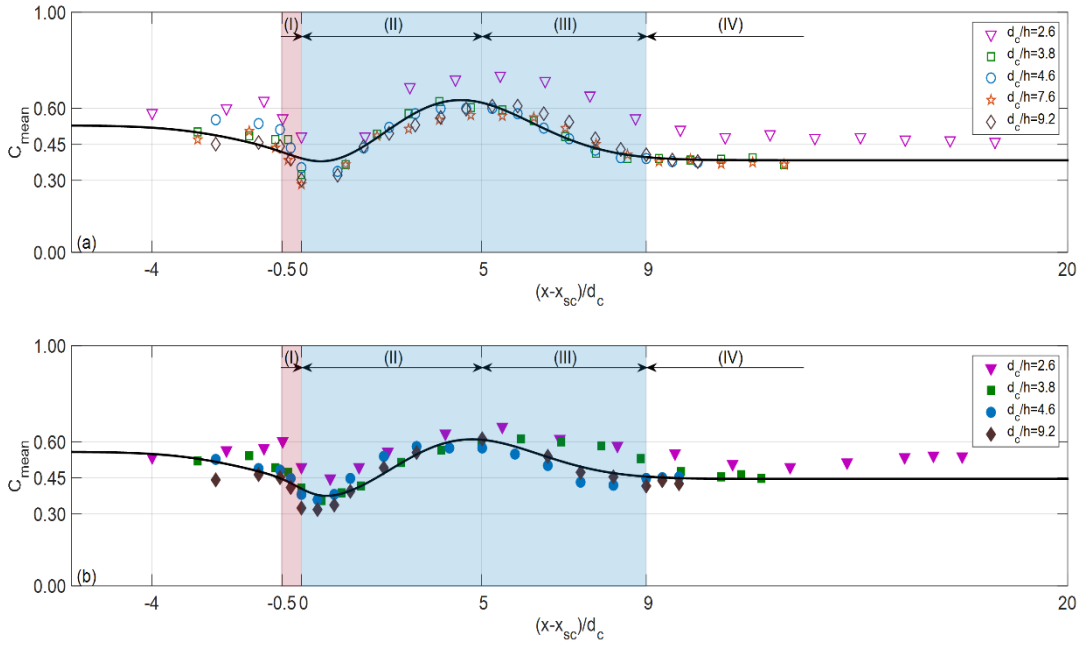

Figure 4.1 Streamwise development of the mean air concentration: a) 50º-18.6º ; b) 50º-30º, where x_{sc} is the distance of the slope change cross-section to the jetbox, measured along the chute (sketch in Fig. 3.4a); (-) global trend lines for $2.6 \leq d_c/h \leq 9.2$.

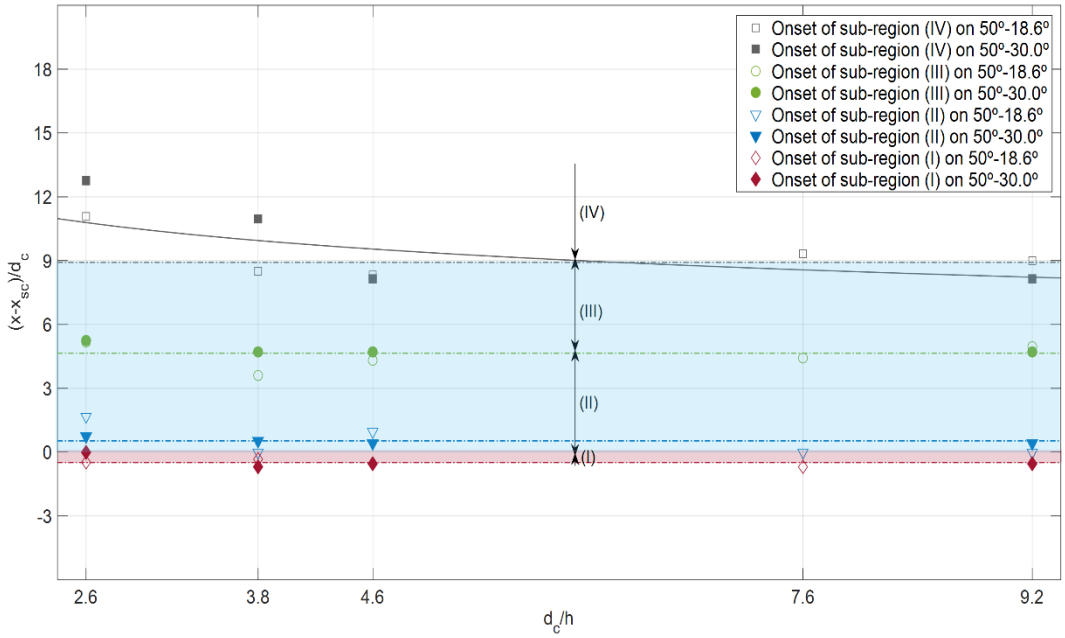

Figure 4.2 Dimensionless location of the onset of sub-regions (I), (II), (III) and (IV), in function of the relative critical depth: dashed lines are representative of the mean values of the onset of each sub-region, and shaded areas refer to the sub-regions under the influence of slope change; a trend line is also included for the onset of sub-region (IV).

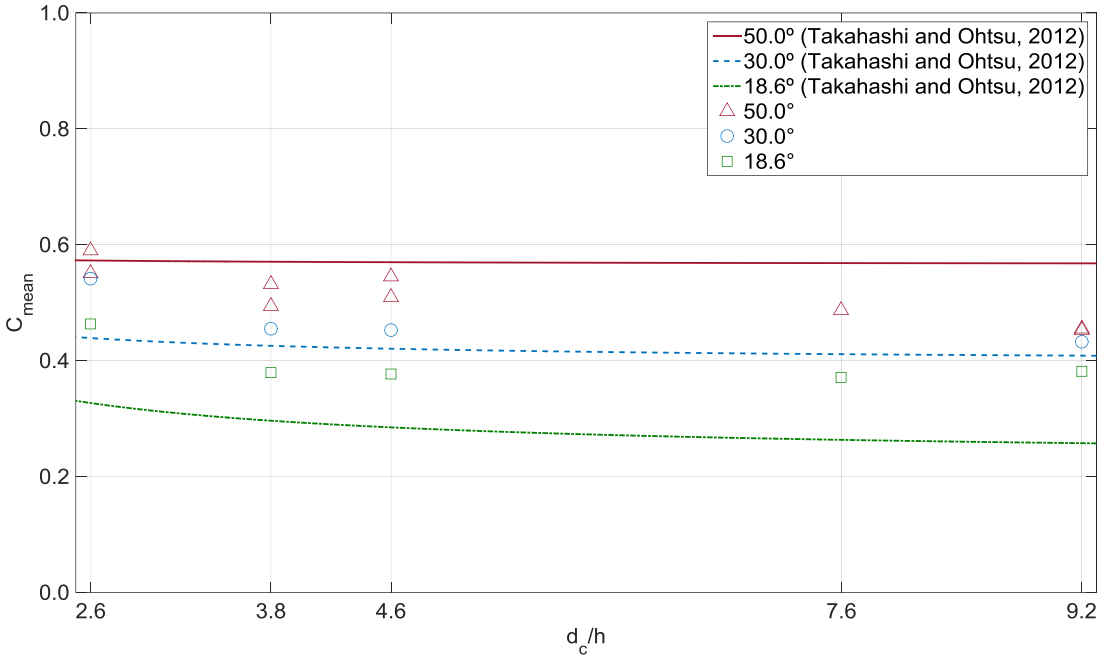

Figure 4.3 Mean air concentration upstream and far downstream of the slope change, in the absence of the slope change effect: comparison with the uniform mean air concentration calculated from Takahashi and Ohtsu (2012), for identical chute slopes.

In order to overcome the drawback related to the significant influence of the lower relative critical depth on the mean air concentration development, in comparison to larger relative critical depths, a mean air concentration ratio C_{mean} / $C_{mean\ ups}$ was introduced, where $C_{mean\ ups}$ is the mean air concentration upstream of, but not influenced by, the slope change (i.e., average of the C_{mean} at steps -09 and -05). The results are plotted in Fig. 4.4, along with empirical equations for the mean air concentration development in sub-regions (I), (II) and (III), under the influence of the slope change (Eq. 4.1). Even though some scatter is noticeable, particularly in sub-region (III) for d_c/h = 4.6, the overall curve fit is considered acceptable.

$$\frac{C_{mean}}{C_{mean\ ups}} = a\, e^{-\left(\frac{(X-b)}{c}\right)^2} \tag{4.1}$$

where $X=(x-x_{sc})/d_c$ and x_{sc} is the distance of the slope change cross-section to the jetbox, measured along the chute.

Table 4.1 Coefficients of Eq. (4.1)

Test No.	Slope configuration	d_c/h	Sub-region	a	b	c	R^2
1 to 5	50º-18.6º	2.6 to 9.2	(I)	0.94	-0.63	1.09	0.80
			(II) and (III)	1.19	4.95	6.33	0.79
6 to 9	50º-30.0º	2.6 to 9.2	(I)	0.98	-0.57	1.20	0.70
			(II) and (III)	1.15	5.48	8.06	0.75

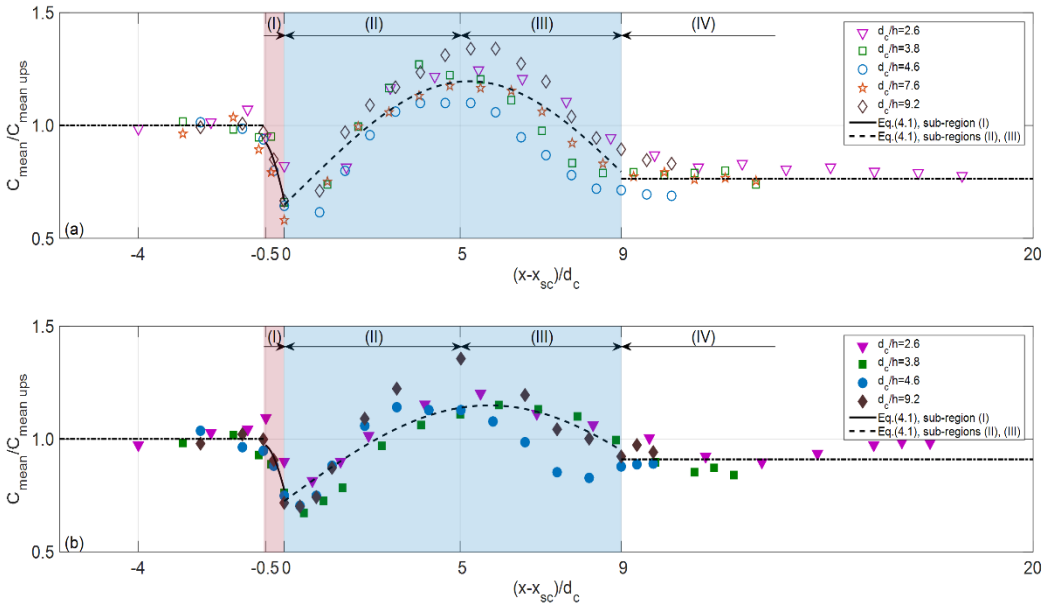

Figure 4.4 Streamwise development of the mean air concentration ratio: a) 50º-18.6º; b) 50º-30º, where x_{sc} is the distance of the slope change cross-section to the jetbox, measured along the chute. The horizontal lines represent the mean values upstream of sub-region (I), in gradually varied or quasi-uniform flow, and on sub-region (IV).

4.3. Air concentration distribution

Air concentration profiles were acquired in skimming flow upstream and downstream of the slope change, on both 50º-30º and 50º-18.6º configurations, for various flow rates and step heights (Table 3.1). In Figs. 4.5 and 4.6, dimensionless distributions are plotted for various cross-sections, for d_c/h = 4.6. The sub-regions previously referred in section 4.2 are also applied to the air concentration distribution.

The air concentration was found to decrease from the quasi-uniform flow values when approaching the slope change cross-section, for identical distance to the pseudo-bottom. Figures 4.5a and 4.6a show that for steps -09 and -05, the air concentration distribution is fairly similar to that predicted by the advection-diffusion model for the air bubbles proposed by Chanson (1997), on uniform flow on a similar sloping chute; identical conclusion cannot be drawn shortly downstream of the slope change, where a considerable decrease on the local air concentration occurs (particularly on steps -02 and -01), compared to the quasi-uniform profiles. This is expected to be due to the appearance of flow curvature (compression) slightly upstream of the slope change cross-section. The compression generates a non-hydrostatic pressure profile with extrema at the chute bottom. This reduces the volume of air bubbles and induces them to rise, thus decreasing locally the air concentration.

In sub-region (II), the air concentration generally increases shortly downstream of the slope change (steps +02 to +06 on 50º-18.6º, and steps +02 to +09 on 50º-30º, Figs. 4.5b and 4.6b), evolving from a S-shape distribution towards a more stretched profile, which is judged to be caused by the flow curvature reversal in the vicinity of the slope change (Fig. 3.9).

Further downstream, in sub-region (III), the air concentration decreases along the chute (Figs. 4.5c, 4.6c), until an approximately constant profile is reached, typical of a gradually varied flow as found in sub-region (IV) (Figs. 4.5d, 4.6d).

Therefore, the reach under the influence of slope change include steps -03 to +21 - on the 50˚-30 ˚, and steps -03 to +12 on the 50˚-18.6˚slope change configuration, as shown exemplary in Fig. 4.7.

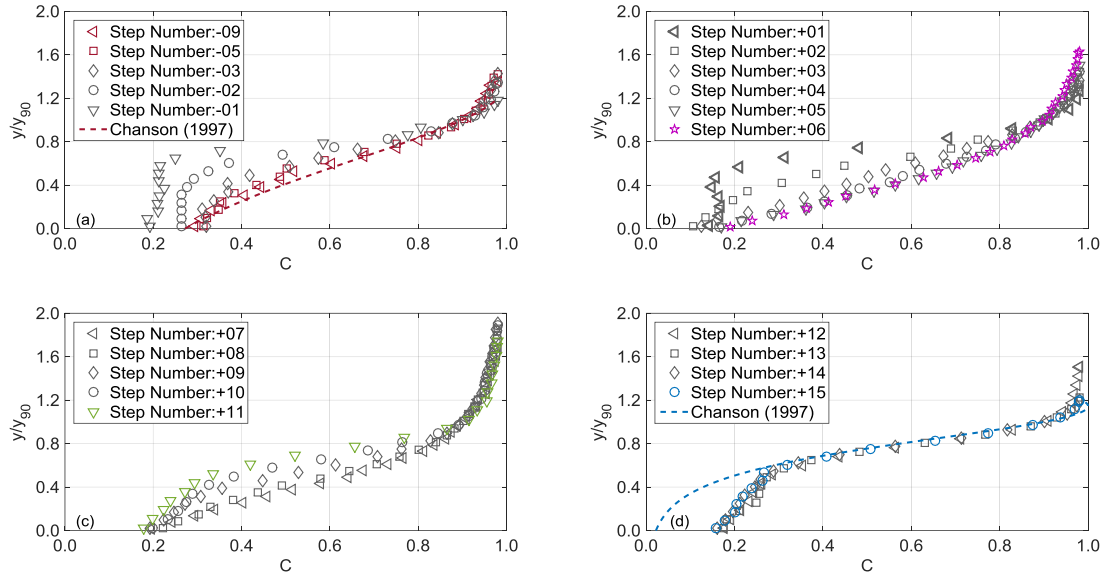

Figure 4.5 Air concentration distribution along the 50˚-18.6˚ slope change configuration, for d_c/h = 4.6 ("-" and "+" signs represent the steps upstream and downstream of the slope change cross-section, respectively, as per Fig. 3.9b): (a) sub-region (I); (b) sub-region (II); (c) sub-region (III); (d) sub-region (IV). "*C* theory" refers to the advection-diffusion model for the air bubbles (Chanson, 1997), where C_{mean} was estimated from Takahashi and Ohtsu (2012), for a similar sloping chute.

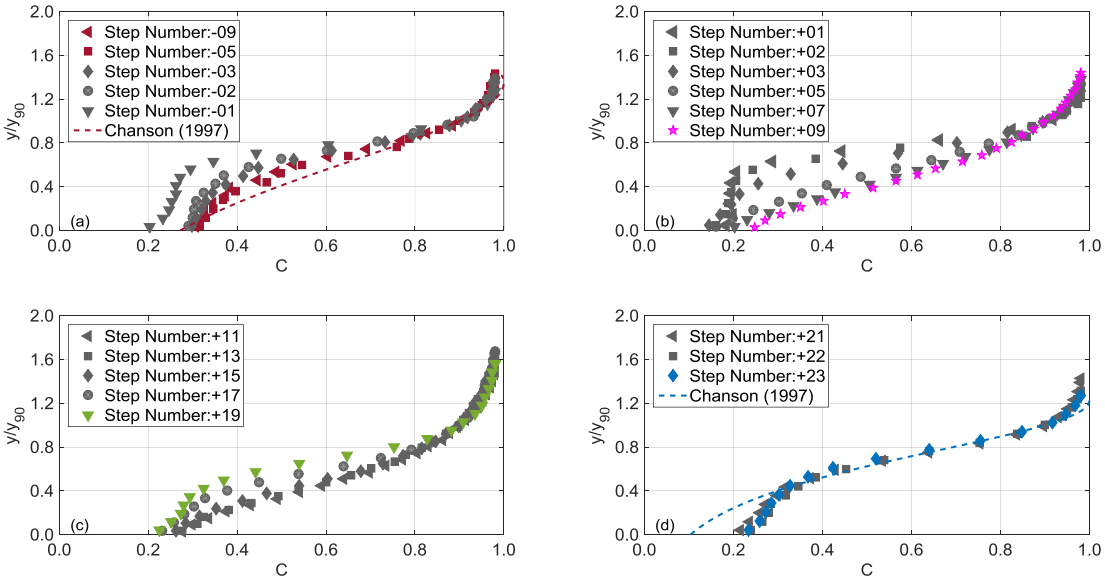

Figure 4.6 Air concentration distribution along the 50˚-30˚ slope change configuration, for d_c/h = 4.6 ("-" and "+" signs represent the steps upstream and downstream of the slope change cross-section, respectively, as per Fig. 3.9d): (a) sub-region (I); (b) sub-region (II); (c) sub-region (III); (d) sub-region (IV). "*C* theory" refers to the advection-diffusion model for the air bubbles (Chanson, 1997), where C_{mean} was estimated from Takahashi and Ohtsu (2012), for a similar sloping chute.

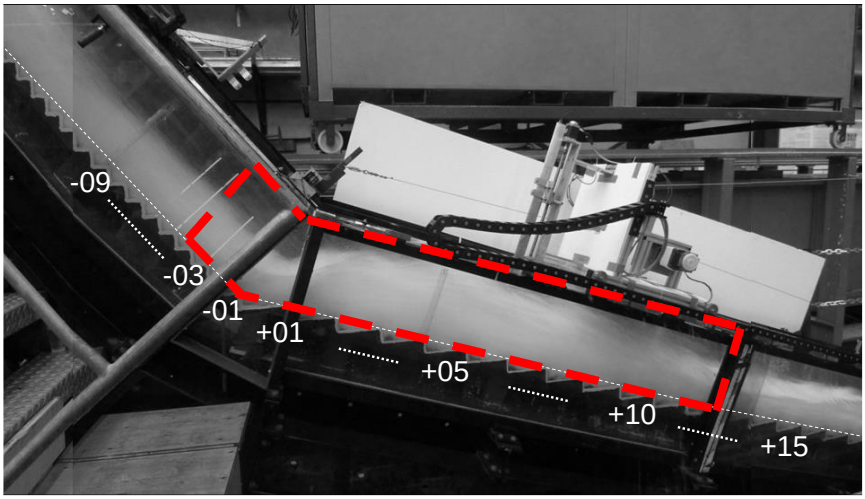

Figure 4.7 The reach under the influence of 50˚-18.6˚ slope change configuration, highlighted in red (--).

The reaches not affected by the slope change include steps -09 to -03 on the 50˚ upstream slope, +12 to +15 on the 18.6˚donwstream slope, and +21 to +23 on the 30˚ downstream slope (Figs. 4.5a, d and 4.6a, d). Along these regions, the air concentration distribution exhibits a S-shape profile similarly as obtained in other experimental studies on quasi-uniform or gradually varied flow on constant chute slopes, as well as described by the advection-diffusion model for the air bubbles (e.g., Chanson, 1997; Chanson and Toombes, 2002).

The comparison of such model with the experimental data seem to strengthen the conclusion that quasi-uniform flow was attained upstream of the slope change, whereas uniform flow conditions were not reached near the downstream end of the chute, particularly on the flatter one (Figs. 4.5d and 4.6d). In fact, markedly different values of the air concentration were obtained close to the pseudo-bottom.

Overall, a similar development of the air concentration profiles occur on the 50º-18.6º and 50º-30º slope changes, as shown in Figs. 4.5 and 4.6. However, the influence of the slope change is slightly more pronounced in the former situation, leading to reduced values of the air concentration close to the pseudo-bottom, in the vicinity of the slope change (e.g., steps -01, +01).

The above conclusions, drawn for d_c/h = 4.6, can also be extended for a broad range of relative critical depths, as illustrated in Fig. 4.8, for d_c/h ranging between 2.6 and 9.2 on the 50º-18.6º slope change configuration. With the exception of the profiles obtained for d_c/h = 2.6, a quite similar development of the air concentration distribution occurs on all sub-regions, irrespective of the relative critical depth.

For all discharges, a significant modification in the air concentration profiles occurs in the vicinity of the slope change (steps -01 and +01), with a significant decrease of the air concentration in the lower flow region (i.e., for y/Y_{90} < 0.5-0.6). The evolvement from a S-shape distribution towards a more stretched, linear profile, occurs on sub-region (II), for y/Y_{90} < 0.9 (step +05); in sub-region (III), the profiles tend to regain their original S-shape form (step +10); finally the consolidation of the S-shape profile takes place in sub-region (IV) (step +15).

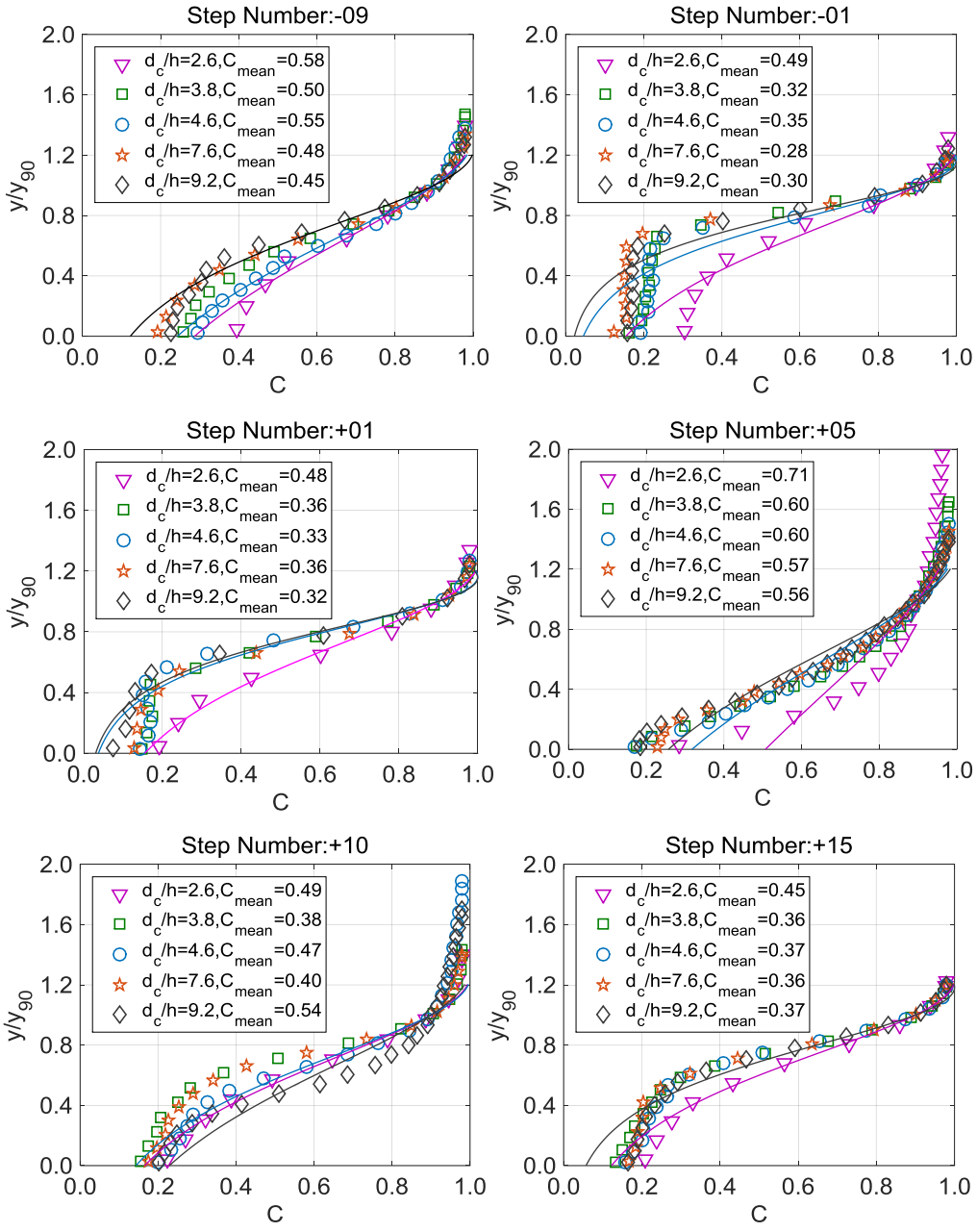

Figure 4.8 Air concentration distribution on typical cross-sections along the 50˚-18.6˚ slope change configuration, for various relative critical depths ("-" and "+" signs represent the steps upstream and downstream of the slope change cross-section, respectively, as per Fig. 3.9b); the plotted curves (-), (-),

(-) refer to the advection-diffusion model for the air bubbles (Chanson, 1997), for values of C_{mean} equal to those obtained experimentally in the present study for d_c/h = 2.6, 4.6, and 9.2, respectively.

4.4. Pseudo-bottom air concentration

The streamwise development of the air concentration close to the pseudo-bottom (at about 0.005 m from the step edges) follows a trend similar to that observed for the mean air concentration (section 4.2, Fig. 4.1), as illustrated in Fig. 4.9. It decreases in the vicinity of the slope change cross-section, exhibits a significant increase shortly downstream, reaching a maximum (at $X \approx 5$), and subsequently decreases (up to $X \approx 9$), until an almost constant value is reached.

Slightly smaller values of the pseudo-bottom air concentration were measured for the flatter chute, as a result of the increased de-aeration. However, for both slope changes, the minimum value of the pseudo-bottom air concentration is larger than 10%, which is judged to be high enough to assure safety against cavitation damage on the step surfaces (e.g., Peterka, 1953, Matos et al., 2000, Boes and Minor, 2000). In Frizell et al. (2013; 2015), it is shown that cavitation damage might occur on high velocity flow over stepped chutes, in the absence of flow aeration, whereas relevant successful prototype experience has been reported for high velocity flows with significant flow aeration (e.g., Guo et al., 2003; Chanson, 2015). It was found that with increasing the slope change magnitude from $\Delta\Theta$=20˚ *to* $\Delta\Theta$=31.4˚, de-aeration increased 28%.

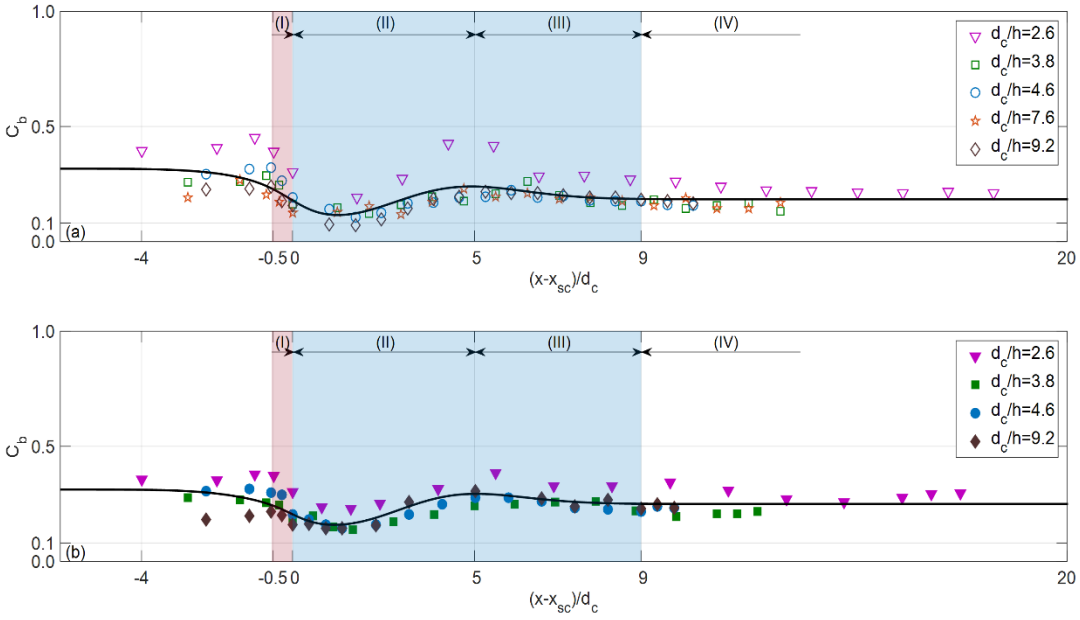

Figure 4.9 Streamwise development of the pseudo-bottom air concentration: a) 50º-18.6º; b) 50º-30º. (-) global trend line for $2.6 \leq d_c/h \leq 9.2$.

4.5. Air-phase frequency

The dimensionless air-phase frequency fd_c/V_c can be expressed as a function of y/Y_{90}, where f is the average number of detected air bubbles per second, d_c the critical flow depth and $V_c = \sqrt{g d_c}$ the critical flow velocity. Felder and Chanson (2009b; 2011a) and Pfister and Hager (2011) showed that on constant sloping stepped spillways, the number of entrained air bubbles increases in the streamwise direction, for a given y/Y_{90}. In Pfister and Hager (2011) it is also shown that close to the inception point of air entrainment, the maximum value of fd_c/V_c is located near the flow surface, while it is located close to the pseudo-bottom far downstream of the inception point. Also maximum air-phase frequency was observed in the intermediate flow region for void fractions between 35% and 65% (Felder and Chanson, 2011a). According to Chanson (2002), the relationship between local air concentration and dimensionless air-phase frequency presents some self-similarity, see Eq. (2.3).

In Figs. 4.10 and 4.11, dimensionless air-phase frequency distributions fd_c/V_c are presented at various cross-sections along the 50º-30º and 50º-18.6º chute configurations as a function of y/Y_{90}, for d_c/h = 4.6. The sub-regions previously referred for the mean air concentration and air concentration profiles (sections 4.2 and 4.3) may also be applied to the dimensionless air-phase frequency distribution.

Sufficiently upstream of slope change (steps -09 and -05 of Figs. 4.10a and 4.11a), the shape of the fd_c/V_c profiles are similar to those found in quasi-uniform flow on 50º steeply sloping chutes, namely by Pfister and Hager (2011), where the maximum cross-sectional value of fd_c/V_c is located near the pseudo-bottom ($y/Y_{90} \approx$ 0.2-0.3).

In the vicinity of the slope change cross-section (e.g., steps -01 and +01, Figs. 4.10a, b and 4.11a, b), a significant change occurs in the fd_c/V_c profiles; the maximum cross-sectional value of fd_c/V_c increases and its location moves towards the free surface ($y/Y_{90} \approx$ 0.6-0.7). Shortly downstream of the slope change, in sub-region (II), the shape of the profiles tend to that observed far upstream of slope change, and the maximum cross-sectional value of fd_c/V_c decreases and its location moves towards the pseudo-bottom ($y/Y_{90} \approx$ 0.2) (Figs. 4.10b and 4.11b).

Subsequently, in sub-region (III) (Figs. 4.10c and 4.11c) the fd_c/V_c profiles continue to readjust until their shape approach that corresponding to the gradually or quasi-uniform flow on the downstream flatter slope (Figs. 4.10d and 4.11d). Therein, the maximum cross-sectional value of fd_c/V_c is located at $y/Y_{90} \approx$ 0.7, on the 18.6º slope, and at $y/Y_{90} \approx$ 0.5, on the 30º slope. In the reaches not affected by the slope change, hence in gradually varied or quasi-uniform flow, the dimensionless air-phase frequency distribution seems to be influenced by the chute slope.

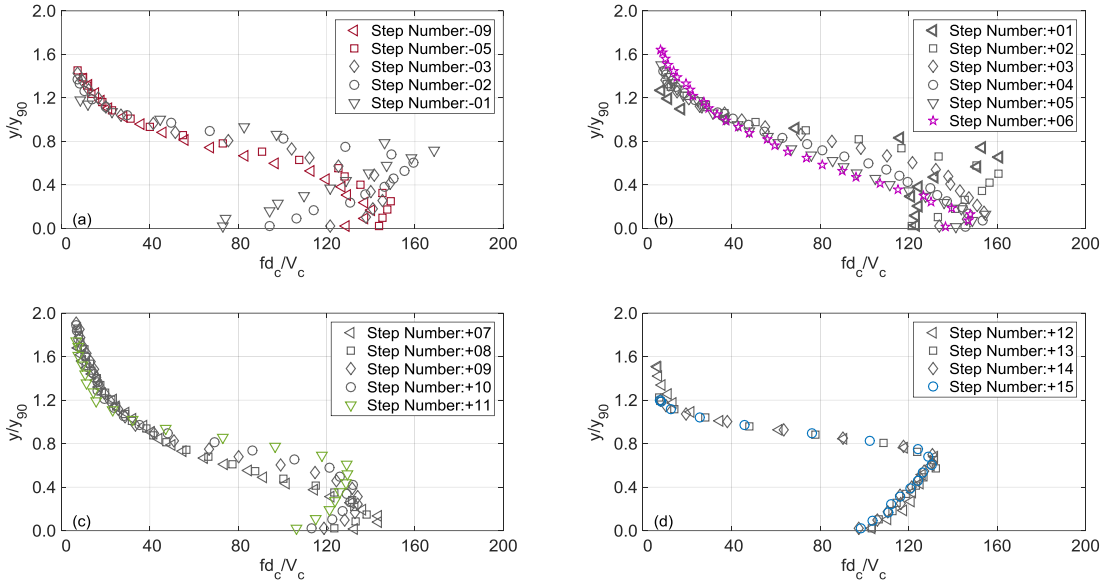

Figure 4.10 Dimensionless air-phase frequency distribution along the 50˚-18.6˚ slope change configuration, for d_c/h = 4.6 ("-" and "+" signs represent the steps upstream and downstream of the slope change cross-section, respectively, as per Fig. 3.9b): (a) sub-region (I); (b) sub-region (II); (c) sub-region (III); (d) sub-region (IV).

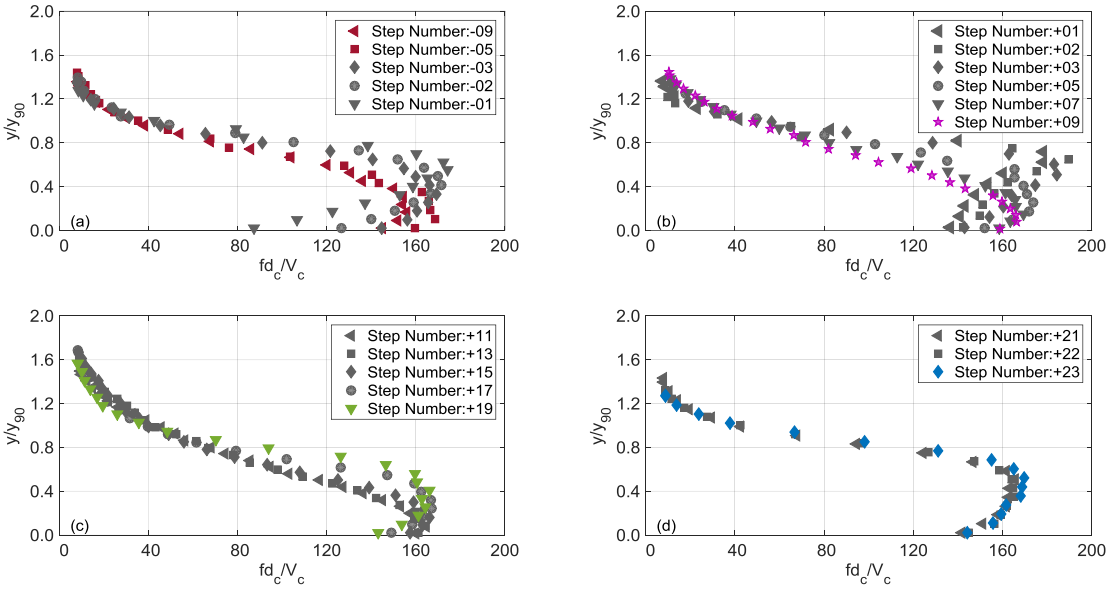

Figure 4.11 Dimensionless air-phase frequency distribution along the 50˚-30˚ slope change configuration, for d_c/h = 4.6 ("-" and "+" signs represent the steps upstream and downstream of the slope change cross-section, respectively, as per Fig. 3.9d): (a) sub-region (I); (b) sub-region (II); (c) sub-region (III); (d) sub-region (IV).

Overall, the magnitude of the slope change has a relatively small but non-negligible influence on the development of the dimensionless air-phase frequency distribution along the reach under the influence of the slope change. In fact, smaller values of the dimensionless air-phase frequency can be observed closer to the pseudo-bottom on the 18.6º than on the 30°

sloping chute, namely in sub-regions (II) (e.g., steps +01 to +03 of Figs. 4.10b and 4.11b) and (III) (Figs. 4.10c and 4.11c).

The above conclusions, drawn for d_c/h = 4.6, may also apply for a broad range relative critical depths, as shown in Fig. 4.12, for d_c/h ranging between 2.6 and 9.2 on the 50º-18.6 slope change configuration. A similar development of the air dimensionless air-phase frequency distribution occurs on all sub-regions, irrespective of the relative critical depth.

For all discharges, a significant modification in the dimensionless air-phase frequency occurs in the vicinity of the slope change (steps -01 and +01), with a significant increase in the location of the maximum cross-sectional value of fd_c/V_c, varying from $y/Y_{90} \approx 0.2$, on step -09, to $y/Y_{90} \approx 0.6$-0.8 on steps -01 to +01.

Downstream of the slope change, near the peak value of the mean air concentration, the location of the maximum cross-sectional value of fd_c/V_c moves towards the pseudo-bottom ($y/Y_{90} \approx 0.1$-0.3, on step +05). Further downstream, in sub-region (III), the location of the maximum dimensionless air-phase frequency distribution varies between $y/Y_{90} \approx 0.3$ and 0.6 (step +10), depending on the relative critical depth. The influence of d_c/h on the location of the maximum cross-sectional value of fd_c/V_c becomes small on sub-region (IV), not affected by the slope change, where $y/Y_{90} \approx 0.6$-07 (step +15).

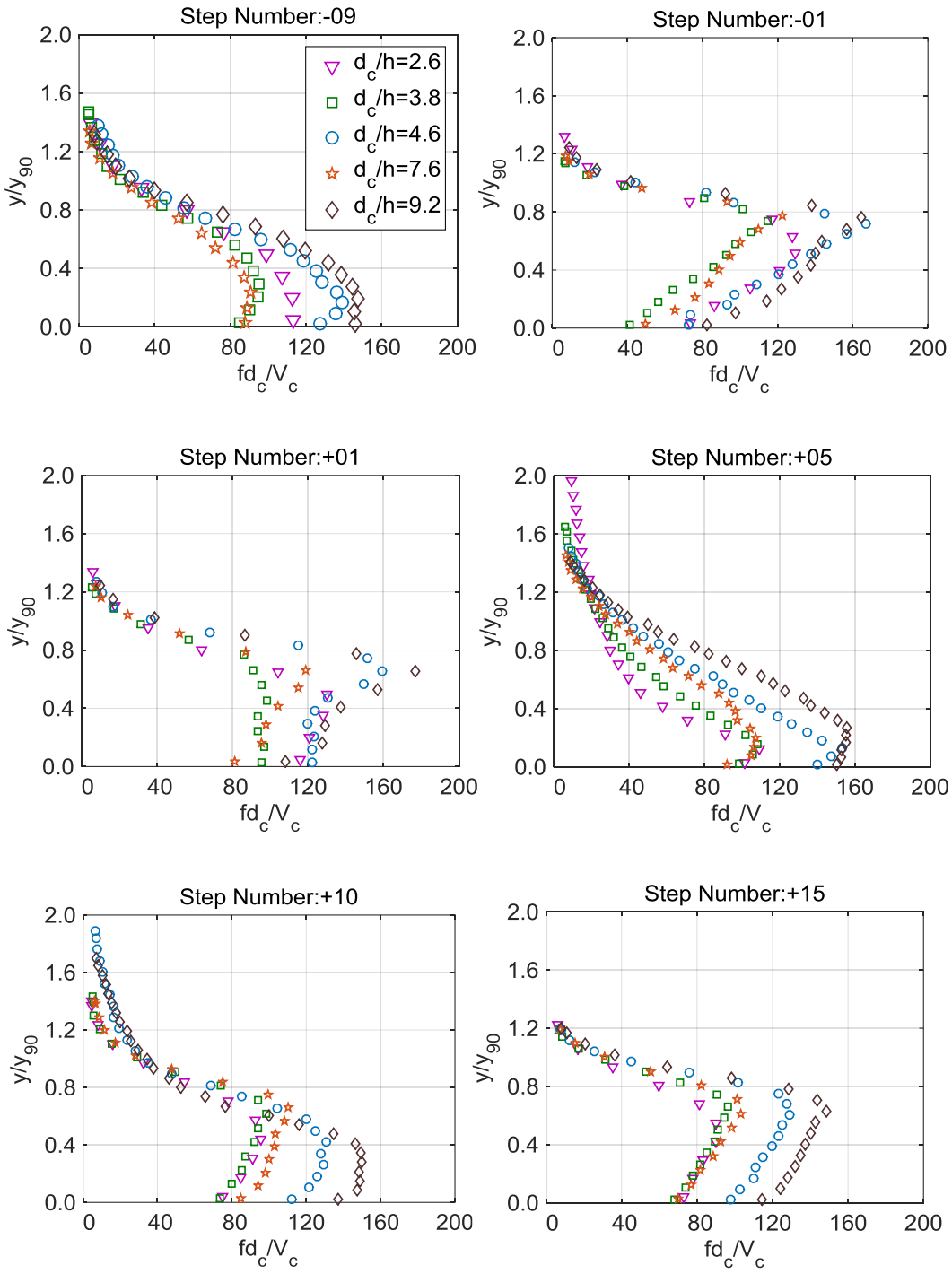

Figure 4. 12 Dimensionless air-phase frequency distribution on typical cross-sections along the 50˚-18.6˚ slope change configuration, for various relative critical depths ("-" and "+" signs represent the steps upstream and downstream of the slope change cross-section, respectively, as per Fig. 3.9b).

In Figs. 4.13 and 4.14, dimensionless air-phase frequency distributions fd_c/V_c are presented for various cross-sections along the 50º-30º and 50º-18.6º chute configurations as a function of the local air concentration, for d_c/h = 4.6. The present data indicate that the maximum air-phase frequency occurs approximately for C equal to 30-40%, regardless of the

slope change. Slighter sharper profiles are noticeable for the 50º sloping chute, when compared to those found on the 18.6º and 30º slopes. The data fd_c/V_c versus C show a skewed distribution as has been reported in the literature rather than an agreement with Eq. (2.3).

The results are within the range of those previously reported on skimming flow over stepped spillways: Toombes (2002) observed that the maximum dimensionless air-phase frequency occurs for an air concentration slightly lower than 50%; Bung (2011) found maximum dimensionless air-phase frequency for C_{mean} = 45% and 43%, for 18.4º and 26.6º sloping chutes, respectively; and the results of Felder and Chanson (2011a), on a 26.6º sloping chute, indicated a maximum dimensionless air-phase frequency for air concentrations between 35% and 65%.

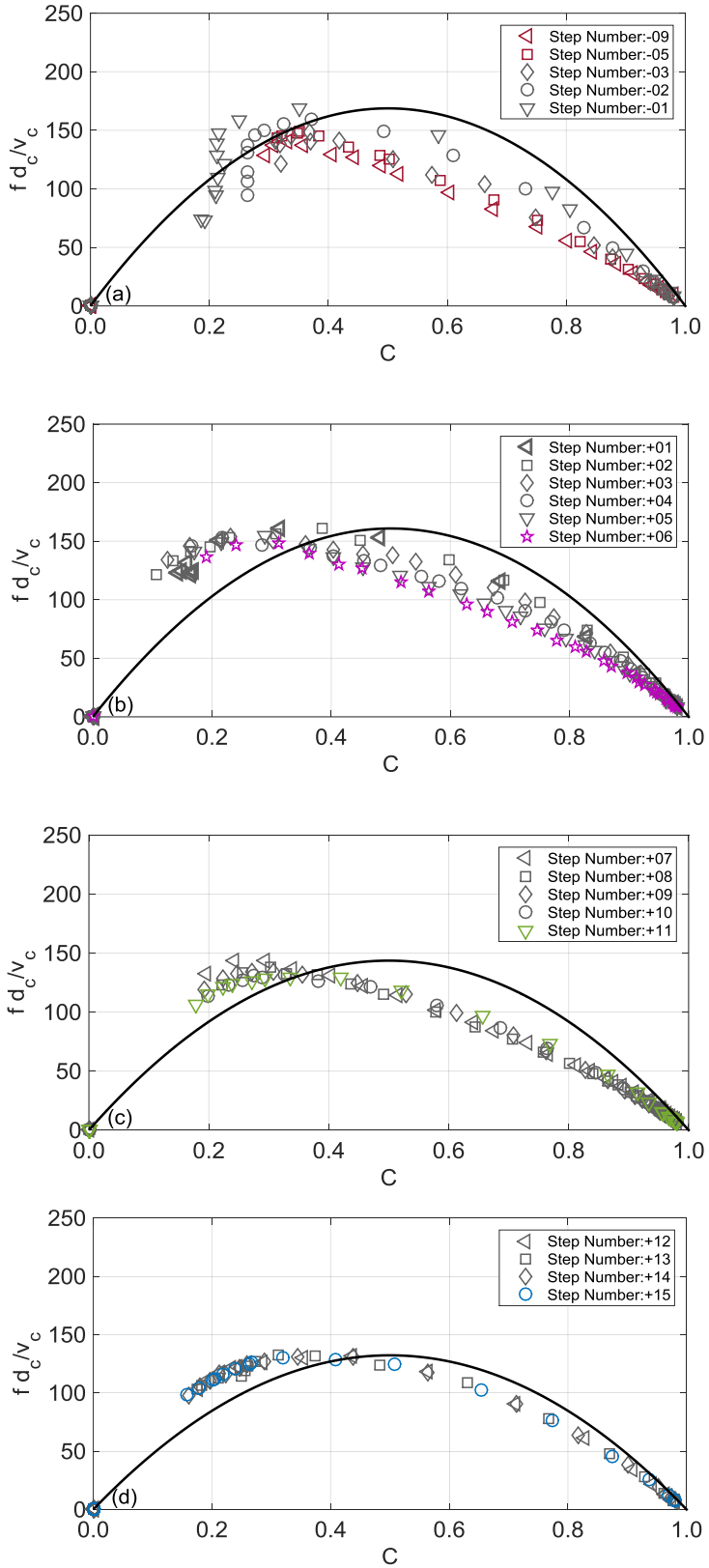

Figure 4.13 Dimensionless air-phase frequency versus local air concentration, comparison with parabolic law (Eq. 2.3) along the 50˚-18.6˚ slope change configuration, for d_c/h = 4.6 ("-" and "+" signs represent the steps upstream and downstream of the slope change cross-section, respectively, as per Fig. 3.9b): (a) sub-region (I); (b) sub-region (II); (c) sub-region (III); (d) sub-region (IV).

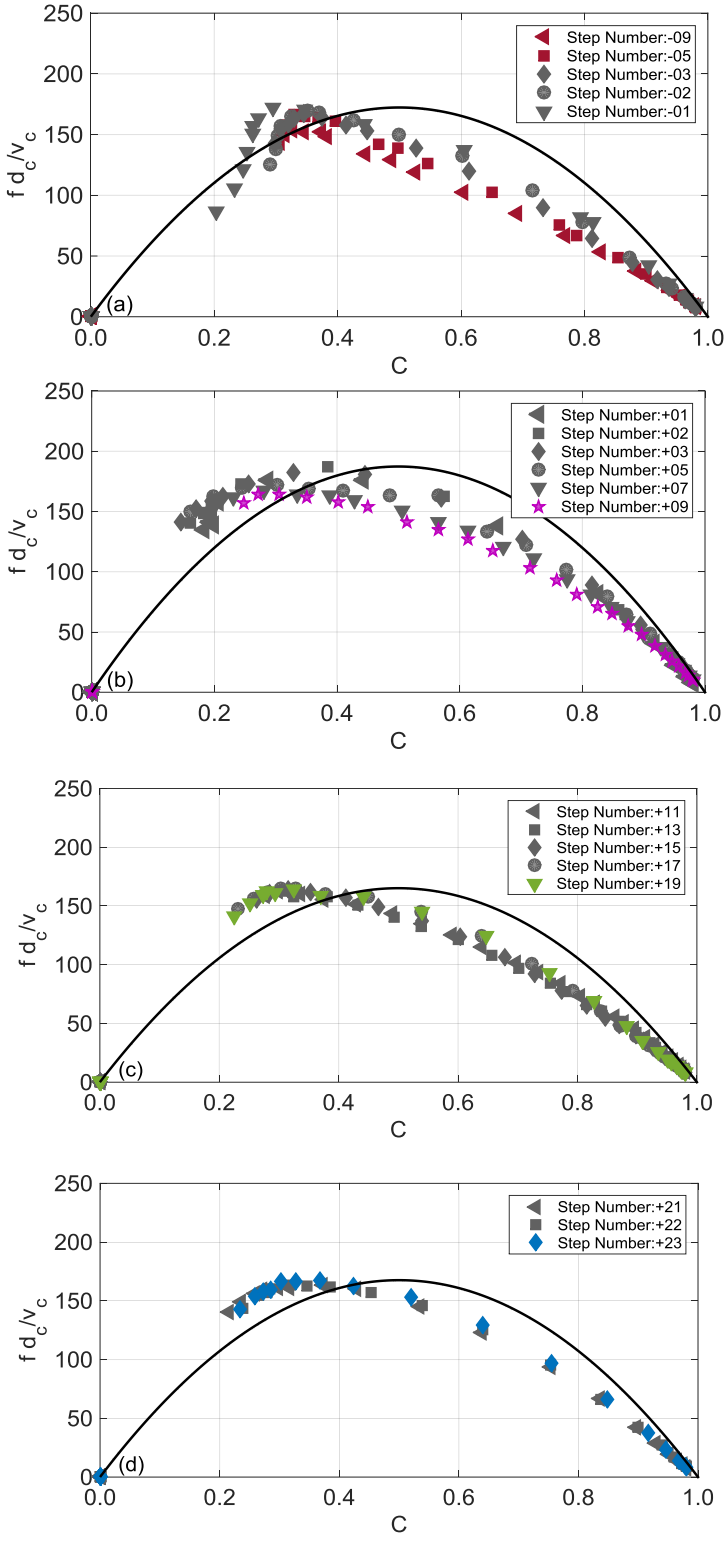

Figure 4.14 Dimensionless air-phase frequency versus local air concentration, comparison with parabolic law (Eq. 2.3) along the 50˚-30˚ slope change configuration, for d_c/h = 4.6 ("-" and "+" signs represent the steps upstream and downstream of the slope change cross-section, respectively, as per Fig. 3.9d): (a) sub-region (I); (b) sub-region (II); (c) sub-region (III); (d) sub-region (IV).

4.6. Characteristic flow and equivalent clear water depths

Figures 4.15, 4.16, and 4.17, show the streamwise development of the characteristic flow depths Y_{90}, Y_{95}, Y_{99} along the 50º-30º and 50º-18.6º sloping chutes. A typical air concentration contour plot is included in Fig. 4.18.

In contrast with the results found for the mean air concentration, the dimensionless characteristic flow depths Y_{90}, Y_{95}, Y_{99} remain practically constant in sub-region (I), when approaching the slope change cross-section, irrespective of the relative critical depth (e.g., $y_{90}/d_c \approx 0.5$ as per Fig. 4.15). A decrease in such characteristic flow depths occur in a very limited reach immediately downstream of the slope change cross-section (i.e., between steps -01 and +01), followed by a considerable increase until a maximum value is reached, at the downstream end of sub-region (II); further downstream the characteristic flow depths decrease until a quasi-constant value is reached, at the downstream end of sub-region (III). Even though the data collapse reasonably well in a single curve for Y_{90}, the characteristic flow depths Y_{95} and Y_{99} are considerably larger on the 18.6º sloping chute for the lowest relative critical depth ($d_c/h = 2.6$); for such conditions, the effect of the slope change becomes more pronounced on Y_{95} and Y_{99}.

Empirical formulae have been fitted to the experimental data for sub-regions (II) and (III) (Eq. 4.2 and Table 4.2); the curves are also plotted in Figs. 4.15 to 4.17, along with the experimental data. In general, the curve fit is judged satisfactory for predicting the characteristic flow depths along the downstream reach under the influence of the slope change.

$$\frac{Y_\psi}{d_c} = a\, e^{-\left(\frac{(X-b)}{c}\right)^2} \qquad (4.2)$$

where $X=(x-x_{sc})/d_c$ and x_{sc} is the distance of the slope change cross-section to the jetbox, measured along the chute.

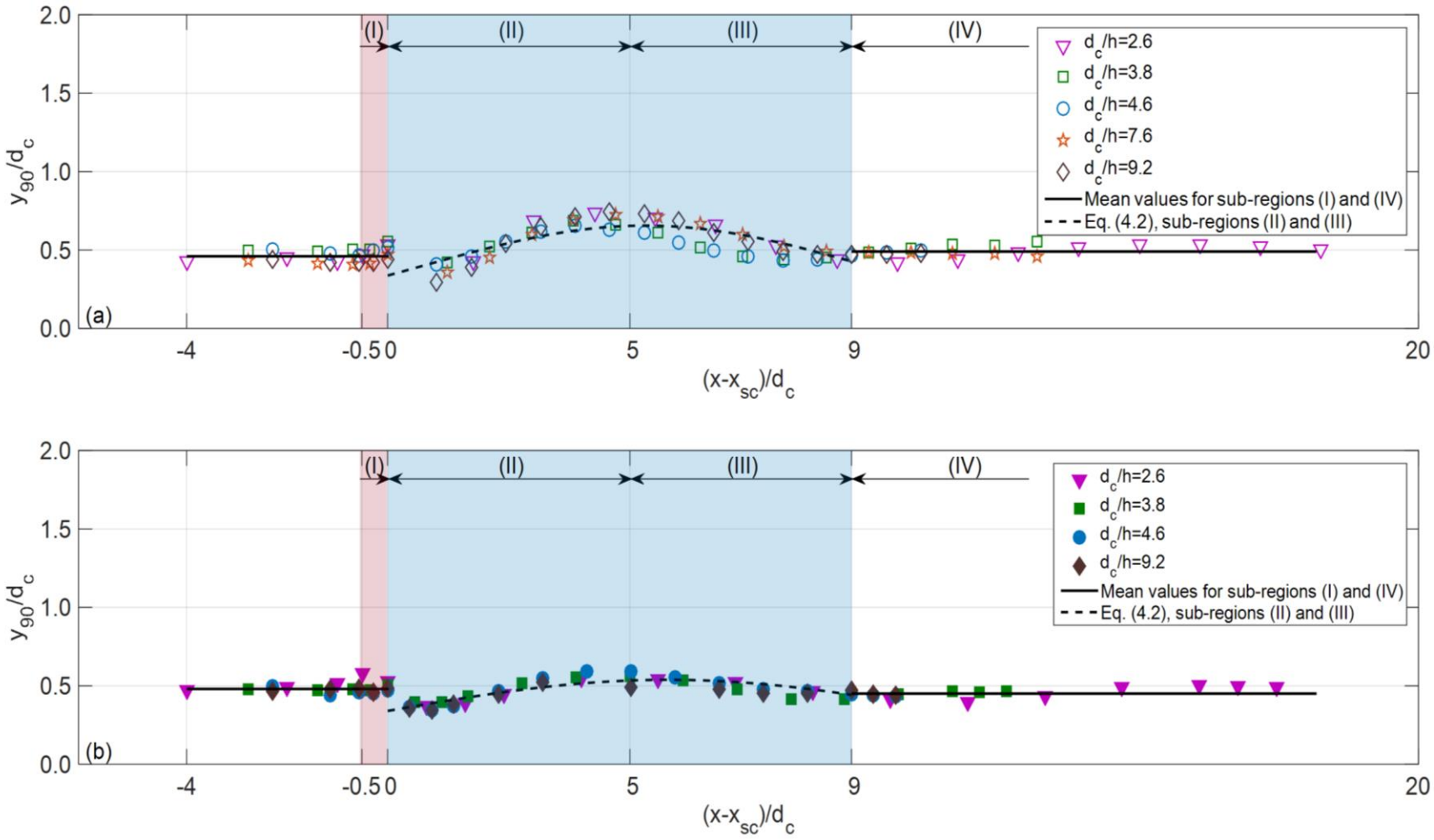

Figure 4.15 Streamwise development of the dimensionless characteristic flow depth Y_{90}/d_c: a) 50º-18.6º; b) 50º-30º.

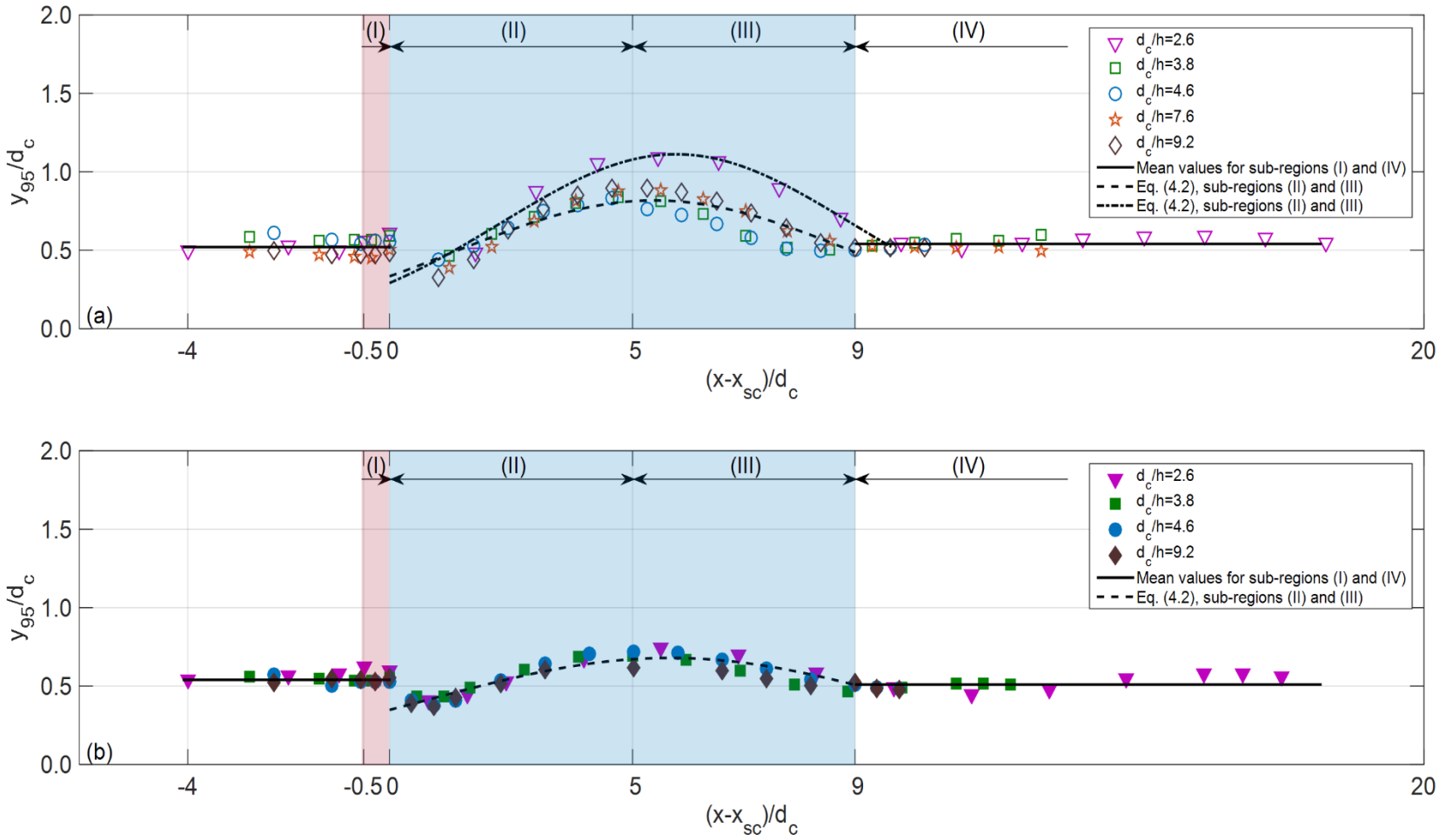

Figure 4.16 Streamwise development of the dimensionless characteristic flow depth Y_{95}/d_c: a) 50º-18.6º; b) 50º-30º.

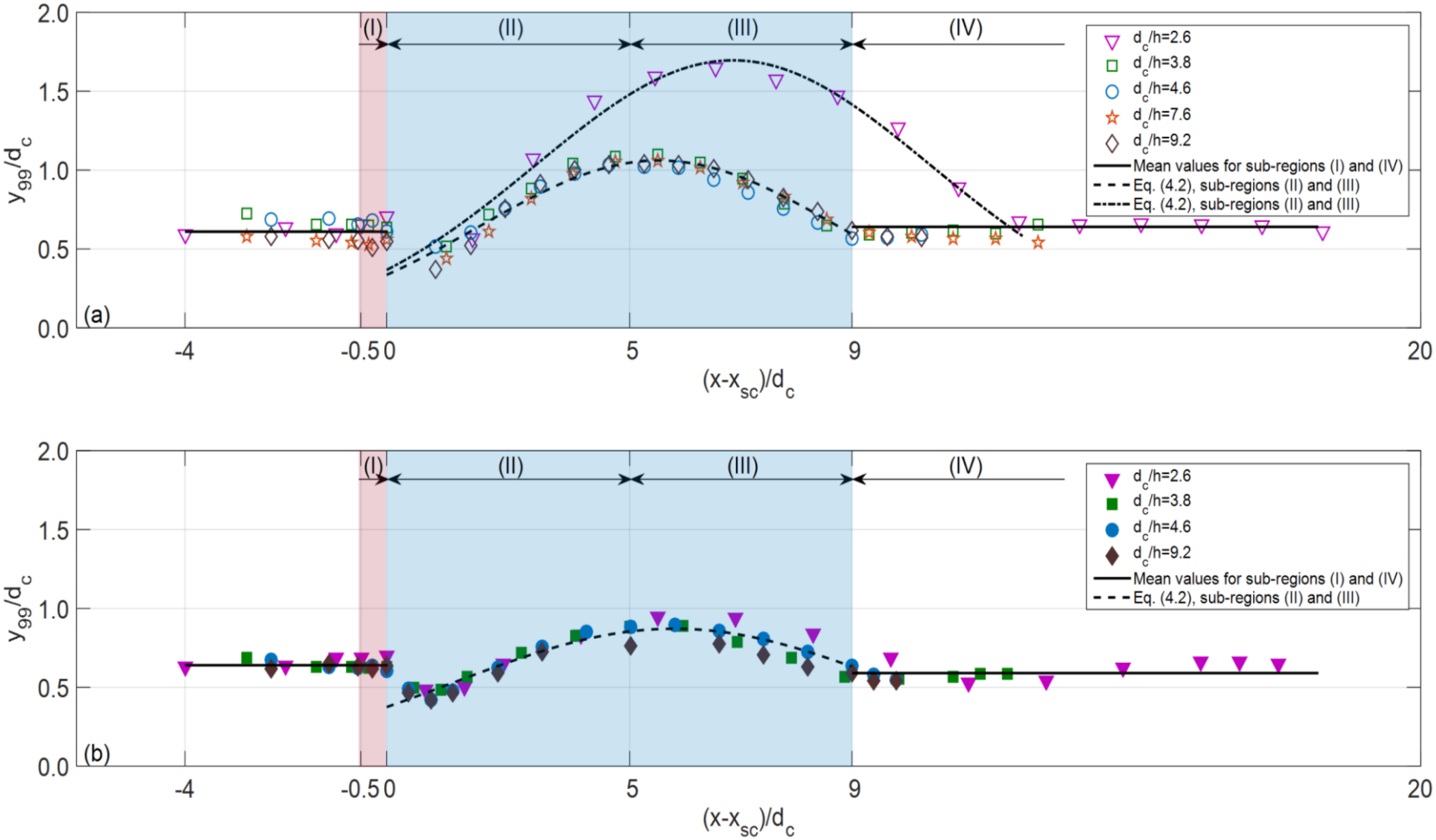

Figure 4.17 Streamwise development of the dimensionless characteristic flow depth Y_{99}/d_c: a) 50º-18.6º; b) 50º-30º.

Table 4.2 Coefficients of Eq. (4.2) for Y_{90}/d_c, Y_{95}/d_c and Y_{99}/d_c in sub-regions (II) and (III)

	Test No.	Slope configuration	d_c/h	a	b	c	R^2
Y_ψ (ψ = 90)	1 to 5	50º-18.6º	2.6 to 9.2	0.65	4.99	6.12	0.71
	6 to 9	50º-30.0º	2.6 to 9.2	0.53	5.44	8.02	0.80
Y_ψ (ψ = 95)	1 to 5	50º-18.6º	2.6	1.11	5.53	4.78	0.95
			3.8 to 9.2	0.81	5.11	5.40	0.80
	6 to 9	50º-30.0º	2.6 to 9.2	0.67	5.42	6.63	0.85
Y_ψ (ψ = 99)	1 to 5	50º-18.6º	2.6	1.69	6.70	5.41	0.94
			3.8 to 9.2	1.06	5.26	4.91	0.93
	6 to 9	50º-30.0º	2.6 to 9.2	0.87	5.56	6.05	0.88

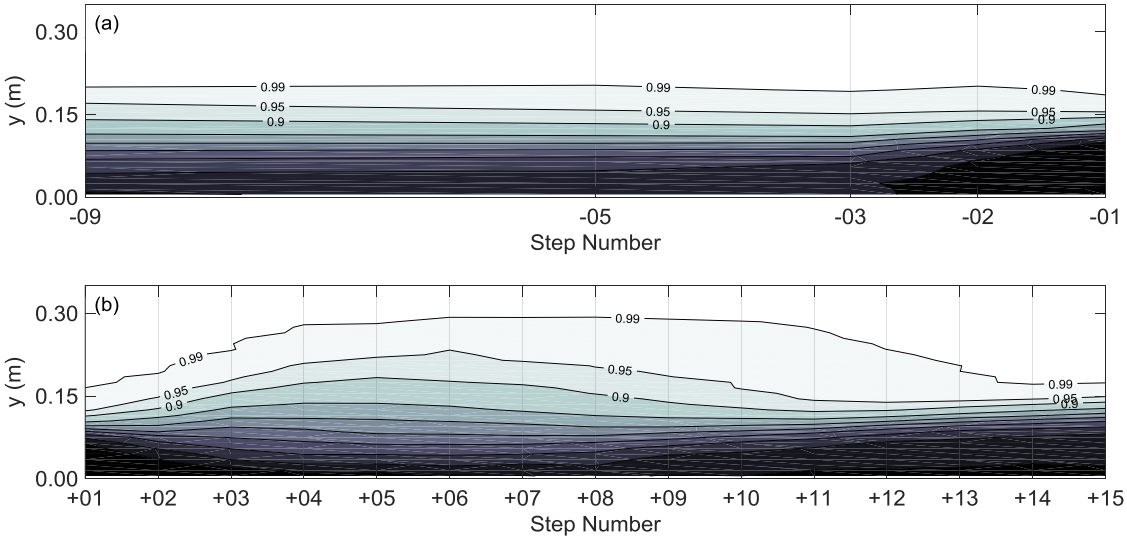

Figure 4.18 Typical air concentration contour plot: a) upstream the slope change; b) downstream of the slope change; test number 3, as per Table 3.1 (Θ_1 = 50º; Θ_2 = 18.6º; d_c/h = 4.6; R_e = 4.6×10^6).

In Fig. 4.19, the maximum dimensionless characteristic flow depths are presented as a function of the relative critical depth, for all experimental tests (Table 3.1). For 3.8 ≤ d_c/h ≤ 9.2, they are practically independent of the d_c/h; the maximum bulked flow depth attained in sub-region (III) is in general lower than or approximately equal to the critical depth, but for d_c/h = 2.6, on the 50º-18.6º slope change configuration, where considerable larger values were obtained, Y_{99max}/d_c ≈ 1.6. It was found that with increasing the slope change magnitude from $\Delta\Theta$=20˚ *to* $\Delta\Theta$=31.4˚, the maximum flow depth Y_{99max}/d_c increased 25%.

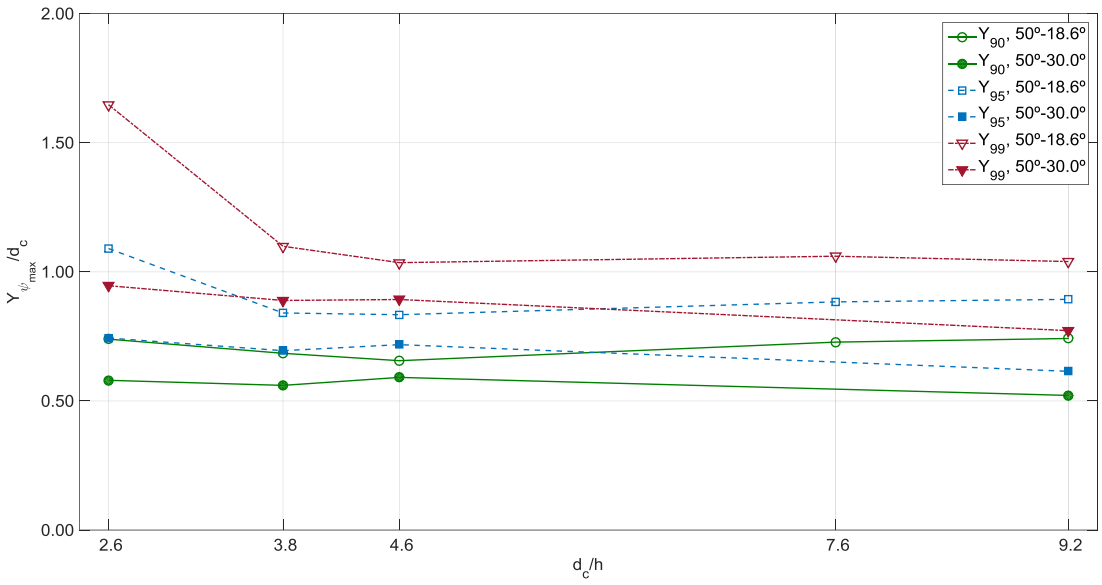

Figure 4.19 Maximum dimensionless characteristic flow depths obtained on the reach under the influence of the slope change, versus the relative critical depth.

The streamwise development of the dimensionless equivalent clear water depth (d_w/d_c) is illustrated in Fig. 4.20, along with horizontal lines representing the mean value of d_w/d_c in the reaches not influenced by the slope change (d_w/d_c = 0.23, 0.23 and 0.29 for 50º, 30º and 18.6º sloping chutes, respectively), as well as d_w/d_c obtained from Boes and Hager (2003a), for uniform skimming flow over stepped chutes (d_w/d_c = 0.23, 0.27 and 0.31 for 50º, 30º and 18.6º sloping chutes, respectively).

A quite good agreement was obtained using the formula of Boes and Hager (2003a) for the 50º sloping chute, whereas in sub-region (IV), downstream of the slope change, it overestimates the mean value calculated from the respective experimental data, namely for 30º and 18.6º sloping chutes. These results may be expected considering that quasi-uniform flow conditions were attained mostly on the 50º sloping chute, upstream of the slope change.

A noticeable increase of d_w/d_c is observed in the vicinity of the slope change cross-section, in sub-region (I), which is judged to be due to the flow curvature initiated slightly upstream of the slope change cross-section (Fig. 4.18), leading to an increased pressure close to the pseudo-bottom. However, d_w/d_c does not vary significantly along sub-regions (II) to (III), for a given relative critical depth.

In the sub-regions influenced by the slope change, d_w was estimated from Eq. (2.5), where Eq. (4.1) (along with Table 4.1) and Eq. (4.2) (along with Table 4.2) were applied for estimating C_{mean} and Y_{90}, respectively. The application of the above formulae was found to provide a reasonable estimate of the increasing and subsequently quasi-constant trends of d_w/d_c along the reach under the influence of the slope change.

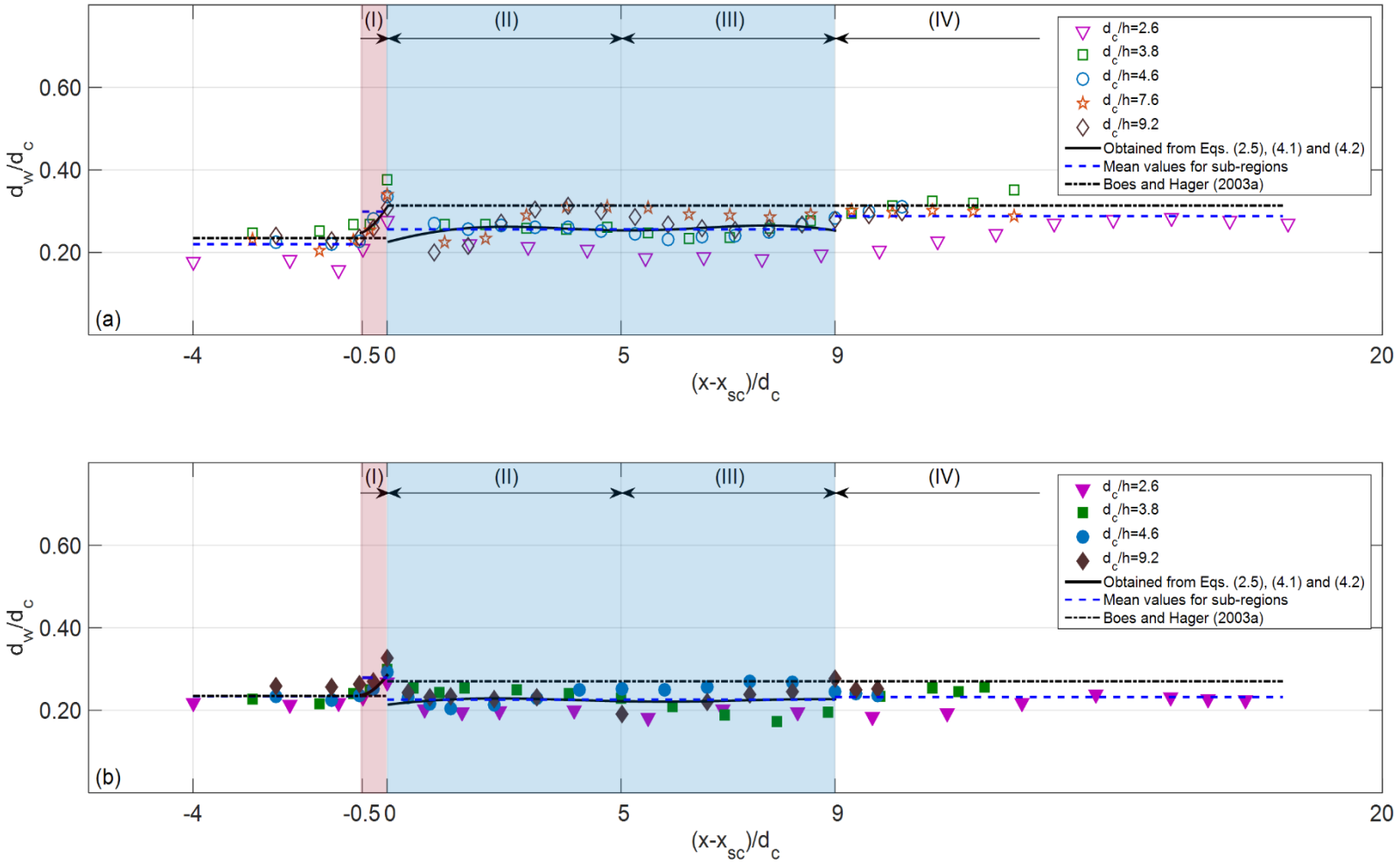

Figure 4.20 Streamwise development of the dimensionless equivalent clear water depth, a) 50º-18.6º and b) 50º-30º.

4.7. Conclusions

The effect of an abrupt slope change on the air entrainment and flow bulking in skimming flow on stepped chutes is analysed in the present chapter. Experimental tests were conducted at various cross-sections on a relatively large scale model of 50º-30º and 50º-18.6º abrupt slope changes, assembled at the Laboratory of Hydraulic Constructions (LCH) of EPFL. Several sets of experiments were carried out for different step heights, approach flow depths and Froude numbers. Empirical equations were developed for estimating the mean air concentration and characteristic flow depths along the reach under the influence of the slope change for $2.6 \leq d_o/h \leq 9.2$. The tests were conducted in skimming flow, so that all observations described herein strictly apply to this regime. The following results and conclusions may be drawn:

- Abrupt slope change on stepped chutes have a major effect on the air entrainment and flow bulking in the vicinity of the slope change. The magnitude of the tested slope change has a relatively small but non-negligible influence on the air-water flow properties along the reach under the influence of the slope change.

- In general, the reach of influence of the slope change is initiated shortly upstream of its cross-section ($X=(x-x_{sc})/d_c \approx -0.5$), and extends further downstream to $X \approx 9$, for practically all studied range of slope changes and relative critical depths. Hence, for practical purposes, the total length of the chute under the influence of the slope change can be taken as $L_t \approx 9.5 d_c$.

- Four main local sub-regions have been found to describe the typical air-water flow patterns in the vicinity and further downstream of the slope change cross-section, namely with regard to the mean (depth-averaged) air concentration, air concentration distribution, pseudo-bottom air concentration, air-phase frequency and characteristic flow depths.

- In general, both the mean (depth-averaged) air concentration and the local air concentration (for identical distance to the pseudo-bottom), decrease when approaching the slope change cross-section, in sub-region (I), whereas they increase shortly downstream, in sub-region (II). A peak in the mean air concentration is reached for $X \approx 5$, followed by its decrease until an approximately constant value is reached, at the downstream end of sub-region (III) ($X \approx 9$). Within the reach under the influence of the slope change, the air concentration distribution evolves from a S-shape distribution towards a more stretched profile. Despite de-aeration in vicinity of slope change for the tested range of upstream and downstream slopes, the air concentration close to the

pseudo-bottom remains larger than 10%, which is expected to assure protection of the step surfaces against cavitation damage.

- In the vicinity of the slope change, a significant modification occurs in dimensionless air-phase frequency (fd_c/V_c) profiles, and the maximum cross-sectional value of fd_c/V_c increases and its location moves towards the free surface ($y/Y_{90} \approx$ 0.6-0.8). Shortly downstream of the slope change, the maximum cross-sectional value of fd_c/V_c decreases and its location moves towards the pseudo-bottom ($y/Y_{90} \approx$ 0.1-0.3). Further downstream, the fd_c/V_c profiles continue to readjust until their shape approach that corresponding to the gradually or quasi-uniform flow on the flatter slope.
- In the reaches not affected by the slope change, hence in gradually varied or quasi-uniform flow, the location of the maximum dimensionless air-phase frequency seems to be influenced by the chute slope ($y/Y_{90} \approx$ 0.2 and 0.7 for 50º and 18.6º chute slopes, respectively).
- Maximum air-phase frequency occurs approximately for C equal to 30-40%, regardless of the slope change configuration. Slight sharper profiles were observed for the 50º sloping chute, when compared to those for the 18.6º and 30º slopes.
- The characteristic flow depths (i.e., Y_{90}, Y_{95}, Y_{99}) remain practically constant upstream of the slope change cross-section, whereas a significant increase is noticeable further downstream, followed by a decrease until an approximately constant value is reached. In general, peak values are obtained for $X \approx 5$ which has to be considered for designing the side walls. In contrast, the streamwise development of the equivalent clear water depth is not significantly influenced by the slope change, except in its vicinity.
- The maximum bulked flow depth Y_{99max} is in general lower than or approximately equal to the critical depth, but on the 50º-18.6º slope change configuration, for d_c/h = 2.6, considerable larger values were obtained ($Y_{99max}/d_c \approx 1.6$).
- Minimum discharges in the lower skimming flow regime or even the transition flow regime could perform differently, as the tests with $d_c/h \geq 2.6$ suggest. Such flows would generate higher local C_{mean} and C_b values, related to a more pronounced spray occurrence.
- The tested slope change was abrupt. A gradual change would certainly reduce the flow bulking and the de-aeration up to a certain degree, as the pressure gradient is distributed on longer flow distance.

5

Velocity distribution and energy dissipation

5.1. Introduction

In the last 3 decades, numerous stepped spillways have been designed and constructed, particularly with the application of the roller compacted concrete (RCC), as a cheaper, quicker and easier technique of construction (Chanson, 2002; Felder and Chanson, 2011b). Thus a significant number of hydraulic physical modelling research has been conducted to investigate the flow features on stepped spillways.

Most of the design and associated physical modelling studies were conducted on a constant sloping stepped chute (e.g., Sorenson, 1985; Chamani and Rajaratnam, 1999; Matos et al., 1999; Boes, 2000a,b; Matos, 2000; Sánchez-Juny et al., 2000, 2007; Chanson and Toombes, 2002; Boes and Hager, 2003a; André et al., 2004; Takahashi et al., 2005; Pfister et al., 2006a,b; Gonzalez and Chanson, 2008; Kavianpour and Masoumi, 2008; Amador et al., 2009; Schleiss, 2009; Bung and Schlenkhoff, 2010; Meireles et al., 2012; Zare and Doering, 2012a,b; Felder, 2013; Frizell, et al., 2013; Hunt and Kadavy, 2013; Matos and Meireles, 2014; Felder and Chanson, 2015). Only a few prototypes such as the Upper Stillwater dam in Utah, USA (Houston, 1987) and lower Siah-Bishe dam in northern Iran (Baumann et al., 2006) incorporated the stepped spillway with an abrupt slope change. However there is presently insufficient information available on the flow behaviour on an abrupt slope change on stepped spillways.

In the present study, the effect of an abrupt slope change on flow properties over the stepped spillway is tested systematically with a uniform step height for a wide range of discharges. It is the aim of this chapter to assess the effect of different abrupt slope change configuration, with the upstream chute slope of 50º (1V:0.84H) and downstream chute slope of

30º (1V:1.7H), or 18.6º (1V:3H), particularly on the velocity profile and energy dissipation evolution.

5.2. Velocity distribution

5.2.1. Quasi-uniform flow region

5.2.1.1. Definition

Quasi-uniform flow conditions are generally attained if the local time-averaged air concentration C and the flow velocity v remain practically constant in the flow direction (Bung 2011). It was revealed that the development of quasi-uniform flow requires a flow distance of around 2 to 3 times the inception point length (Pfister & Hager 2011, Bung 2011).

Due to the jet-box, quasi-uniform conditions related to air concentration and velocity were achieved shortly upstream of the slope change (near the end of the upper module) as well as downstream of the slope change (near the end of the lower module), see also section 4.2. Figure 5.1 shows air concentration and velocity profiles measured on the last three consecutive steps in the quasi-uniform flow region at the end of the 50º, 30º, and 18.6º modules for d_c/h=4.6 (test runs 3 and 8, see Table 3.1).

5.2.1.2. Air concentration profile

The air concentration profiles are compared with the S-shape associated to the advection-diffusion model proposed by Chanson (1997). The latter is a function of the mean (depth-averaged) air concentration C_{mean} per profile, obtained herein from the last three consecutive steps per module in quasi-uniform flow. As shown in Fig. 5.1, the last three profiles are similar to each other. Further, the prediction of Chanson fits well with the present profiles. The bottom air concentration is slightly overestimated herein. The measured values are C_b=0.28, 0.21 and 0.16 at the end of the 50º, 30º, and 18.6º modules for d_c/h=4.6. The results also show that the bottom air concentration decreases with decreasing chute slope, which is in consistency with other studies on constant sloping stepped chutes. Boes & Hager (2003b) observed $0.05 \leq C_b \leq 0.1$ on 30º chute, whereas Bung (2011) obtained C_b=0.05 and 0.01respectively on 26.6º and 18.4º chutes (with h=0.06 m). Boes & Hager (2003b) and Pfister and Hager (2011) give $C_b \approx 0.20$ for 50º chute respectively for h=0.06 and h=0.093 m.

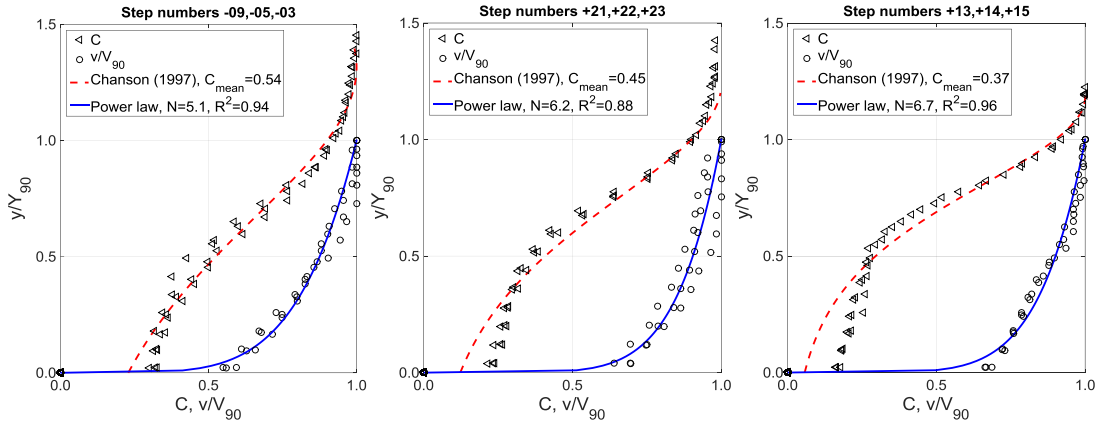

(a) (b) (c)

Figure 5.1 Air concentration C and dimensionless velocity v/V_{90} profiles indicating quasi-uniform flow at the end of a module, (a) Θ_1=50º, (b) Θ_2=30º, and (c) Θ_2=18.6º. All for d_c/h=4.6.

5.2.1.3. Velocity profile

The dimensionless time-averaged velocity v/V_{90} profile on stepped chutes is approximated by a power function, as Eq. (2.13), (Chanson, 1994; Felder and Chanson, 2015). As shown in Fig. 5.1, the measured velocity profiles collapse with the power function. Note that the exponent N increases with decreasing chute angle. Further, N may vary from one step to the consecutive one, due to some interference between adjacent shear layers and cavity flows (Felder & Chanson 2009a, b; 2011a; 2015). However, relatively homogenous velocity profiles were measured on the last three consecutive steps, indicating quasi-uniform flow conditions for d_c/h=4.6, (Fig. 5.1).

The above conclusions can be extended to smaller relative discharges comprising $2.6 \leq d_c/h \leq 4.6$ and to both investigated slope configurations on Θ_1=50º, Θ_2=30º and 18.6º (Fig. 5.2). This suggests that quasi-uniform flow conditions were achieved in the model. Besides, it indicates that the slope change does not affect the velocity profile anymore after a certain flow distance. Finally, the relative discharge has no effect on the dimensionless velocity profiles, as noted by Bung (2011).

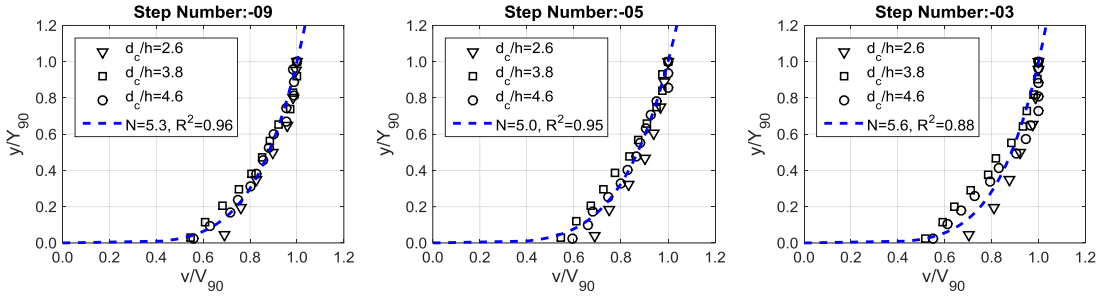

(a)

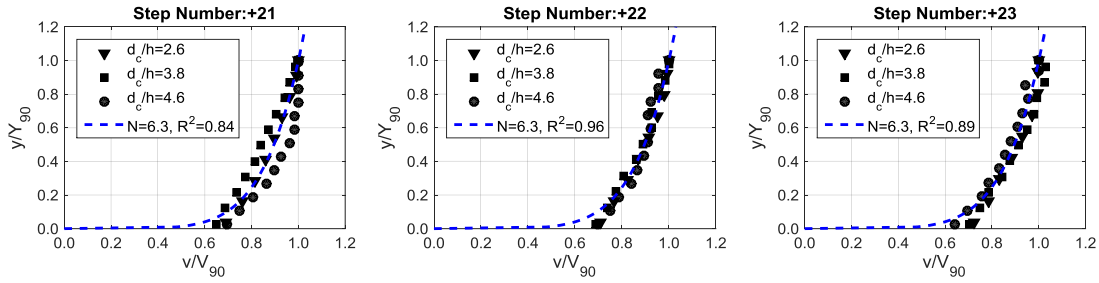

(b)

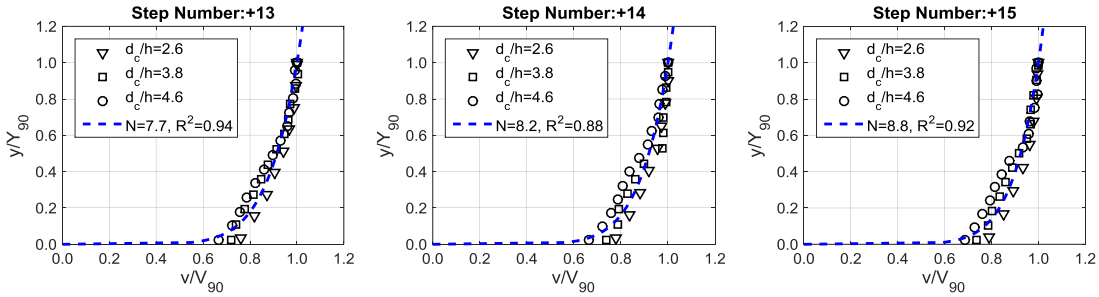

(c)

Figure 5.2 Dimensionless velocity profiles for quasi-uniform flow, at modules ends, for the a) 50º, b) 30 º and c) 18.6º chute slope.

Figure 5.3 compares the dimensionless velocity profiles of the three tested slopes with Eq. (2.13). Despite of a small scatter, Eq. (2.13) fits with the data independent of the dimensionless discharge if N=5.6, 6.2 and 8.2 according to Θ_1=50º, Θ_2=30º and 18.6º ($2.6 \leq d_c/h \leq 4.6$). The upper and lower limits of shadowed area corresponds to N=4.1 and N=13, respectively as the minimum and maximum values obtained in the present work on the steps in the quasi-uniform flow region.

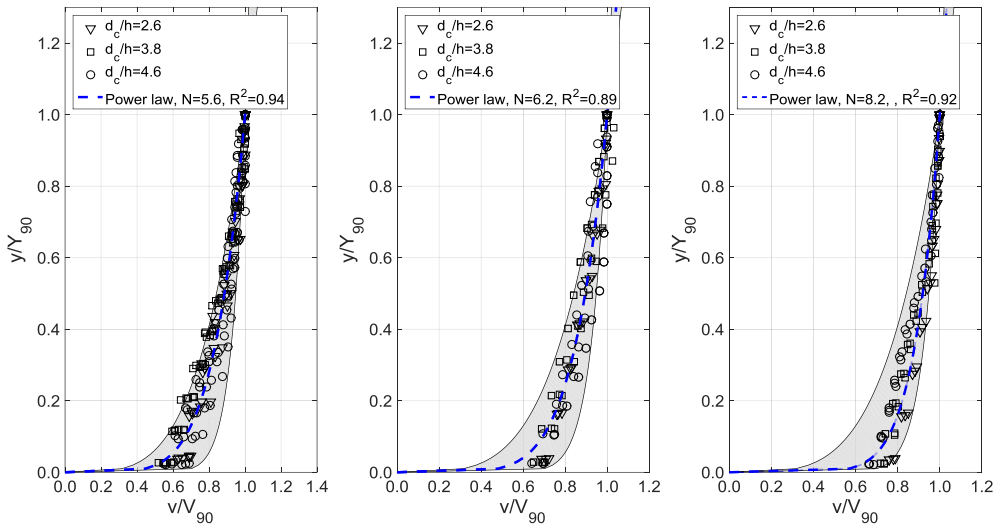

(a) (b) (c)

Figure 5.3 Dimensionless velocity profile on the last 3 steps in quasi-uniform flow region on a) 50º, b) 30º and c) 18.6º sloping chute, for $2.6 \leq d_c/h \leq 4.6$, compared with the fitted power law curves (dashed blue lines). Shadowed area is formed by power law curves with the exponent equals to *N*=4.1 and *N*=13, respectively as the minimum and maximum values obtained on the steps in quasi-uniform flow region.

Figure 5.4 compares the exponents *N* resulting from the present experimental velocity profiles with those defined by Eq. (2.14). Generally, a reasonable agreement is observed. The link between *N* and the values V_{mean} and V_{90} seems thus appropriate to describe the velocity profile.

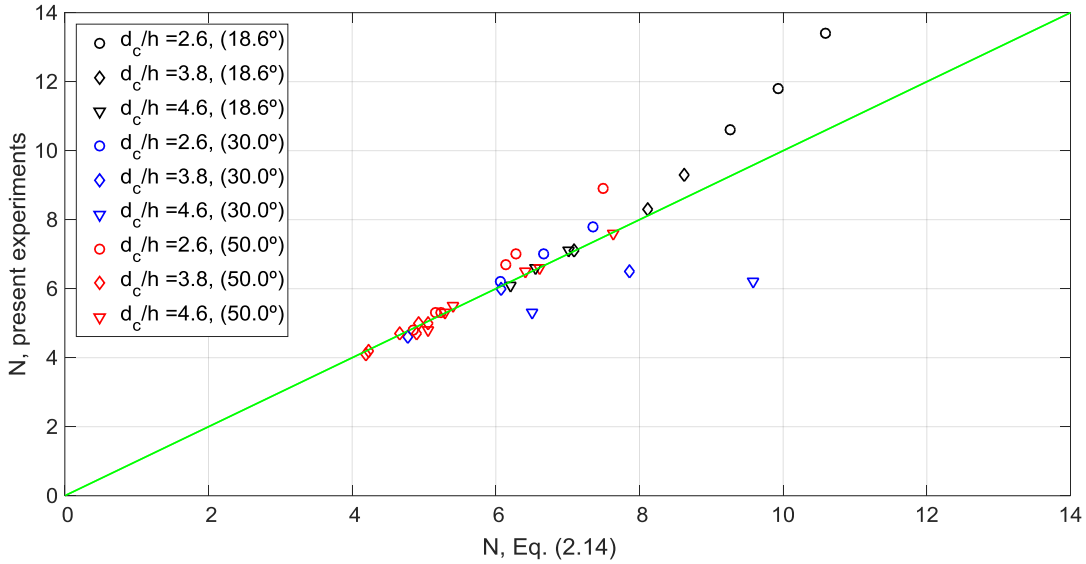

Figure 5.4 Exponents *N* from present experimental velocity profiles versus the values provided by Eq. (2.14) (Bung 2011).

The exponents *N* from the present velocity profiles are compared in Fig. 5.5 with those predicted by Eqs. (2.16) and (2.17). The data of the 18.6º and 30º chute angle follow the trend of Eq. (2.16), while the individual data of the 50º chute angle agree better with Eq. (2.17). Note that the applicability of Eq. (2.16), proposed by Bung (2011), is limited to the chute slope ranging between 18.4 º to 26.6 º.

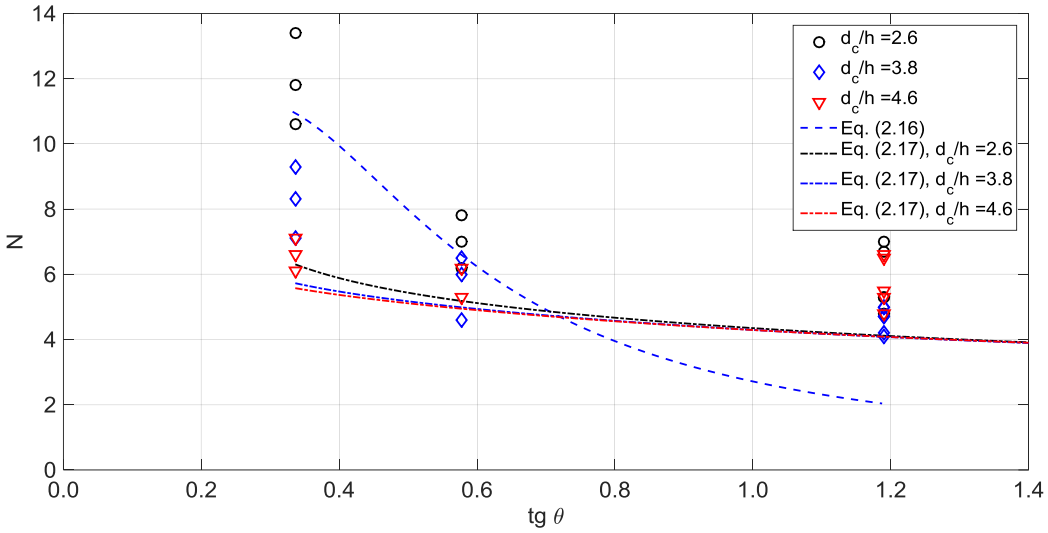

Figure 5.5 Exponents *N* from present experimental velocity profiles versus values predicted by Eqs. (2.15) and (2.16) (Bung 2011, Takahshi & Ohtsu 2012).

5.2.2. Slope change region

The mean velocity V_{mean} (Eq. 2.15) is normalized with the critical flow velocity being $v_c=(gd_c)^{0.5}$. The streamwise development of this normalized velocity is shown in Fig. 5.6. The dimensionless streamwise coordinate is defined as $X=(x–x_{sc})/d_c$, with x as streamwise coordinate starting at the jet-box and x_{sc} as location of the slope change. By using X the origin is set at the slope change and the distance is normalized with the critical flow depth d_c.

The normalized velocity tends to increases slightly upstream of the slope change (at X≈–0.5 in Fig. 5.6) for both slope change configurations, even though with a considerable data scatter. Shortly downstream of the slope change, the velocity tends to decrease until an almost constant trend is observed on the downstream flat module. The latter is achieved at latest at X≈9 (Fig. 5.6). The slope change thus generates a flow compression and deviation, inducing a local acceleration. The observed tendency of slight increase of the mean velocity upstream of the slope change is not fully consistent with the previously noticed increase of the equivalent clear water depth on identical reach. Such a result may be due to the inaccuracy of estimating the mean velocity in the vicinity of the slope change, where the flow curvature is not negligible.

The influence reach of the slope change includes some $-0.5 \leq X = (x-x_{sc})/d_c \leq 9$, being independent of the slope change configuration (50º-18.6º and 50º-30º) as well as of the relative discharge (d_c/h). This observation is confirmed by the development of the air concentration profiles and flow depths (see Chapter 4, section 4.2).

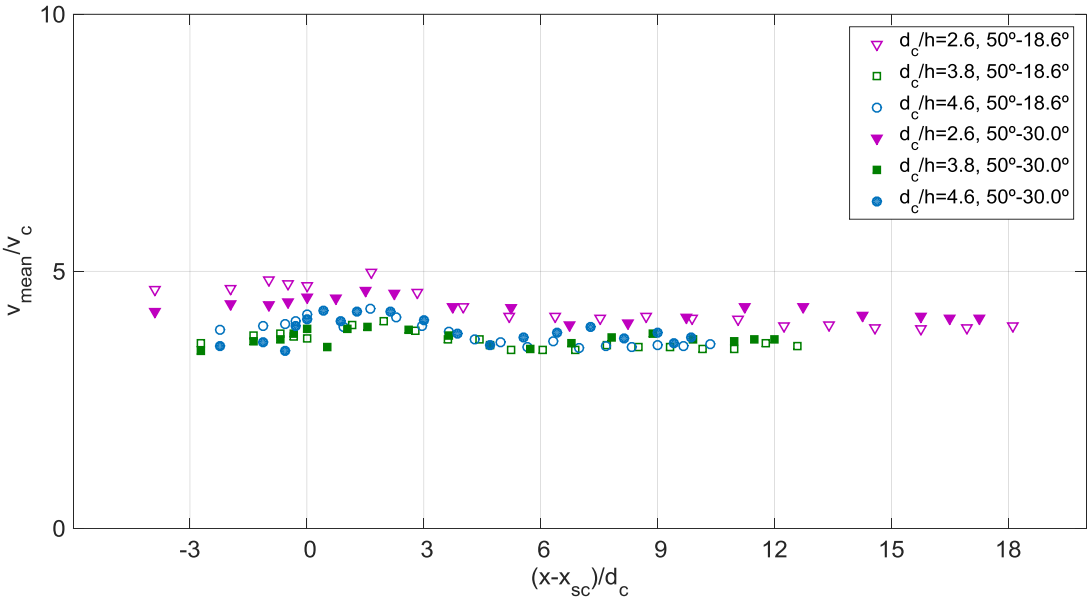

Figure 5.6 Streamwise development of the normalized mean velocity on 50º-18.6º and 50º-30º, where the critical flow velocity is $V_c = \sqrt{gd_c}$, and x_{sc} is the distance between the jetbox and the slope change cross-section, measured along the chute.

Velocity profiles were acquired in skimming flow upstream and downstream of the slope change, on both 50º-30º and 50º-18.6º configurations, for various flow rates (test runs 1 to 3 and 6 to 8; Table 3.1). In Figs. 5.7 and 5.8, dimensionless velocity distributions are plotted for various cross-sections, for d_c/h = 2.6. Figures 5.7a and 5.8a show that for steps -09 and -05, the velocity distribution follows the before-mentioned power law function as expected for quasi-uniform flow on a similar sloping chute. The velocity generally increases shortly downstream of the slope change (steps +01 to +06 on 50º-18.6º, and steps +01 to +09 on 50º-30º, Figs. 5.7b and 5.8b), evolving towards those profiles which do not follow the power law distribution. This is judged to be due to the strong flow curvature reversal and higher pressure in the vicinity of the slope change (Ostad Mirza et al., 2015a,b), (Fig. 3.9b,d). Further downstream, the velocity generally tends to decrease along the chute (Figs. 5.7c, 5.8c), until an approximately constant profile with the power law distribution is reached, typical of a gradually varied flow on similar sloping chute (Figs. 5.7d, 5.8d).

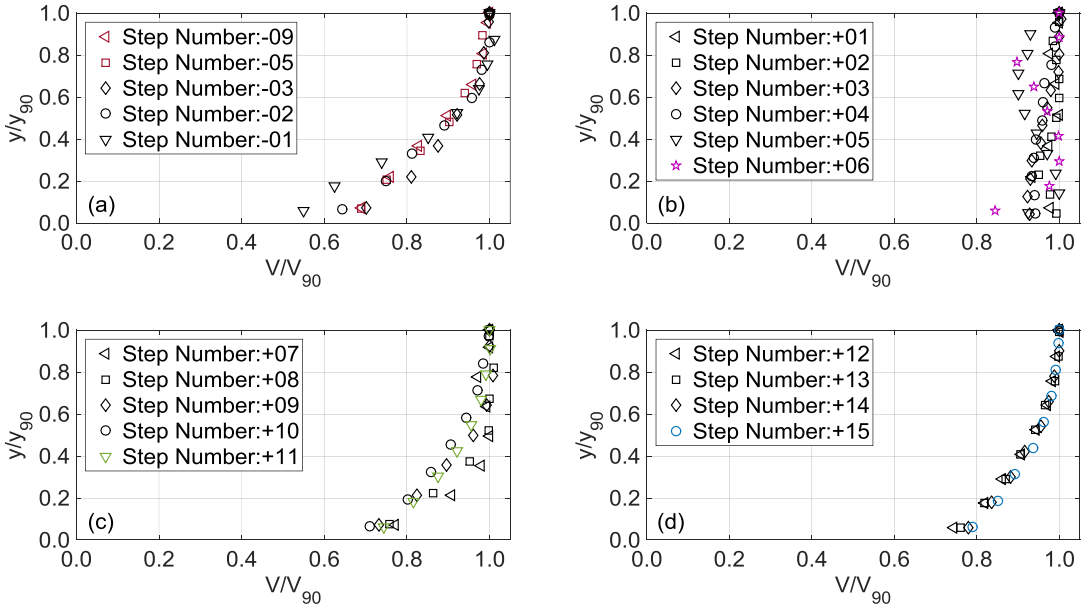

Figure 5.7 Velocity distribution along the 50˚-18.6˚ slope change configuration, for d_c/h = 2.6 ("-" and "+" signs represent the steps upstream and downstream of the slope change cross-section, respectively, as per Fig. 3.9b).

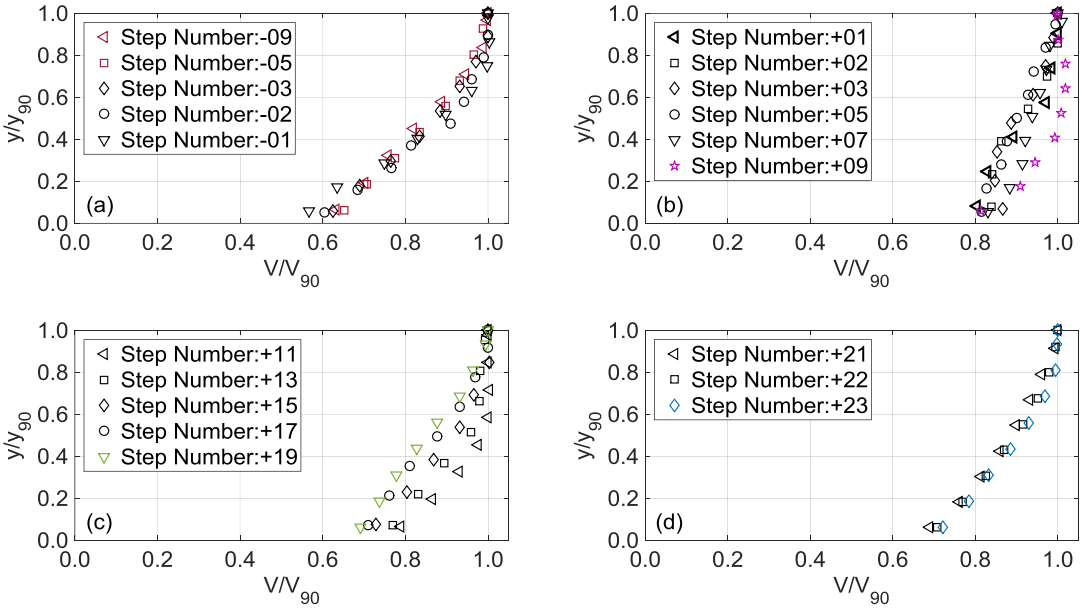

Figure 5.8 Velocity distribution along the 50˚-30˚ slope change configuration, for d_c/h = 2.6 ("-" and "+" signs represent the steps upstream and downstream of the slope change cross-section, respectively, as per Fig. 3.9d).

According to the previous chapter (section 4.2) and section 5.2.1 of present chapter, the reaches not affected by the slope change include steps -09 to -03 on the 50˚ upstream slope (*X*

≤ -0.5), +12 to +15, and +21 to +23 respectively on the 18.6˚ and 30.0˚ downstream slope ($9 \leq X$), (Figs. 5.7a, d and 5.8a, d). Along these regions, the dimensionless velocity exhibits the power law distribution similarly as obtained in other experimental studies in quasi-uniform or gradually varied flow on constant chute slopes (e.g., Bung, 2011; Felder and Chanson, 2011a). The achieved experimental data gathered on 3 consecutive step edges along these regions, which are fairly similar, strengthens the conclusion that gradually varied or quasi-uniform flow was attained. Overall, a similar development of the velocity profiles occurs on the 50º-18.6º and 50º-30º slope changes, as shown in Figs. 5.7 and 5.8. However, the influence of the slope change is more pronounced in the 50º-18.6º configuration, comparing the modifications observed on the velocity profiles, particularly in the vicinity of the slope change (e.g., +01).

5.3. Energy dissipation

The energy dissipation on stepped chutes with an abrupt slope change may be caused not only by the momentum exchange between the mainstream and the step niche vortices, but furthermore by flow deflection and re-attachment. Therefore, an abrupt slope change on stepped spillways is an interesting issue with regards to the probable effect on the energy dissipation rate as a basic parameter to be considered for the design of stepped spillways. Based on the air concentration and velocity profiles, local kinetic energy correction coefficient (α) (obtained from Eq. 2.19) and specific energy (E) (obtained from Eq. 2.18) values were computed along the stepped chute, upstream and downstream of the slope change.

The streamwise development of the kinetic energy correction coefficient α is shown in Fig. 5.9, with horizontal lines representing the mean value of α in quasi-uniform flow. A local peak of α is observed at the slope change due to flow curvature generating a non-hydrostatic pressure distribution, affecting also the typical velocity profile (Figs. 5.7a and 5.8a, steps –2 to +1). However, along not affected reaches (outside of $-0.5 \leq X \leq 9$) α remains practically constant with α=1.06 upstream and α=1.03 far downstream of the slope change, (Fig. 5.9).

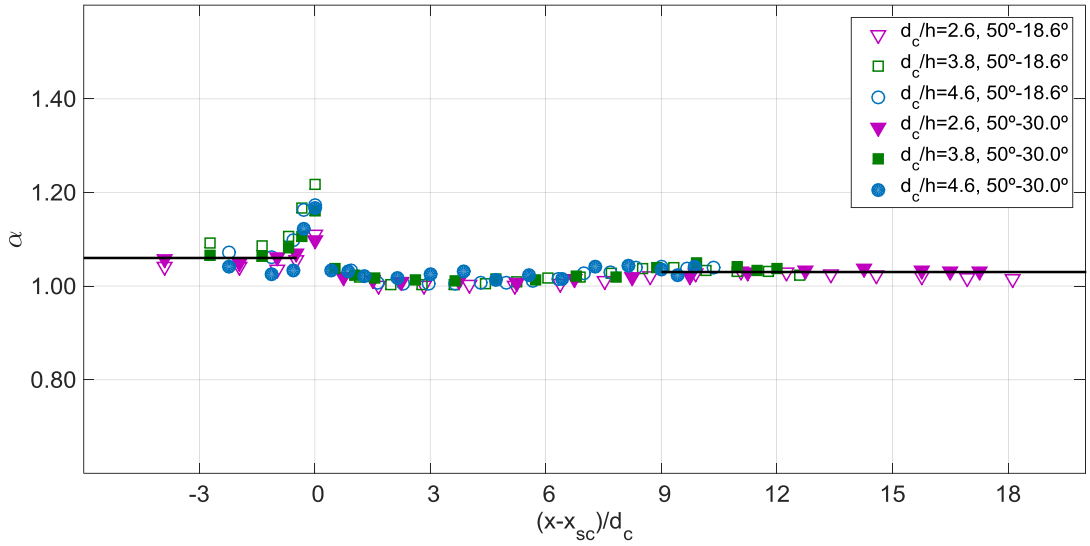

Figure 5.9 Streamwise development of the kinetic energy correction coefficient on 50º-18.6º and 50º-30º slope change configurations, where x_{sc} is the distance between the jetbox and the slope change cross-section, measured along the chute.

Figure 5.10 shows the streamwise development of the dimensionless specific energy E/d_c. The latter tends to increase immediately upstream of the slope change, which is mainly due to the slight increase in the mean velocity and considerable increase in the kinetic energy correction coefficient. It should also be noticed that the estimation of the mean velocity and the kinetic energy correction coefficient, and consequently the specific energy, is expected to be inaccurate in the vicinity of the slope change.

Immediately after the slope change and up to roughly X=6, the dimensionless specific energy decreases, indicating an over-proportional energy dissipation, as typical for diverging streamlines. Downstream of roughly $X > 9$ an almost constant value is reached under gradually varied or quasi-uniform flow conditions. The dimensionless specific energies of d_c/h=3.8 and 4.6 overlap, but a higher dimensionless energy is observed for d_c/h=2.6.

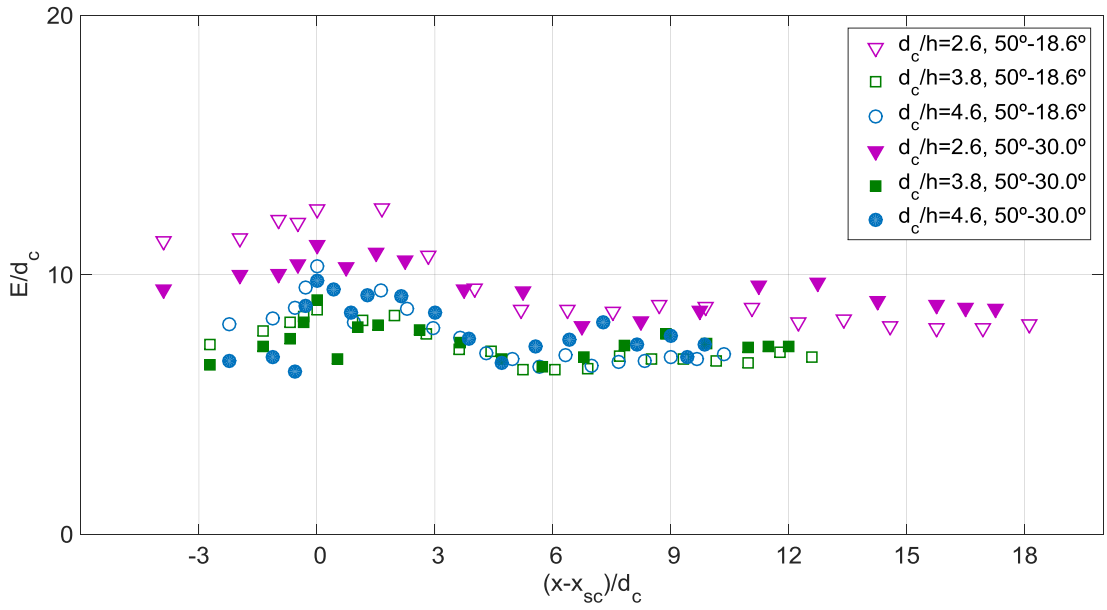

Figure 5.10 Streamwise development of the dimensionless specific energy on 50º-18.6º and 50º-30º slope change configurations, where x_{sc} is the distance between the jetbox and the slope change cross-section, measured along the chute.

Considering H_{usc} the total head obtained immediately (at the first step) upstream of the reach under the influence of slope change ($X \approx -0.5$), above the datum cross-section defined by the downstream end of the region influenced by the slope change ($X \approx 9$), then $H_{usc}=E_{usc}+\Delta Z_{sc}$, where E_{usc} is the specific energy immediately upstream of the reach under the influence of slope change and ΔZ_{sc} is the elevation above the datum cross-section. The head loss on the region influenced by the slope change is given as:

$$\Delta H_{sc} = H_{usc} - H_{dsc} \tag{5.1}$$

where H_{dsc} is the total head at the downstream end of the region influenced by the slope change ($X \approx 9$). Thus, the relative head loss corresponding to the reach under the influence of the slope change, can be expressed as:

$$\frac{\Delta H_{sc}}{H_{usc}} = \frac{H_{usc} - H_{dsc}}{H_{usc}} \tag{5.2}$$

Figure 5.11 shows the relative head loss on the 50º-30º and 50º-18.6º slope change regions. The relative head loss tends to decrease with increasing relative critical depths and varied roughly between 38% to 51%, depending on the relative critical depth and slope change configuration. The following simple equation was found to fit roughly to the data:

$$\frac{\Delta H_{sc}}{H_{usc}} = 0.63 - 0.05\frac{dc}{h} \tag{5.3}$$

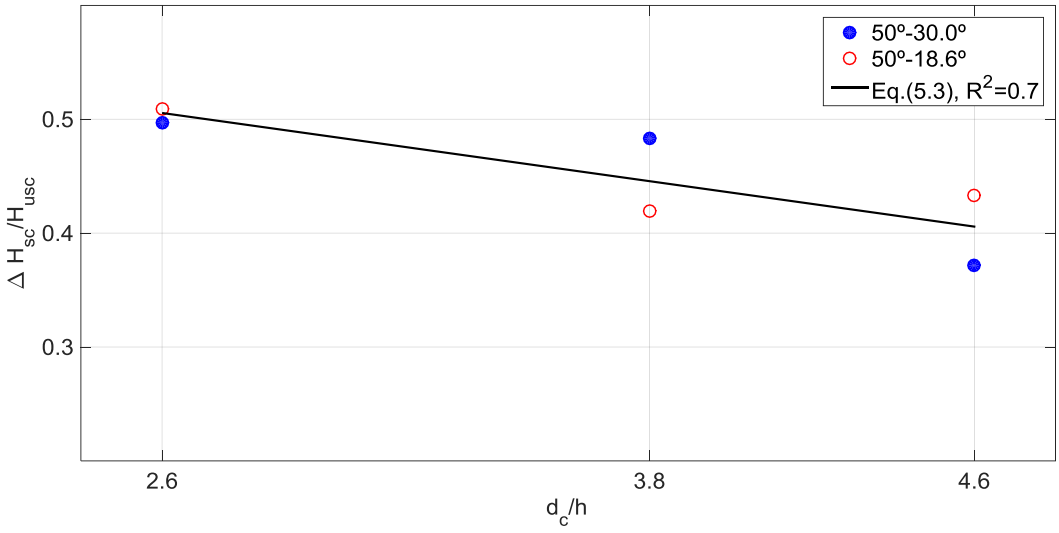

Figure 5. 11 Relative head loss caused under the influence of slope change, on 50º-18.6º and 50º-30º slope change configurations; measurements at the first step edge upstream and downstream of the reach under the influence of slope change.

5.4. Conclusions

A significant number of physical model studies were conducted on the hydraulics of skimming flow over constant sloping stepped spillways. Although some prototype of stepped spillways with an abrupt slope change have been built and operated for a long period, there is a lack of understanding of its influence on the flow characteristics. This chapter discussed the effect of an abrupt slope change on the velocity distribution and energy dissipation in skimming flow on stepped chutes. Six sets of experiments were carried out for a range of flow rates ($2.6 \leq d_c/h \leq 4.6$), on a relatively large scale model of 50º-30.0º and 50º-18.6º abrupt slope change.

The basic results demonstrated that along the reaches not influenced by the slope change, the dimensionless velocity distribution is a function of the chute slope and follows the power law distribution, corresponding to the gradually or quasi-uniform flow. The power law exponent (N) decreases with increasing chute slope. Accordingly, typical N exponent observed on 50º, 30º and 18.6º sloping chutes were respectively equal to 5.6, 6.2, 8.2. Within the reach under the influence of the slope change, a significant modification occurs in dimensionless velocity distribution and profiles do not follow the power law distribution. Downstream of the reach under the influence of slope change, the profiles readjust their shape to the power law distribution.

The development of the V_{mean}/V_c, α, and E/d_c along the chute showed an increase upstream of the slope change cross-section (X≈-0.5), whereas it decreased shortly downstream of slope change cross-section to reach to the values corresponding to the flatter sloping chute (X≈9). However, the results obtained in the vicinity of the slope change are expected to be inexact, due to the considerable flow curvature in such reach.

The results also indicated that the head loss in the region influenced by the slope change tends to decrease with increasing relative critical depth, varying roughly between 38% to 51% for the tested relative critical depths and slope change configurations.

6

Distribution of dynamic pressures at slope changes

6.1. Introduction

The hydrodynamic pressure distribution and its prediction play an important role in structural analysis of smooth and stepped chutes. They were investigated extensively over a constant sloping stepped chutes (e.g., Matos et al., 2000; Sánchez-Juny et al., 2000, 2007, 2008; André, 2004; Sánchez-Juny and Dolz, 2005; André and Schleiss, 2008; Amador et al., 2009; Zhang et al., 2012; Frizell et al., 2013, 2015; Chanson, 2015).

Nevertheless, an abrupt slope change of the chute may change the dynamic pressure pattern in the flow either over smooth or stepped spillways. To date, there are a limited number of numerical and experimental studies evaluating the dynamic pressure development in the flow over a sudden slope change on smooth chutes (e.g. Zarrati et al., 2004). According to Zarrati et al. (2004), a sudden change in pressure and velocity distribution occurs as the flow passes over a sudden change in smooth sloping chutes. They indicated that the slope change of $\Delta\Theta$=15º may lead to an increase in the pressure in vicinity (up and downstream) of the slope change cross-section up to 25 times the hydrostatic pressure. However, except a few model studies of stepped chute prototypes incorporating a slope change (e.g. Houston, 1987 on Upper Stillwater dam in Utah, USA and Baumann et al., 2006 on Lower Siah-Bishe dam in northern Iran), there is no detailed information regarding pressure development in skimming flows over stepped spillways with an abrupt slope change (Ostad Mirza et al., 2015a). The purpose of the present chapter is to highlight the effect of an abrupt slope change on the distribution of the dynamic pressure across the slope changes. Dynamic pressure measurements were gathered in four

model test runs (number 3 and 6 to 8, see Table 3.1) for slope change configurations of 50º-18.6º ($\Delta\Theta$=31.4º) and 50º-30º ($\Delta\Theta$=20º).

6.2. Results and analysis

6.2.1. Measurement methodology

As explained in Chapter 3 (see section 3.2.2.), the pressure measurements were collected by piezoresistive pressure transmitters (Keller-druck PR-23/8465.2). The pressure transducers arrangement is shown in Fig. 3.13. Therein the values of *z/h* are equal to 0.30, 0.55 and 0.70, irrespective of the chute slope (*z* is the distance from the step edge, along the vertical face, and *h* is the step height: *h*=0.06 m). *x/l* values for different sloping chute are presented in Table 3.2, where *x* is the distance from the step edge, along the horizontal face, and *l* is the step length.

To understand the influence of the slope change on dynamic pressure development and to compare with earlier findings on conventional constant sloping stepped spillways, the results have been presented along the horizontal and vertical face of steps in vicinity (under the influence) and far upstream and downstream (not being influenced) of the slope change cross-section. According to Chapter 4 (see section 4.2), the steps which are not influenced by the slope change are defined as step number -3 (upstream of slope change cross-section, on the steeper sloping chute of 50º), and steps number +31, and +20 (far downstream of slope change cross-section, on the flatter sloping chutes of 30º and 18.6º respectively).

6.2.2. Dynamic pressure distribution on the horizontal step faces

Figures 6.1 and 6.2, indicate the mean, 95th and 5th percentiles of the dimensionless dynamic pressures ($p/\gamma/h$) obtained on the horizontal step faces in the vicinity and far downstream of 50º-18.6º and 50º-30º slope changes, for d_c/h=4.6, where p is the measured dynamic pressure, γ is water specific weight and h is step height. Both the mean and the 95th percentile tend to increase in the direction of the outer step edge, essentially due to the influence of the impact of the flow on the horizontal step faces, (Figs. 6.1 and 6.2). As it can be seen, the minimum pressure values are observed along the upstream portion of the horizontal step faces, ($x/l > 0.5$), whereas the maximum values are observed along the portion closer to the step edges ($x/l < 0.5$). The highest pressure was recorded at $0.15 < x/l < 0.35$, for d_c/h=4.6. The above findings are consistent with other studies on constant sloping stepped chutes from 30º to 51.2º (Sánchez-Juny et al., 2000, 2007, 2008; André, 2004; André and Schleiss, 2008; Amador et al., 2009), stating that the outer step edge is under the influence of the flow impact and the inner

step edge is under the influence of flow recirculation, and the highest absolute pressures occurs at the flow separation in between these two regions ($x/l \approx 0.2$). S-shape pressure distribution on horizontal step faces, observed for instance by Sánchez-Juny et al. (2007) and Zhang et al. (2012), is more evident at step number +20 (on 18.6º sloping chute), possibly due to covering a larger portion of the step by the higher number of the measuring pressure taps (Fig. 6.1c).

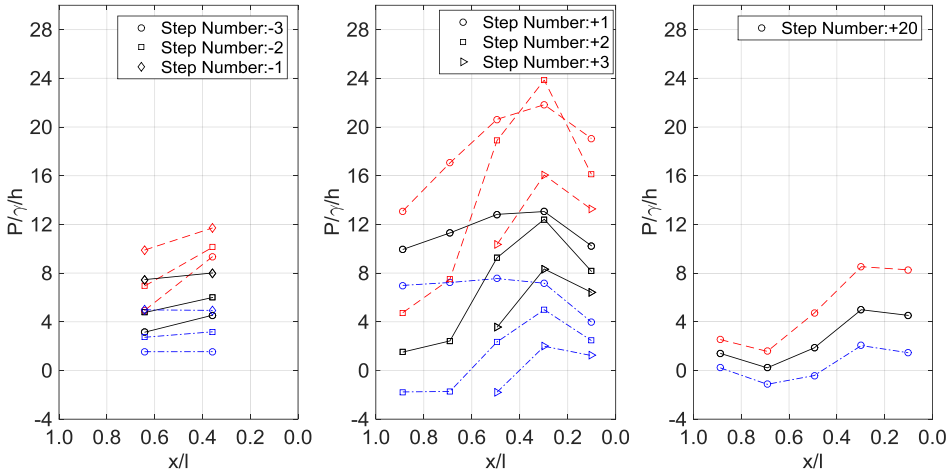

(a) (b) (c)

Figure 6.1 Mean (-), 95th (- -) and 5th (- .) percentiles of the dimensionless pressure on the horizontal step faces, in vicinity and far downstream of the 50º-18.6º slope change, for d_c/h =4.6; l is the step length and x is the distance from the step edge, along the horizontal face (see Fig. 3.13a).

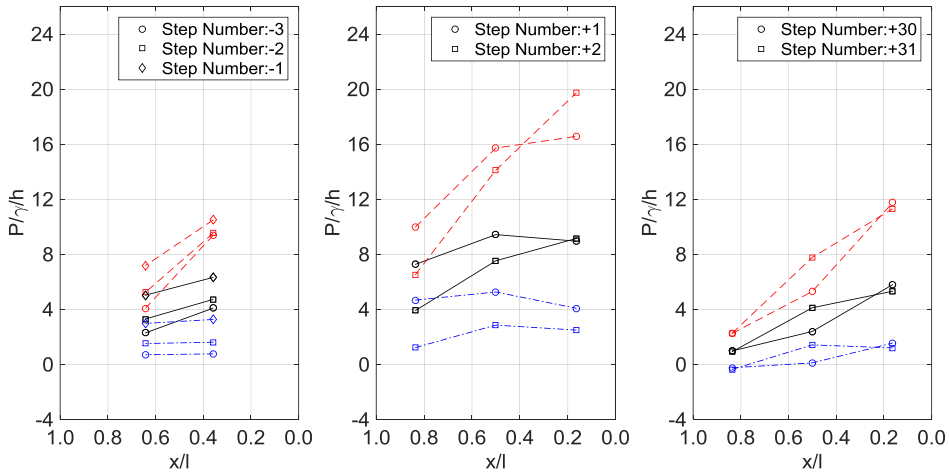

(a) (b) (c)

Figure 6.2 Mean (-), 95th (- -) and 5th (- .) percentiles of the dimensionless pressure on the horizontal step faces, in vicinity and far downstream of the 50º-30º slope change, for d_c/h =4.6; l is the step length and x is the distance from the step edge, along the horizontal face (see Fig. 3.13b).

The pressure starts to increase by approaching the slope change (step number -2 and -1, Figs. 6.1a and 6.2a). Immediately downstream of the slope change cross-section, considerably larger values of the mean, 5th and 95th pressure percentiles were found (step number +1 and +2, Figs. 6.1b and 6.2b). Similar trends have been observed on earlier studies on an abrupt slope change on smooth (Zarrati et al., 2004) and stepped (Houston, 1987) sloping chutes. Zarrati et al., (2004), observed that the modification in pressure and velocity initiates slightly upstream of slope change, despite of supercritical flow. The later is judged to be due to the back internal pressure waves, corresponding to the non-hydrostatic pressure distribution upstream of the slope change, which leads to influence the flow properties upstream of the slope change, even in the supercritical flows.

A higher magnitude of the slope change resulted in ≈16% higher 95th percentile pressure values in vicinity of 50º-18.6º cross-section, in comparison with the results obtained in vicinity of 50º-30º slope change cross-section. At the downstream end of the flatter sloping chute the pressure values are almost of the same order of magnitude as those upstream of the slope change cross-section on the steeper sloping chute, in particular for the 50º-30º slope change configuration (Figs. 6.1c and 6.2c).

The above findings for d_c/h = 4.6, are also observed for a broad range of relative critical depths ($2.6 \leq d_c/h \leq 4.6$), as shown on the 50º-30º slope change configuration (Fig. 6.3). It is also evident that the greater the discharge, the greater the pressure values were observed for mean, 95th and 5th percentiles.

Sánchez-Juny et al. (2007) and André (2004) observed maximum pressures respectively up to ≈7 and 5.5 time the step height on horizontal step faces of 51.2º and 30º sloping stepped chutes for d_c/h=2.25 and 2.65. This is in fair agreement with the present results on the horizontal face of steps not influenced by the slope change along the 50º-30º slope change configuration (step numbers -3 and +31, Fig. 6.3a), where the maximum pressure was found to be ≈7.5 times the step height for d_c/h= 2.6.

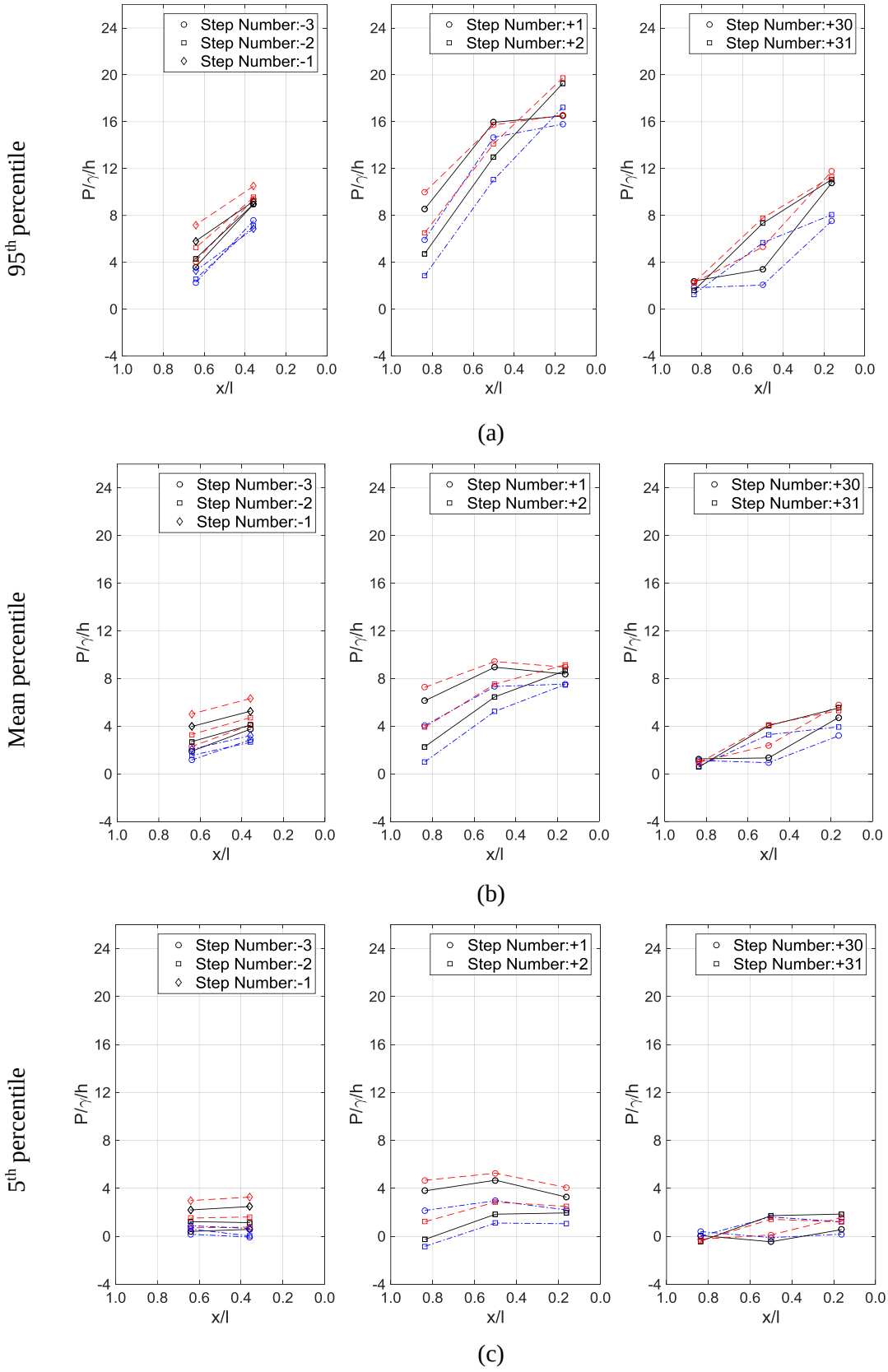

Figure 6.3 Mean, 95th and 5th percentiles of the dimensionless pressure obtained on the horizontal step faces, in vicinity and far downstream of the 50°-30° slope change, for d_c/h = 2.6 (- .), 3.8 (-), and 4.6 (- -).

6.2.2.1. Streamwise development of maximum pressures

The streamwise development of the maximum measured mean, 95th and 5th percentiles of the dynamic pressure on horizontal step faces (obtained at x/l =0.35, 0.17 and 0.3 respectively on 50º, 30º and 18.6º sloping chute steps) are shown in Figs. 6.4 and 6.5 respectively for 50º-18.6º and 50º-30º configurations. The influence of the slope change, as explained before, start slightly upstream of the slope change cross-section and a significant increase occurs approximately from step -2 to step +2. Further downstream, the pressure decreases significantly, and the values at the downstream end of the flatter sloping chute are of the same order of magnitude as those upstream of the slope change cross-section.

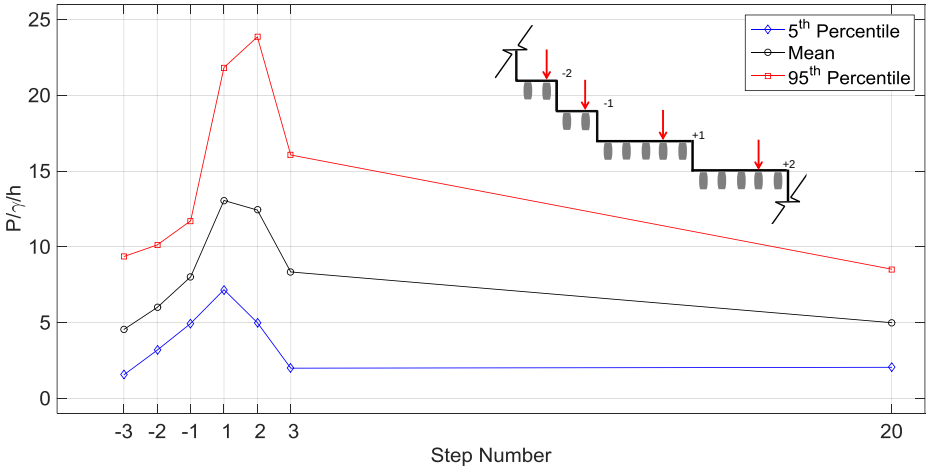

Figure 6.4 Streamwise development of the mean, 95th and 5th percentiles of the dimensionless pressure on the horizontal step faces in vicinity and far downstream of 50º-18.6º slope change, at x/l= 0.35 on 50º sloping chute and x/l= 0.3 on 18.6º sloping chute, for d_c/h =4.6.

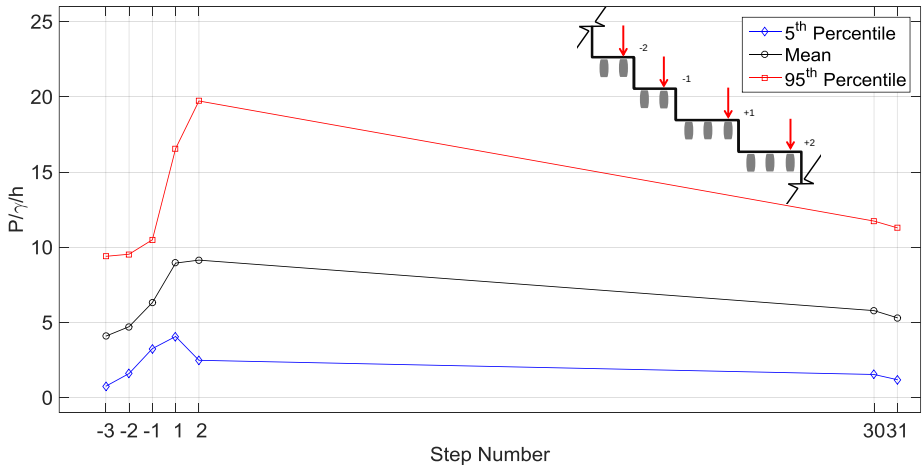

Figure 6.5 Streamwise development of the mean, 95th and 5th percentiles of the dimensionless pressure on the horizontal step faces in vicinity and far downstream of 50º-30º slope change, at x/l= 0.35 on 50º sloping chute and x/l= 0.17 on 30º sloping chute, for d_c/h =4.6.

6.2.2.2. Streamwise development of the equivalent clear water depth and maximum mean pressures in vicinity of the slope change

The streamwise development of the dimensionless equivalent clear water depth (d_w/h) in the vicinity of 50º-18.6º and 50º-30º slope changes is illustrated in Fig. 6.6. The clear water depth shows a considerable increase when approaching the slope change, followed by a sudden decrease shortly downstream of that cross-section. On the flatter sloping chute, the values are slightly smaller but of the same order of magnitude as upstream of the slope change (on steeper sloping chute). As expected, the higher the discharge, the higher clear water depths were observed.

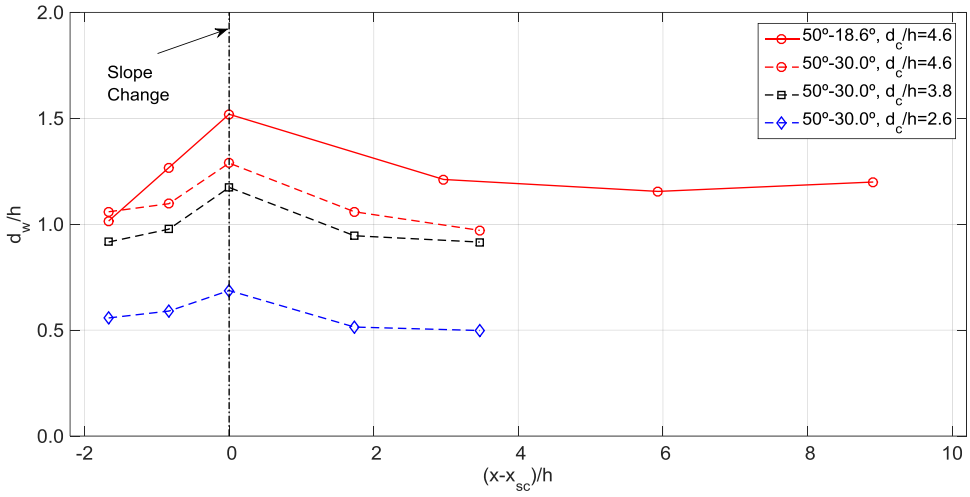

Figure 6.6 Streamwise development of dimensionless equivalent clear water depth (d_w) in the vicinity of 50º-18.6º and 50º-30º slope changes cross-section.

In order to show the significant modification of the pressure development on horizontal step faces in vicinity of slope change, $P/(\gamma d_{w\,up} cos\theta)$ was introduced, where $d_{w\,up}$ is the equivalent clear water depth upstream of, but not influenced by, the slope change (obtained at step -3). The collected results over 50º-18.6º ($\Delta\Theta$=31.4º) and 50º-30º ($\Delta\Theta$=20º) slope change configurations are plotted in Fig. 6.7 (mean pressures obtained at x/l =0.35, 0.17 and 0.3 respectively on 50º, 30º and 18.6º sloping chute steps). As it can be seen, when approaching the slope change, the pressure ratio increases noticeably. Short downstream of the slope change (step numbers +1 and +2), mean pressures between 13 to 21 times the equivalent clear water depths were observed on the horizontal step faces for the range of tested relative flow rates ($2.6 \leq d_c/h \leq 4.6$). A similar trend has been observed also on earlier studies on an abrupt slope change ($\Delta\Theta$=15º) on a smooth sloping chute (Zarrati et al., 2004). They observed pressures up to 25 times the hydrostatic pressure near the slope change cross-section.

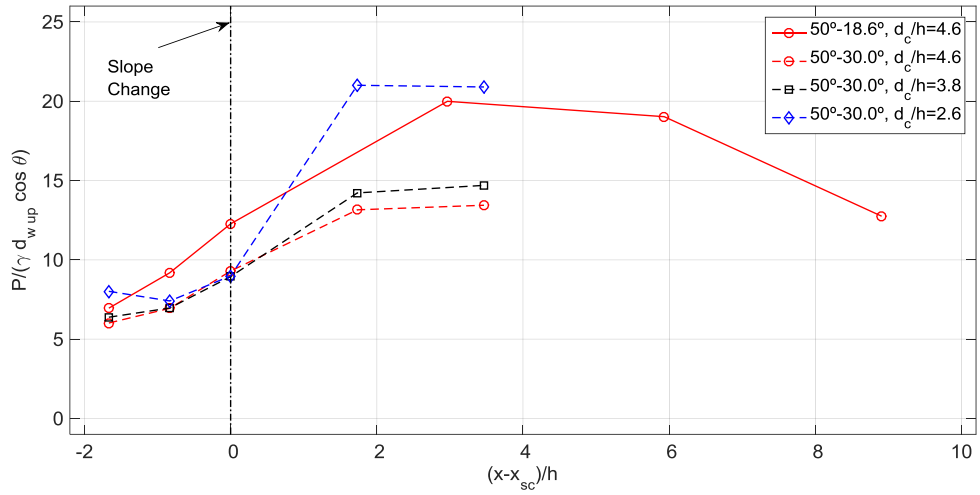

Figure 6.7 Ratio of the mean pressure over equivalent clear water depth in vicinity of 50º-18.6º and 50º-30º slope changes cross-section, (pressures obtained at *x/l* =0.35, 0.17 and 0.3 respectively on 50º, 30º and 18.6º sloping chute steps).

It was found that with increasing the slope change magnitude from $\Delta\Theta$=20˚ *to* $\Delta\Theta$=31.4˚, maximum dimensionless mean pressures ($p/\gamma/h$) and maximum $P/(\gamma d_{w\,up} cos\theta)$ increased 29% and 32% respectively .

6.2.2.3. Spectral contents of the pressure signals

The power spectral density (PSD) content of the pressure fluctuations at a given frequency in turbulent flows is the mean energy in that frequency and may provide information about the flow features and how the eddies of different sizes exchange energy with each other (Tennekes and Lumley, 1972). Therefore, to study the influence of the slope change, Welch's power spectral density of the pressure fluctuations (P_{xx}) was estimated by means of 2^{16} recorded signals on each sensor (by Hamming windowing with 25% overlapping).

The results showed that the dominant frequencies of skimming flows are between 5 to 20 Hz, which is in fair agreement with those obtained in aerated and non-aerated flows by Amador (2005), Gomes (2006) and Sánchez-Juny et al. (2007). Figure 6.8 indicates the PSD of the pressure fluctuations on the horizontal faces of the steps which were not influenced by the slope change on 50º, 30º and 18.6º sloping chutes, for d_c/h=4.6. As can be noticed, the signals obtained from the pressure sensors which are located closer to the outer step edge (downstream portion of the horizontal step faces) contain higher spectral energy. They are clearly distinguishable from the spectral energy graphs obtained from the pressure sensors located closer to the inner step edge (upstream portion of the horizontal step face). This is in agreement with earlier findings on constant sloping stepped chutes. Therein it is shown that the

downstream portion of the horizontal step face is subject to the jet impact, whereas the upstream portion involves a boundary layer separation due to step vorticity and recirculating internal eddies (Sánchez-Juny et al., 2000, 2007; André and Schleiss, 2008). It can be shown that for a given chute slope, the initiation of the decay is shifted to the higher frequency with decreasing *x/l*.

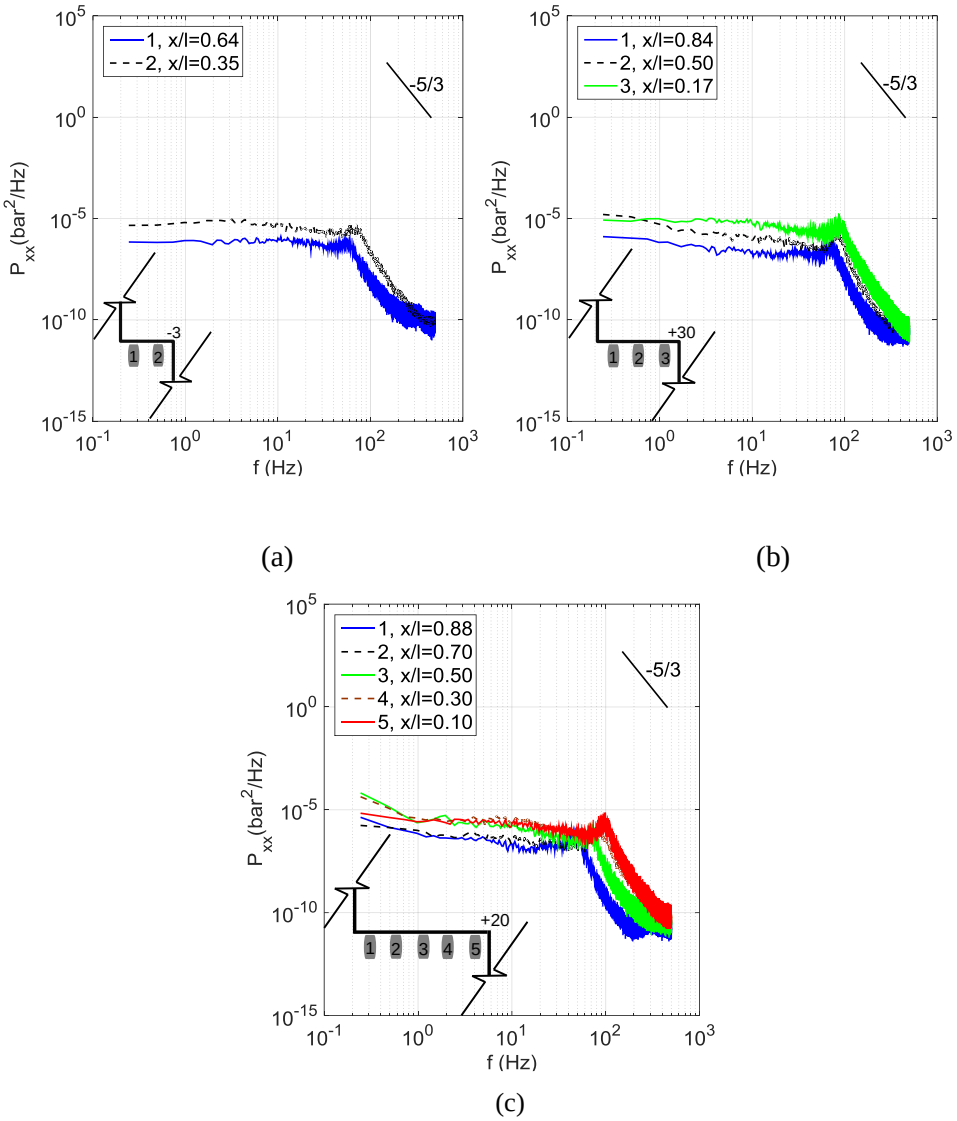

Figure 6.8 PSD of the dynamic pressure fluctuations obtained on the horizontal face of the steps not influenced by slope change for d_c/h =4.6: a) step number -3 (on the 50º sloping chute), b) step number +31 (on the 30º sloping chute), and c) step number +20 (on the 18.6º sloping chute). The typical turbulent slope decay of -5/3 is shown as well.

For better understanding the effect of the slope change, power spectrums were computed also on the steps in vicinity of the slope change and were compared with the spectral density curves obtained on the steps not influenced by the slope change. Figure 6.9 exemplary compares the spectral contents obtained near the outer edge on the horizontal step face (at *x/l*

=0.35, 0.17 and 0.3 respectively on 50º, 30º and 18.6º sloping chute) in vicinity and downstream of the slope change cross-sections, for d_c/h=4.6. As it can be seen, when approaching the slope change, a higher spectral energy is produced, while further downstream the energy content reduces and reaches to lower values corresponding to the steps not influenced by slope change on the flatter sloping chute. Hence, a slope change may lead to higher spectral energy content, as observed on the tested slope change configurations.

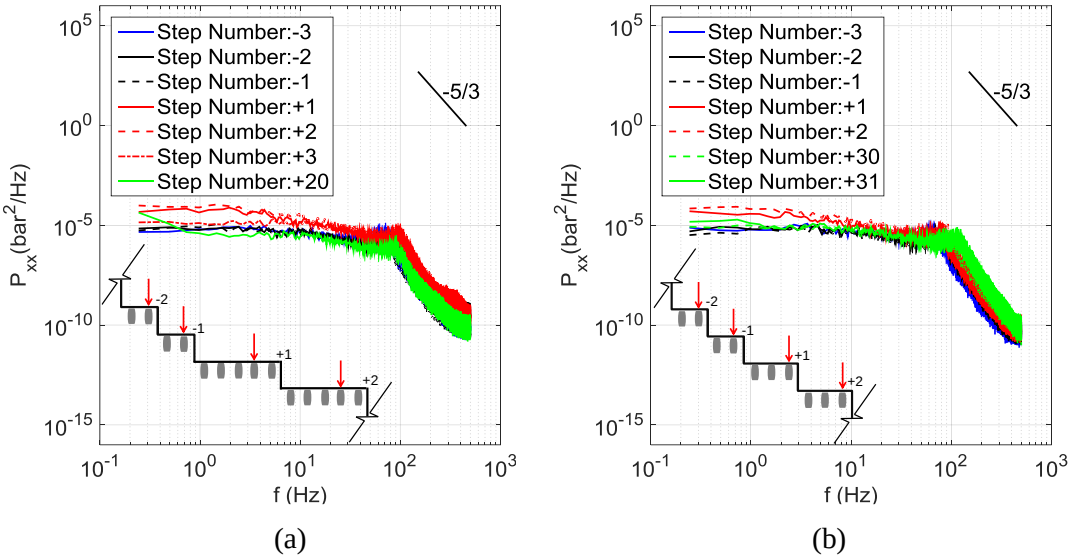

Figure 6.9 PSD of the dynamic pressure fluctuations obtained on the horizontal step faces in vicinity and far downstream of a) 50º-18.6º slope change configuration, at x/l= 0.35 (on 50º sloping chute) and x/l= 0.3 (on 18.6º sloping chute), and b) 50º-30º slope change configuration, at x/l= 0.35 (on 50º sloping chute) and x/l= 0.17 (on 30º sloping chute), for d_c/h =4.6.

6.2.2.4. Probability distribution of the dynamic pressures

Probability distribution of dynamic pressures on the horizontal faces of the steps not influenced by the slope change are compared with the Normal (Gaussian) distribution (straight dashed line) on 50º, 30º and 18.6º sloping chutes for d_c/h=4.6 in Figs. 6.10, 6.11 and 6.12 respectively. Skewness (S_k) and kurtosis (k_u) values are also given. The results indicate that the Normal probability plots obtained along the upstream portion of the horizontal step faces are (x/l>0.5) different from those obtained along the downstream portion (x/l<0.5), irrespective of the sloping chute. For x/l<0.5, a higher and positive skewness was found, showing that large negative pressure values are not as frequent as large positive values (Tennekes and Lumley, 1972), hence a Gaussian model will underestimate the maximum pressures on the step edges

(Amador et. al., 2009). Close to the outer step edge, negative pressures with very low probability were found.

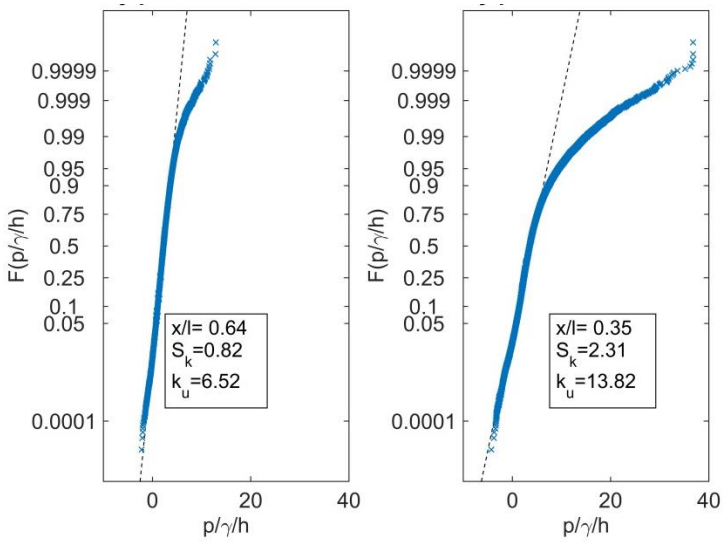

(a) (b)

Figure 6.10 Normal probability plots of dimensionless pressure on the horizontal face of step number -3 (on 50º sloping chute): a) *x/l*=0.64 and b) *x/l*=0.35, for d_c/h =4.6.

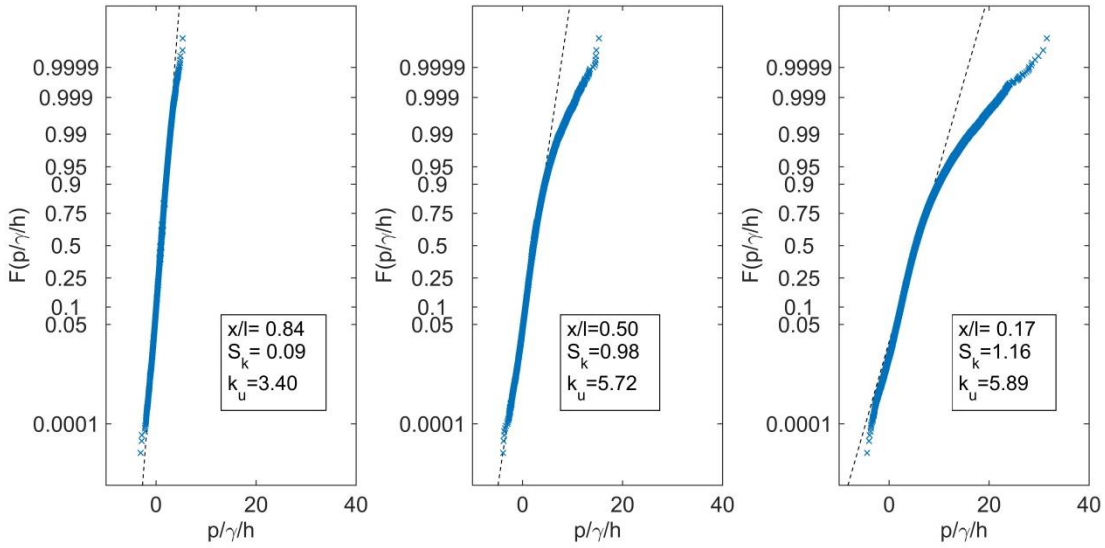

(a) (b) (c)

Figure 6.11 Normal probability plots of dimensionless pressure on the horizontal face of step number +31 (on 30º sloping chute): a) *x/l*=0.84, b) *x/l*=0.50 and c) *x/l*=0.17, for d_c/h =4.6.

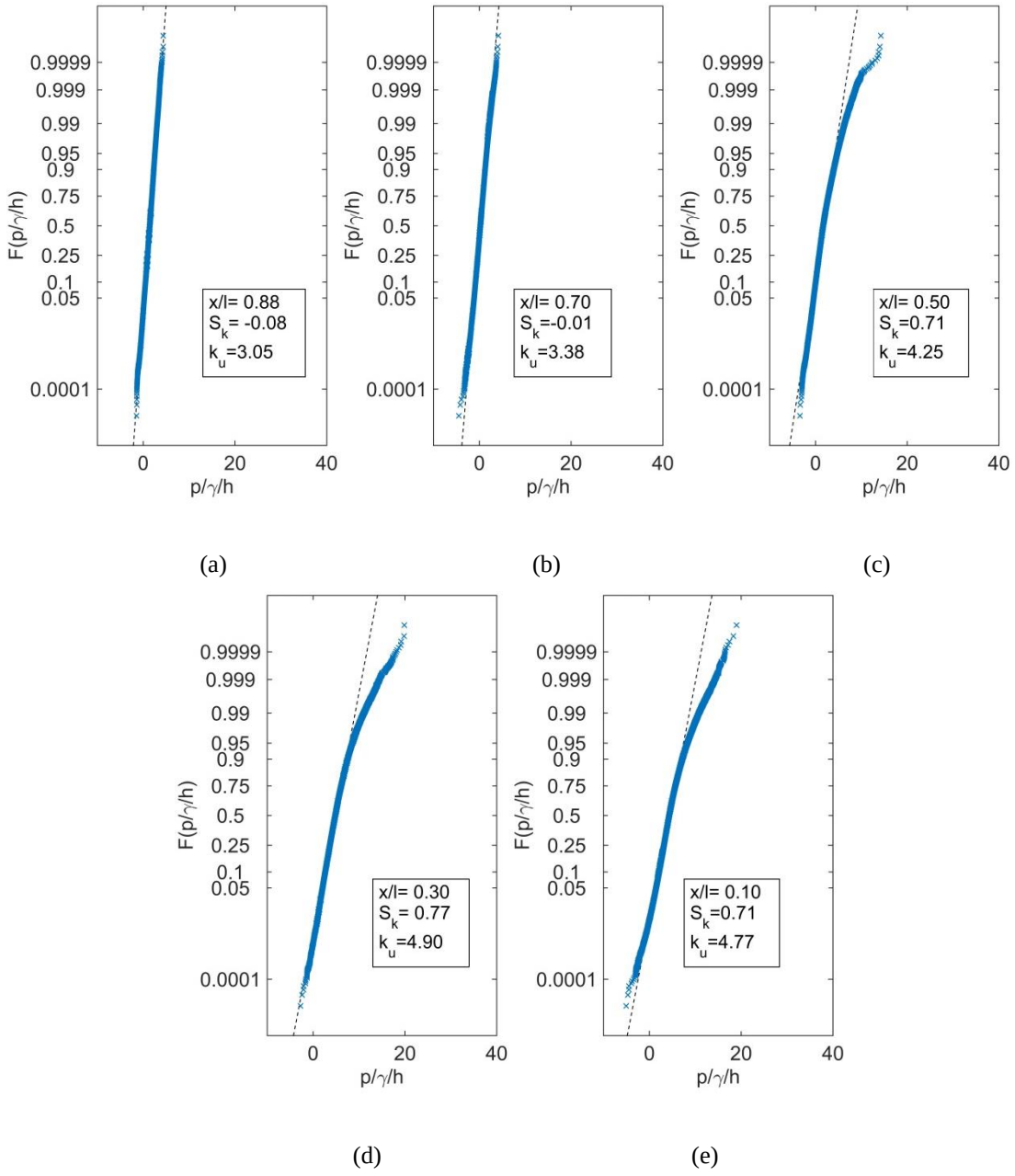

Figure 6.12 Normal probability plots of dimensionless pressure on the horizontal face of step number +20 (on 18.6º sloping chute): a) *x/l*=0.88, b) *x/l*=0.70, c) *x/l*=0.50, d) *x/l*=0.30 and e) *x/l*=0.10, for d_c/h =4.6.

For *x/l*>0.5, smaller pressure fluctuations were found compared with the downstream portion of the steps (*x/l*<0.5) and negative skewness was observed on some recorded signals (e.g. at *x/l*=0.70 and 0.88 on 18.6º sloping chute, Fig. 6.12a,b). The minimum pressure of larger magnitude was observed near to the step inner edges (*x/l*=0.64, 0.84, and 0.88 respectively on 50º, 30º and 18.6º sloping chute steps). Along the inner region of the steps, the pressure distribution was found to be more in agreement with the Gaussian distribution, if compared to

that at the downstream portion of steps. In all cases, the kurtosis greater than 3 was observed. The above-mentioned conclusions are consistent with the findings of Amador et al. (2009).

6.2.3. Dynamic pressure distribution on the vertical step faces

Figures 6.13 and 6.14, indicate the mean, 95th and 5th percentiles of the dimensionless pressure ($p/\gamma/h$) obtained on vertical step faces in the vicinity and far downstream of 50º-18.6º and 50º-30º slope changes, for d_c/h=4.6, where p is the measured dynamic pressure , γ is water specific weight and h is step height. The results indicate a small influence of the location of the pressure sensors, for z/h ranging from 0.3 to 0.7.

When approaching the slope change cross-section, a general trend of increase trend is observed for the mean, 95th and 5th percentiles of the dynamic pressure on the vertical step face, as were observed on horizontal step faces (see section 6.2.1), but with less pronounced maxima. Immediately downstream, the pressure decrease considerably. Minimum negative values of the 5th percentile of the pressure were found on step number +3 (p/γ/h ≈ -4) but not low enough to lead to cavitation, similarly as found in Houston (1987). Regardless of the step number, lower pressures were observed on the vertical step faces in comparison with those on the horizontal step faces, which is consistent with earlier studies on constant sloping stepped chutes (e.g. Sánchez-Juny et al., 2000, 2007, 2008; André, 2004; Amador, 2009; Zhang et al., 2012).

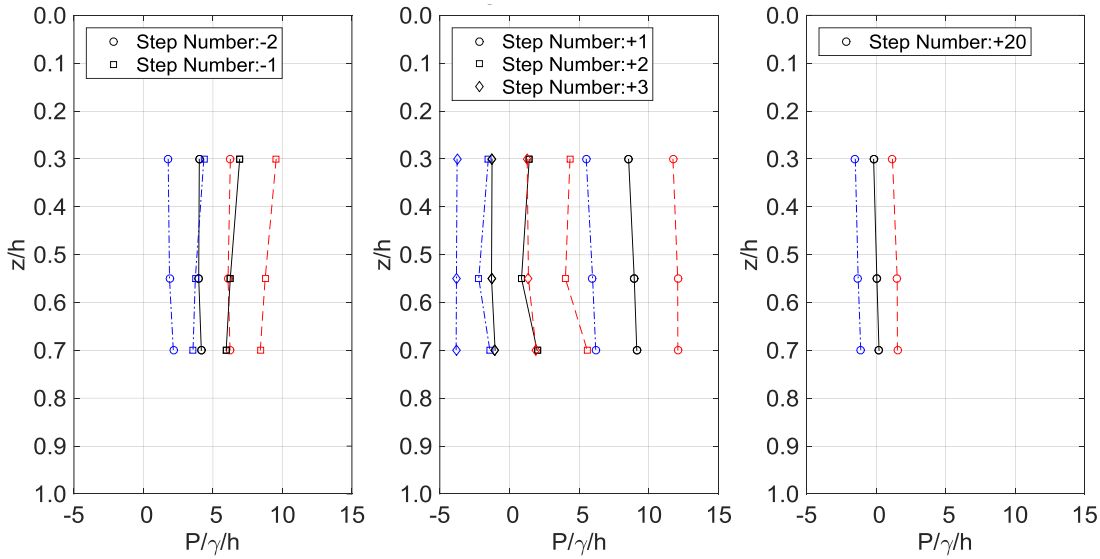

(a) (b) (c)

Figure 6.13 Mean (-), 95th (- -) and 5th (- .) percentiles of the dimensionless pressure on the vertical step faces, in the vicinity and far downstream of the 50º-18.6º slope change, for d_c/h =4.6; h is the step height and z is the distance from the step edge, along the vertical face (see Fig. 3.13a).

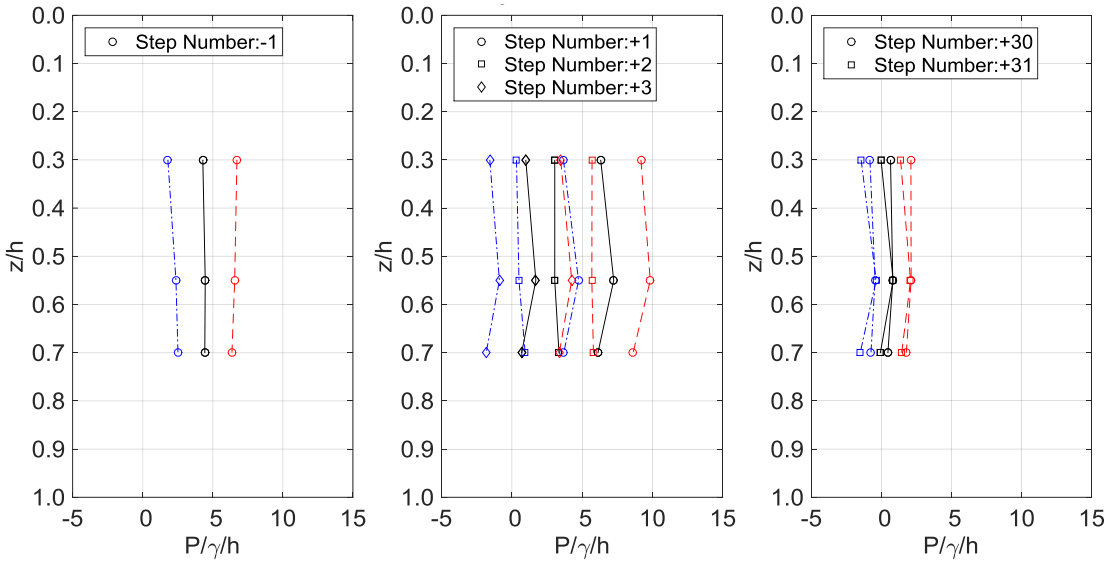

(a) (b) (c)

Figure 6.14 Mean (-), 95th (- -) and 5th (- .) percentiles of the dimensionless pressure on the vertical step faces, in the vicinity and far downstream of the 50º-30º slope changes, for d_c/h =4.6; h is the step height and z is the distance from the step edge, along the vertical face (see Fig. 3.13b).

The above findings for d_c/h = 4.6, are also observed for a broad range of relative critical depths ($2.6 \leq d_c/h \leq 4.6$), as shown in Fig. 6.15, on the 50º-30º slope change configuration. The results show that the higher the discharge, the greater the pressure values observed for the mean, 95th and 5th percentiles.

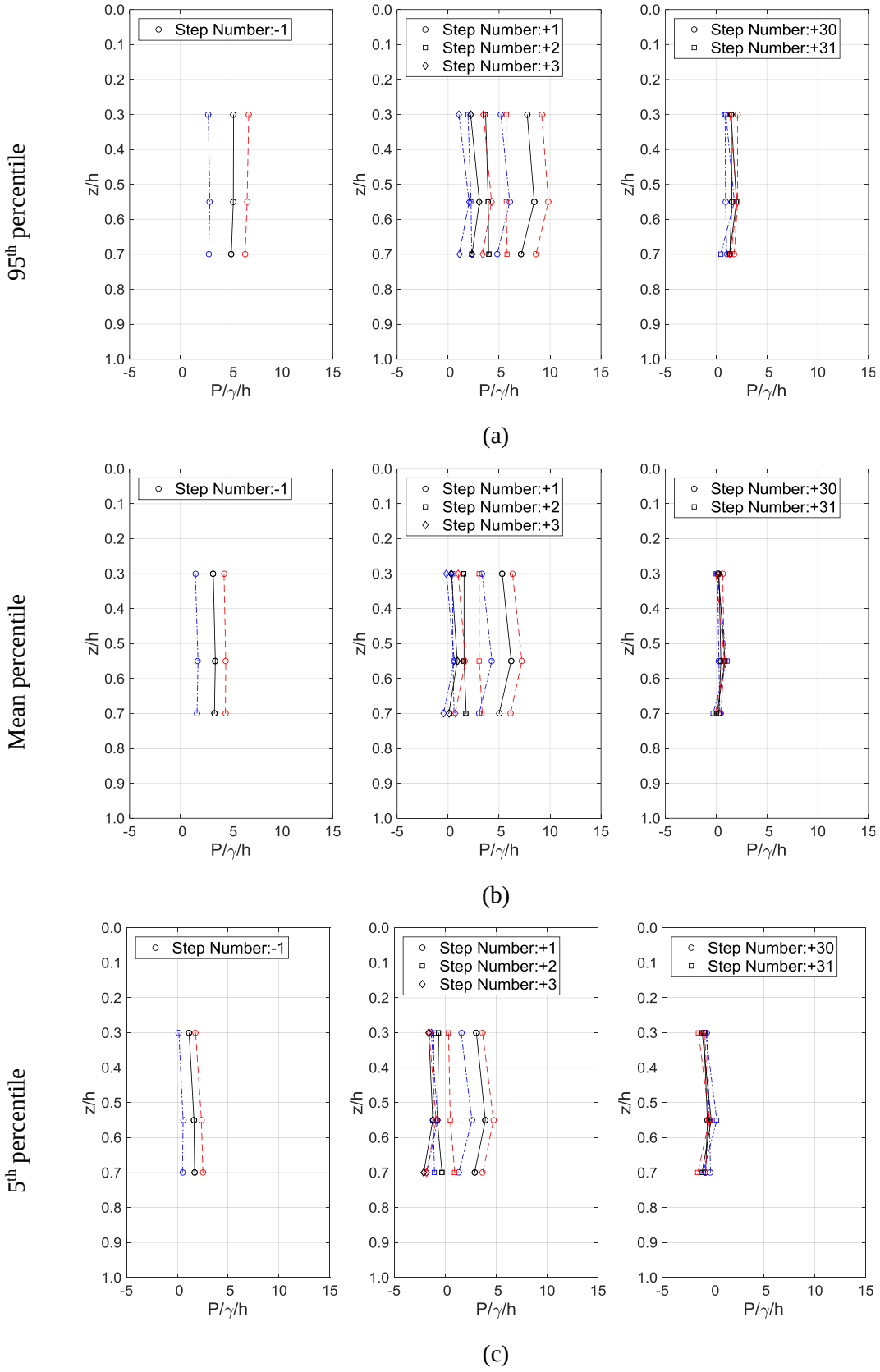

Figure 6.15 Mean, 95th and 5th percentiles of the dimensionless pressure obtained on the vertical step faces, in the vicinity and far downstream of the 50º-30º slope change, for d_c/h = 2.6 (- .), 3.8 (-) and 4.6 (- -).

6.2.3.1. Spectral contents of the pressure signals

Figure 6.16 compares the spectral energy contents obtained near the outer edge of vertical step face (z/h =0.3) in vicinity and downstream of slope change cross-sections, for d_c/h=4.6. The energy content on the vertical step faces increases when approaching the slope change. Near the downstream end of the flatter slopes, lower energy content of flow can be observed which may be expected due to the reduction of the flow velocity with decreasing slope, irrespective of the slope change configuration. Generally, lower energy contents were observed on the vertical step faces in comparison with the PSD curves obtained on the horizontal step faces (see section 6.2.1, Fig. 6.9).

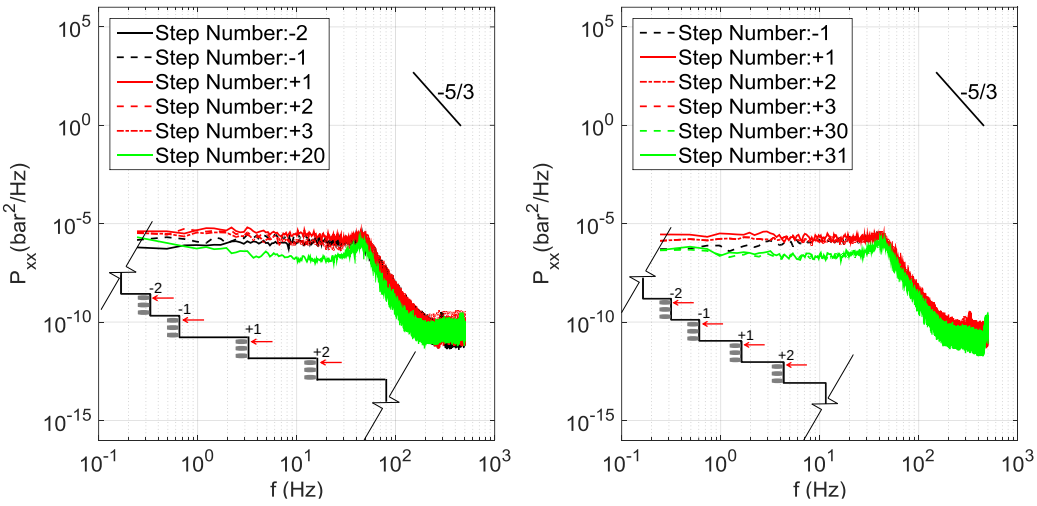

Figure 6.16 PSD of the dynamic pressure fluctuations obtained on the vertical step faces in the vicinity and far downstream of a) 50º-18.6º, and b) 50º-30º slope change, at z/h= 0.3, for d_c/h =4.6.

6.2.3.2. Probability distribution of the dynamic pressures

The probability plot of dynamic pressures on the vertical faces of the steps which were not influenced by the slope change are shown in Figs. 6.17, 6.18 and 6.19 respectively corresponding to 50º, 30º, 18.6º sloping chutes, for d_c/h=4.6. The obtained plots are different from those observed on the horizontal step faces. In the direction of the outer step edge, the skewness decrease and negative values were found for instance at z/h= 0.3 on 50º and 30º sloping chute steps, which indicates that large negative values are more frequent than large positive values (Tennekes and Lumley, 1972). In this case, a Gaussian model underestimates

the extreme minimum pressures, expected to occur close to the step edge on the vertical step faces (Amador et. al., 2009). The pressure sensors located closer to the outer step edge (z/h=0.3) present slightly higher negative pressures, but not low enough to cause cavitation.

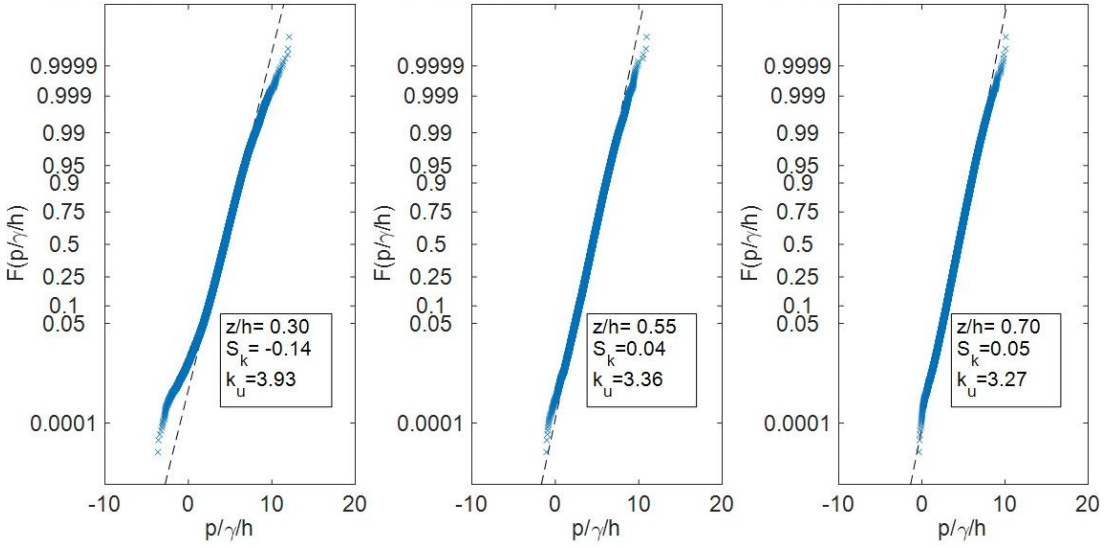

(a) (b) (c)

Figure 6. 17 Normal probability plots of dimensionless pressure on the vertical face of step number -2 (on 50º sloping chute): a) z/h=0.30, b) z/h=0.55 and c) z/h=0.70, for d_c/h =4.6.

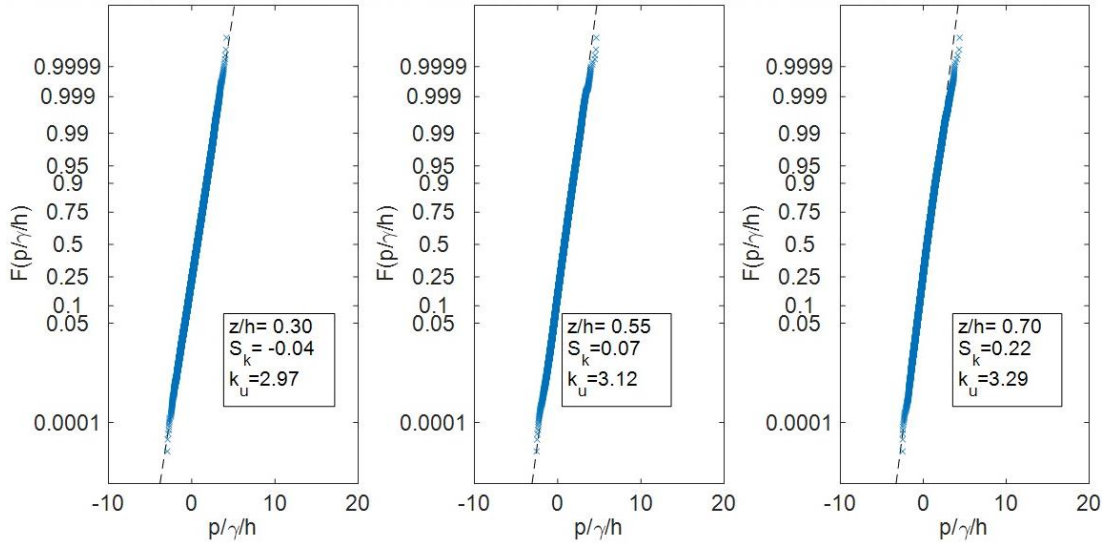

(a) (b) (c)

Figure 6.18 Normal probability plots of dimensionless pressure on the vertical face of step number +31 (on 30º sloping chute): a) z/h=0.30, b) z/h=0.55 and c) z/h=0.70, for d_c/h =4.6.

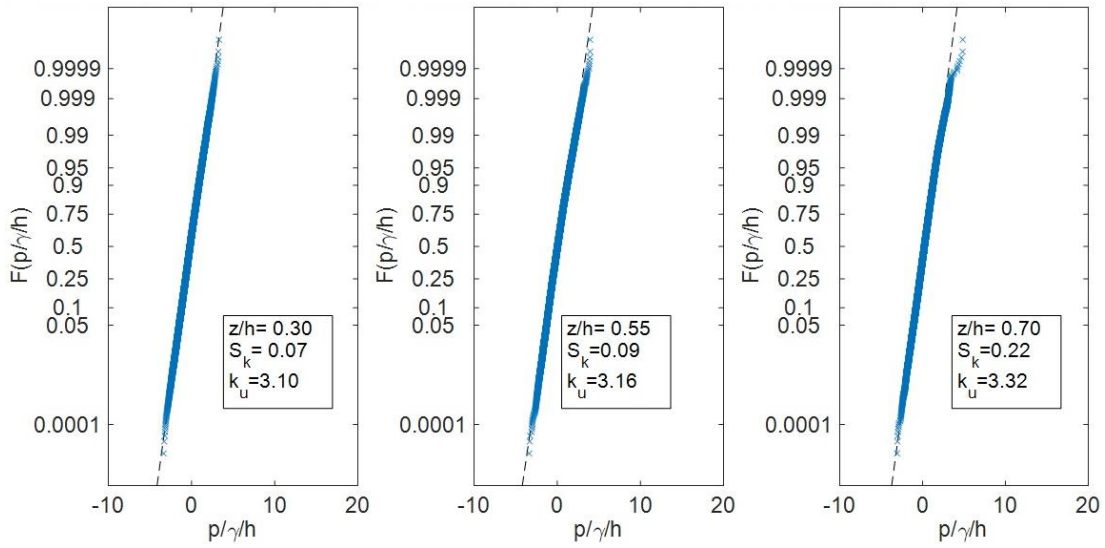

(a) (b) (c)

Figure 6.19 Normal probability plots of dimensionless pressure on the vertical face of step number +20 (on 18.6º sloping chute): a) *z*/*h*=0.30, b) *z*/*h*=0.55 and c) *z*/*h*=0.70, for d_c/h =4.6.

6.3. Conclusions

Even though few prototypes of stepped spillways with abrupt slope changes have been built and operated well to date, there is a lack of understanding on the dynamic pressure field in the vicinity of a slope change. A systematic experimental study was carried out to assess the influence of an abrupt slope change on the dynamic pressure distribution in skimming flow on stepped spillways. Four model test runs were performed on 50º-18.6º ($\Delta\Theta$=31.4º) and 50º-30º ($\Delta\Theta$=20º) slope change configurations, for a range of dimensionless flow rates ($2.6 \leq d_c/h \leq 4.6$). Dynamic pressures were measured on horizontal and vertical step faces in vicinity and far downstream of the slope change cross-section. Time averaged pressures, extreme pressure values, pressure probability distribution and spectral energy content of the pressure fluctuations were analysed.

The basic results showed a significant influence on the pressure development pattern in vicinity of the slope change, in comparison with the typical results on constant sloping stepped spillway flows. A notable increase of the mean, 95th and 5th percentiles of the dynamic pressure and spectral content of pressure signals was observed on the horizontal step faces in the vicinity of the tested slope changes. Mean pressures up to ≈21 times the equivalent clear water depth (≈13 times the step height) were obtained. A similar increasing trend was seen on

the vertical step faces near the slope change, but with less pronounced maxima. Negative values of the 5^{th} percentile of the pressure were found on the vertical step faces, particularly in the vicinity of the slope change. However, they were not found to be severe enough to lead to cavitation. Lower pressure and energy content were observed on vertical step faces in comparison with the horizontal steps faces. Further downstream of the slope change, the pressure and spectral energy content decrease considerably and reach lower values which correspond to the steps not influenced by the slope change, on the flatter sloping chute.

The largest dynamic pressures and associated spectral energy occur on the horizontal step faces near their outer edge, where pressures are influenced by the flow impact, similarly to the results obtained on constant sloping chutes. On the vertical step faces, the pressure sensor location does not have a major influence on the measured pressure values for z/h ranging between 0.3 and 0.7, irrespective of the chute slope.

Along the steps which were not influenced by the slope change, the probability plots obtained on the horizontal step faces differ from those observed on the vertical step faces. On both horizontal and vertical step faces, the pressure distribution does not follow a Gaussian distribution. The dynamic pressures measured near the outer step edge were governed by a higher and positive skewness on the horizontal faces, whereas a lower and even negative skewed distribution was observed near the outer step edge on the vertical step faces.

Part (III)

7

Conclusions and recommendations

7.1. General remarks

A significant number of physical model studies were conducted on the hydraulics of skimming flow over constant sloping stepped spillways. Although some stepped spillways with an abrupt slope change have been built and operated for a considerable period, there is a lack of understanding of its influence on the flow characteristics.

Flow bulking and dynamic pressure development in the vicinity of an abrupt slope change was a particular focus in a few previous experimental and numerical studies (e.g. Houston, 1987; Montes, 1994; 1997; Zarrati et al., 2004). Chanson (2002) and Pfister (2009) addressed the risk of unsatisfactory flow condition on abrupt slope changes, such as jet deflection (on steep to mild slope changes), or a free jet generation (on mild to steep slope changes).

This research investigated the effect of an abrupt slope change on the flow properties in skimming flow on stepped chutes. Nine sets of experiments were carried out including different step heights and discharges on a relatively large scale model of 50º-18.6º ($\Delta\Theta$=31.4º) and 50º-30º ($\Delta\Theta$=20º) abrupt slope changes, assembled at the Laboratory of Hydraulic Constructions (LCH) of EPFL. With the results of the present research project, a better understanding of the effect of an abrupt slope change (steep to mild) on the flow features could be acquired and limited previous findings on flow behaviour over an abrupt slope change on stepped spillways are now more completed. For example, the mean air concentration, characteristic flow depth and consequently equivalent clear water depth development along the influence reach of the slope change can now be estimated by proposed empirical equations for $2.6 \leq d_c/h \leq 9.2$. The tests were conducted in skimming flow, so that all observation described

herein strictly apply to this regime. The following results and conclusions on air entrainment, flow bulking, velocity and pressure distribution as well energy dissipation may be drawn:

7.2. Air entrainment and flow bulking

In this research study, air concentration and air-phase frequency were measured in each of the nine experimental sets. The influence of the tested slope changes on the air entrainment and flow bulking can be summarized in the following conclusions:

- Abrupt slope changes on stepped chutes have a major effect on the air entrainment and flow bulking in the vicinity of the slope change. The magnitude of the tested slope change has a relatively small but non-negligible influence on the air-water flow properties along the reach under the influence of the slope change.

- In general, the reach of influence of the slope change is initiated shortly upstream of its cross-section ($X=(x-x_{sc})/d_c \approx -0.5$), and extends further downstream to $X \approx 9$, for practically all studied range of slope changes and relative critical depths. Hence, for practical purposes, the total length of the chute under the influence of the slope change can be taken as $L_t \approx 9.5 d_c$.

- Four main local sub-regions have been found to describe the typical air-water flow patterns in the vicinity and further downstream of the slope change cross-section, namely with regard to the mean (depth-averaged) air concentration, air concentration distribution, pseudo-bottom air concentration, air-phase frequency and characteristic flow depths.

- In general, both the mean (depth-averaged) air concentration and the local air concentration (for identical distance to the pseudo-bottom), decrease when approaching the slope change cross-section, in sub-region (I), whereas they increase shortly downstream, in sub-region (II). A peak in the mean air concentration is reached for $X \approx 5$, followed by its decrease until an approximately constant value is reached, at the downstream end of sub-region (III) ($X \approx 9$). Within the reach under the influence of the slope change, the air concentration distribution evolves from a S-shape distribution towards a more stretched profile. Despite the de-aeration in vicinity of slope change for the tested range of upstream and downstream slopes, the air concentration close to the pseudo-bottom remains larger than 10%, which is expected to assure protection of the step surfaces against cavitation damage.
- It was found that with increasing the slope change magnitude from $\Delta\Theta=20^{\circ}$ *to* $\Delta\Theta=31.4^{\circ}$, de-aeration increased 28%.

- In the vicinity of the slope change, a significant modification occurs in the dimensionless air-phase frequency (fd_c/V_c) profiles, the maximum cross-sectional value of fd_c/V_c increases and its location moves towards the free surface ($y/Y_{90} \approx$ 0.6-0.8). Shortly downstream of the slope change, the maximum cross-sectional value of fd_c/V_c decreases and its location moves towards the pseudo-bottom ($y/Y_{90} \approx$ 0.1-0.3). Further downstream, the fd_c/V_c profiles continue to readjust until their shape approach that corresponding to the gradually or quasi-uniform flow on the flatter slope.
- In the reaches not affected by the slope change, hence in gradually varied or quasi-uniform flow, the location of the maximum dimensionless air-phase frequency seems to be influenced by the chute slope ($y/Y_{90} \approx$ 0.2 and 0.7 for 50º and 18.6º chute slopes, respectively).
- Maximum air-phase frequency occurs approximately for C equal to 30-40%, regardless of the slope change configuration. Slight sharper profiles were observed for the 50º sloping chute, when compared to those for the 18.6º and 30º slopes.
- The characteristic flow depths (i.e., Y_{90}, Y_{95}, Y_{99}) remain practically constant upstream of the slope change cross-section, whereas a significant increase is noticeable further downstream, followed by a decrease until an approximately constant value is reached. In general, peak values are obtained for $X \approx 5$ which has to be considered for designing the side walls. In contrast, the streamwise development of the equivalent clear water depth is not significantly influenced by the slope change, except in its vicinity.
- It was found that with increasing the slope change magnitude from $\Delta\Theta$=20˚ *to* $\Delta\Theta$=31.4˚, the maximum flow depth Y_{99max}/d_c increased 25%.
- The maximum bulked flow depth Y_{99max} is in general lower than or approximately equal to the critical depth, but on the 50º-18.6º slope change configuration, for d_c/h = 2.6, considerable larger values were obtained ($Y_{99max}/d_c \approx 1.6$).
- Minimum discharges in the lower skimming flow regime or even the transition flow regime could perform differently, as the tests with $d_c/h \geq 2.6$ suggest. Such flows would generate higher local C_{mean} and C_b values, related to a more pronounced spray occurrence.
- The tested slope change was abrupt. A gradual change would certainly reduce the flow bulking and the de-aeration up to a certain degree, as the pressure gradient is distributed on longer flow distance.

7.3. Velocity distribution and energy dissipation

Velocity distribution and energy dissipation were analysed on six test runs with a step height of 0.06 m. The results showed that both the velocity distribution and specific energy are highly influenced by the slope change. The main conclusions are listed below:

- The results demonstrated that along the reaches not influenced by the slope change, the distribution of the dimensionless flow velocity is a function of the chute slope and follows the power law distribution, typical of the gradually or quasi-uniform flow on stepped chutes.
- The power law exponent (N) decreases with increasing chute slope. Accordingly, typical N exponent observed on 50º, 30º and 18.6º sloping chutes were respectively equal to 5.6, 6.2, and 8.2.
- Within the reach under the influence of the slope change, a significant modification occurs in the dimensionless velocity distribution and the respective profiles do not follow the power law distribution.
- Downstream of the reach under the influence of slope change, the velocity profiles readjust their shape to the power law distribution.
- The streamwise development of V_{mean}/V_c, α, and E/d_c along the chute was found to increase upstream of the slope change cross-section ($X \approx -0.5$), whereas it decreases shortly downstream of slope change cross-section, reaching the values corresponding to the flatter sloping chute ($X \approx 9$). The results obtained in the vicinity of the slope change should however be taken with caution, because of the considerable flow curvature in such region.
- The relative head loss on the slope change region varied roughly between 38% to 51% for the tested relative critical depths and slope change configurations.
- The relative head loss was found to decrease with the increase of the relative critical depth.

7.4. Dynamic pressure distribution

The influence of the slope change on the dynamic pressures was analysed on horizontal and vertical step faces in vicinity and far downstream of the slope change cross-section. Time averaged pressures, extreme pressure values, pressure probability distribution and spectral energy content of the pressure fluctuations were also analysed by means of the results of four test runs with step height of 0.06 m. Based on the results of these experiments; the following conclusions can be drawn:

- Basic results showed a significant influence of the pressure development pattern in vicinity of the slope change, in comparison with the typical results on constant sloping stepped spillway flows.
- A notable increase of the mean, 95^{th} and 5^{th} percentiles of the dynamic pressure and spectral content of pressure signals was observed on the horizontal step faces in the vicinity of the tested slope changes.
- Mean pressures up to ≈21 times the equivalent clear water depth (≈13 times the step height) were obtained. A similar increasing trend was seen on the vertical step faces near the slope change, but with less pronounced maxima. Negative values of the 5^{th} percentile of the pressure were found on the vertical step faces, particularly in the vicinity of the slope change. However, they were not expected to be severe enough to produce cavitation.
- It was found that with increasing the slope change magnitude from $\Delta\Theta$=20˚ *to* $\Delta\Theta$=31.4˚, maximum dimensionless mean pressures ($p/\gamma/h$) and maximum $P/(\gamma d_{w\,up} cos\theta)$ increased 29% and 32% respectively .
- Lower pressures and energy content were observed on the vertical step faces in comparison with the horizontal steps faces. Further downstream of the slope change, the pressure and spectral energy content decrease considerably and reach the lower values which correspond to the steps not influenced by the slope change, on the flatter sloping chute.
- The largest dynamic pressures and associated spectral energy occur on the horizontal step faces near their outer edge, where pressures are influenced by the flow impact, similarly to the results obtained on constant sloping chutes.
- On the vertical step faces, the pressure sensor location does not have a major influence on the pressure values for *z/h* ranging between 0.3 and 0.7, irrespective of the chute slope.
- Along the steps not influenced by slope change, the probability plots obtained on the horizontal step faces differ from those observed on the vertical step faces, both being considerably different from a Gaussian distribution.
- The dynamic pressures measured near the outer step edge were governed by a higher and positive skewness on the horizontal faces, whereas a lower and even negative skewed distribution was observed near the outer step edge on the vertical step faces.

7.5. Recommendations for future work

The following issues could be addressed in future research investigations to improve the knowledge on the flow behaviour over abrupt slope changes on stepped chutes:

- As introduced in Chapter 3, the present study investigated only two slope change configurations, with a fixed upstream chute slope of 50º. Future studies could examine additional configurations of slope changes, particularly with distinct upstream chute slope, as well as additional flow regimes and conditions upstream of the slope change, such as transition flow regime or non-uniform skimming flow (not fully developed).
- Further, the present study focused on the pressure distribution only in vicinity of the slope change, namely in sub-regions (I) and (II), ($-0.5 < X \leq 5$). However, it would be interesting to investigate the pressure development along sub-region (III), where the flow impacts on the pseudo-bottom ($5 \leq X \leq 9$).
- Prototype measurements on existing stepped spillways with an abrupt slope change (e.g. Lower Siah-Bishe dam stepped spillway) would be also attractive in order to provide results exempted from scale effects, especially regarding dynamic pressures.
- In addition to the experimental model or prototype measurements, the numerical simulation of air-water flow over slope changes could be conducted in future research.
- Possible solutions to prevent or minimize the flow disturbance (e.g. flow bulking, high pressure impact, and de-aeration) could be also tested by implementing gradual change (transitional steps) in the vicinity of the slope change.
- The study of the flow properties on mild to steep abrupt slope changes on stepped spillways may also be of interest.

Altogether, these investigations may provide a solid ground for the hydraulic design criteria of stepped spillways with slope changes.

Bibliography

Amador, A. (2005). Comportamiento Hidráulico de los Aliviaderos Escalonados en Presas de Hormigón Compactado, *Ph.D. thesis*, UPC, Barcelona, Spain (in Spanish).

Amador, A., Sánchez-Juny, M., and Dolz, J. (2005). Discussion of "two phase flow characteristics of stepped spillways" by Boes, R. and Hager, W.J., in *Journal of Hydraulic Engineering*, 131(5), 419-429.

Amador, A., Sánchez-Juny, M. and Dolz, J. (2009). Developing flow region and pressure fluctuations on steeply sloping stepped spillways. *Journal of Hydraulic Engineering*, 135(12), 1092-1100.

André, M., Ramos, P. and Matos, J. (2005). Dissipação de energia em descarregadores de cheia em degraus. Aplicação a descarregadores com largura constante e com paredes convergentes. *7th SILUSBA*, APRH, Evora, Portugal (in Portuguese).

André, S. (2004). High velocity aerated flows over stepped chutes with macro-roughness elements. *Thesis No. 2993, EPFL, and Communication LCH No. 20*, (Eds.), A.J. Schleiss, Lausanne, Switzerland.

André, S., Matos, J., Boillat, J.-L and Schleiss, A.J. (2004). Energy dissipation and hydrodynamic forces of aerated flow over macro-roughness linings for overtopped embankment dams. in Yazdandoost, F., and Attari, J. (Eds.), *Proceedings of International Conference on Hydraulics of Dams and River Structures*, Tehran, Iran, Taylor&Francis Group, London, ISBN 90 5809 632 7, 189-196.

André, S., and Schleiss, A. J. (2008). Discussion of "Pressure on a stepped spillway" by Sánchez-Juny, M., Bladé, E. and Dolz, J., in *Journal of Hydraulic Research*, 46(4), 574-576.

Baumann A., Arefi F. and Schleiss A.J. (2006). Design of two stepped spillways for a pumped storage scheme in Iran. *Proceedings of the International Conference Hydro 2006, Maximising the benefits of hydropower*, Porto Carras, Greece (CD-ROM).

Boes, R. M. (2000a). Zweiphasenströmung und Energieumsetzung auf Grosskaskaden, *Ph.D. thesis*, VAW, ETH Zurich, Switzerland (in German).

Boes, R.M. (2000b). Scale effects in modelling two-phase stepped spillway flow. *Proceedings of International Workshop on Hydraulics of Stepped Spillways*, VAW, ETH Zurich, Minor, H.-E., and Hager, W.H., (Eds.). Balkema, Rotterdam, 53-60.

Boes, R.M. and Minor, H.-E. (2000). Guidelines for the hydraulic design of stepped spillways. *Proceedings of the International Workshop on Hydraulics of Stepped Spillways*, VAW, ETH Zurich, Minor, H.-E., and Hager, W.H., (Eds.). Balkema, Rotterdam, 163-170.

Boes, R. M. and Hager, W.H. (2003a). Hydraulic design of stepped spillways. *Journal of Hydraulic Engineering*, 129(9), 671-679.

Boes, R. M. and Hager, W.H. (2003b). Two-Phase flow characteristics of stepped spillways. *Journal of Hydraulic Engineering*, 129(9), 661-670.

Bung, D.B. (2009). Zur selbstbelüfteten Gerinneströmung auf Kaskaden mit gemässigter Neigung, *Ph.D. thesis*, Bergische University of Wuppertal, Germany (in German).

Bung, D.B. (2011). Developing flow in skimming flow regime on embankment stepped spillways. *Journal of Hydraulic Research*, 49(5), 639–648.

Bung, D.B. and Schlenkhoff, A. (2010). Self-aerated skimming flow on embankment stepped spillways: the effect of additional micro-roughness on energy dissipation and oxygen transfer. *Proceedings of 1st European IAHR Congress*, Edinburgh, Flash-drive.

Carosi, G., and Chanson, H., (2006). Air-water time and length scales in skimming flow on a stepped spillway. Application to the Spray Characterisation, *Report No. CH59/06*, Division of Civil Engineering, The University of Queensland, Brisbane, Australia.

Carosi, G., and Chanson, H. (2008). Turbulence characteristics in skimming flows on stepped spillways. *Canadian Journal of Civil Engineering*, 35(9), 865-880.

Chamani, M.R. (2000). Air inception in skimming flow regime over stepped spillways. in Minor, H.E. and Hager, W.H. (Eds) *Proceedings of the Int. Workshop on Hydraulics of Stepped Spillways*, Zürich, Switzerland, Balkema, 61-67.

Chamani, M.R. and Rajaratnam, N. (1999). Characteristics of skimming flow over stepped spillways. *Journal of Hydraulic Engineering*, 125(4), 361-368.

Chanson, H. (1994). *Hydraulic design of stepped cascades, channels, weirs and spillways*. Pergamon, Oxford, UK.

Chanson, H. (1997). *Air bubble entrainment in free surface turbulent shear flows*. Academic Press, London.

Chanson, H. (2002). *The hydraulics of stepped chutes and spillways*. Balkema, Lisse, the Netherlands.

Chanson, H. (2006). Hydraulics of skimming flows on stepped chutes: the effects of inflow conditions. *Journal of Hydraulic Research*, 44(1), 51-60.

Chanson, H. (2015). Discussion of "Cavitation potential of flow on stepped spillways" by Frizell, K.W., Renna, F.M., and Matos, J., in *Journal of Hydraulic Engineering*, 141(5), 07014025-1-07014025-2.

Chanson, H. and Gonzalez, C.A. (2005). Physical modelling and scale effects of air-water flows on stepped spillways, *Journal of Zhejiang University*, 6A (3), 243-250.

Chanson, H. and Toombes, L. (2002). Air-water flows down stepped chutes: turbulence and flow structure observations. *International Journal of Multiphase Flow*, 28(11), 1737-1761.

Chanson, H. and Toombes, L. (2004). Hydraulics of stepped chutes: The transition flow. *Journal of Hydraulic Research*, 42(1), 43-54.

Chaumat, H., Billet-Duquenne, A.M., Augier, F., Matthieu, C., and Delmas, H. (2007). On the reliability of an optical fibre probe in bubble column under industrial relevant operating conditions. *Experimental Thermal and Fluid Science*, 31(6), 495-504.

Christodoulou, G. C. (1993). Energy dissipation on stepped spillways. *Journal of Hydraulic Engineering*, 119, (5), 644-650.

Christodoulou, G. (1999). Design of stepped spillways for optimal energy dissipation. *International Journal of Hydropower & Dams*, 5, 90-93.

Estrella, S., Sánchez-Juny, M., Dolz, J., Ibanez, R., Dominguez, M., Balairon, L. and Lopez,D. (2012). Velocity and air concentration in air-water flow: application on a stepped spillway without sidewalls. *IAHR International Symposium of Hydraulic Structures*, Porto, Portugal.

Falvey, H. T. (1990). Cavitation in chutes and spillways. *Engineering monographs 42, USBR ed., U.S. Dept. of the Interior, Bureau of Reclamation*, Denver, Colorado.

Felder, S. (2013). Air-water flow properties on stepped spillways for embankment dams: aeration, energy dissipation and turbulence on uniform, non-uniform and pooled stepped chutes. *PhD. thesis*, School of Civil Engineering, The University of Queensland, Australia.

Felder, S., and Chanson, H. (2009a). Energy dissipation, flow resistance and gas-liquid interfacial area in skimming flows on moderate-slope stepped spillways. *Environmental Fluid Mechanics*, 9(4), 427-441.

Felder, S., and Chanson, H., (2009b), Turbulence, dynamic similarity and scale effects in high-velocity free-surface flows above a stepped chute, *Experimental Fluids*, 47(1), 1-18.

Felder, S., and Chanson, H., (2011a). Air-water flow properties in step cavity down a stepped chute. *International Journal of Multiphase flow*, 37(7), 732-745.

Felder, S., and Chanson, H. (2011b). Energy dissipation down a stepped spillway with non-uniform step heights. *Journal of Hydraulic Engineering*, 137(11), 1543-1548.

Felder, S., and Chanson, H. (2015). Phase-detection probe measurements in high-velocity free-surface flows including a discussion of key sampling parameters, *Journal of Experimental Thermal and Fluid Science*, 61(1), 66-78.

Frizell, K.H. (1990). Hydraulic model study of McClure dam existing and proposed stepped spillways. *Hydraulic Laboratory Report R-90-02*, U.S. Department of the Interior, Bureau of Reclamation, Denver, Colorado, USA.

Frizell, K.H. (2006). Research state-of-the-art and needs for hydraulic design of stepped spillways. *Hydraulic Laboratory Report HL-2005-06, U.S. Department of the Interior, Bureau of Reclamation*, Denver, Colorado, USA.

Frizell, K.W., Renna, F.M., and Matos, J. (2013). Cavitation potential of flow on stepped spillways. *Journal of Hydraulic Engineering*, 139(6), 630-636.

Frizell, K.W., Renna, F.M., and Matos, J. (2015). Closure to "Cavitation potential of flow on stepped spillways", in *Journal of Hydraulic Engineering*, 141(5), 07015009-1-07015009-2.

Gomes, J. F., (2006). Campo de Pressões: Condições de Incipiência à Cavitação em Vertedouros em Degraus com Declividade 1V:0,75H, *Ph.D. thesis*, UFRGS-IPH, Porto Alegre, Brazil (in Portuguese).

Gomes, J. F., Amador, A. T., Marques, M., Matos, J. and Sánchez-Juny, M. (2006). Hydrodynamic pressure field on steeply sloping stepped spillways, in Matos, J., and Chanson, H (Eds). *Proceedings of the International Junior Researcher and Engineer Workshop on Hydraulic Structures* (IJREWHS'06), Montemor-o-Novo, Report CH61/06, Div. of Civil Eng., The University of Queensland, Brisbane, Australia, 71-80.

Gonzalez, C. (2005). An experimental study of free surface aeration on embankment stepped chutes, *Ph.D. thesis*, University of Queensland, Brisbane, Australia.

Gonzalez, C.A., and Chanson, H. (2004). Interactions between cavity flow and main stream skimming flows: an experimental study. *Canadian Journal of Civil Engineering*, 31(1), 33-44 (ISSN 0315-1468)

Gonzalez, C.A. and Chanson, H. (2008). Turbulence and cavity recirculation in air-water skimming flows on a stepped spillway. *Journal of Hydraulic Research*, 46(1), 65-72.

Gonzalez, C.A., Takahashi, M. and Chanson, H. (2008). An experimental study of effects of step roughness in skimming flows on stepped chutes. *Journal of Hydraulic Research*, 46 (Extra Issue 1), 24-35.

Guo, J., Liu, Z., and Lu, Y. (2003). Field observation on the RCC stepped spillways with the flaring pier gate on the Dachaoshan project, in Ganoulis, J. and Prinos, P. (Eds.), *Proceedings of the 30th IAHR Biennial Congress*, Thessaloniki, Greece, Vol. B, 473-478.

Hager, W.H, Pfister, M (2013). Stepped spillways: technical advance from 1900. *35th IAHR World Congress*, Chengdu, 1-8.

Hakoishi, N. and Sumi, T. (2000). Hydraulic design of Nakasujigawa dam stepped spillway. *Proceedings of International Workshop on Hydraulics of Stepped Spillways*, ETH Zurich, Balkema, Rotterdam, 27-34.

Houston, K.L. (1987). Hydraulic model studies of Upper Stillwater dam stepped spillway and outlet works. *Report No. REC-ERC-87-6, U.S. Department of Interior, Bureau of Reclamation*, Denver, USA.

Hunt, S.L., and Kadavy, K.C. (2011). Inception point relationship for flat-slopped stepped spillways. *Journal of Hydraulic Engineering*, 137(2), 262-266.

Hunt, S. L., and Kadavy, K. C. (2013). Inception point for embankment dam stepped spillways. *Journal of Hydraulic Engineering*, 138(9), 796-802.

Hunt, S.L., Kadavy, P.E., Abt, S.R, and Temple, D.M. (2008). Impact of converging chute walls for roller compacted concrete stepped spillways. *Journal of Hydraulic Engineering*, 134(7), 1000-1003.

Kavianpour, M.R and Masoumi, H.R. (2008). New approach for estimating of energy dissipation over stepped spillways. *International Journal of Civil Engineering*, 6(3), 230-237.

Khatsuria, R. M. (2008). Discussion of "Experimental study of transition and skimming flows on stepped spillways in RCC dams: qualitative analysis and pressure measurements" by Sánchez-Juny, M. and Dolz, J. in *Journal of Hydraulic Research*, 46(1), 175-176.

Kobus, H. (1985). *An introduction to air-water flows in hydraulics. Institute of Hydraulic Engineering, University of Stuttgart*.

Mateos, C. and Elviro, V. (1997). Initiation of aeration in stepped spillways. in Holly Jr. F.M. and Alsaffar, A. (Eds) *Proceedings of the 27th IAHR Congress*, Theme D, 589–594.

Mateos, J., Iguacel, C., Garcia, E. V., (2001). Initiation of aeration in stepped spillways. *29th Proceedings of IAHR Congress*, Beijing, China, 589-596.

Matos, J., (1999). Emulsionamento de ar e dissipação de energia do escoamento em descarregadores em degraus, *Ph.D. thesis*, IST, Lisbon, Portugal (in Portuguese).

Matos, J. (2000). Hydraulic design of stepped spillways over RCC dams. *Proceedings of International Workshop on Hydraulics of Stepped Spillways*, VAW, ETH Zurich, Minor, H.-E., and Hager, W.H., (Eds.). Balkema, Rotterdam, 187-194.

Matos, J., Quintela, A. C., and Ramos, C. M. (2001). Sobre a protecção contra a erosão por cavitação em descarregadores em degraus. *Recursos Hídricos*, 23(1) (in Portuguese).

Matos, J., Sánchez-Juny, M., Quintela, A. and Dolz, J. (1999). Characteristic depth and pressure profiles in skimming flow over stepped spillways. in Bergmann, H., Krainer, R. and Breinhälter, H. (Eds.) *Proceedings of the 28th IAHR Congress*, Graz, Austria.

Matos, J., Sánchez-Juny, M, Quintela, A. and Dolz, J. (2000). Air entrainment and safety against cavitation damage in stepped spillways over RCC dams. in Minor, H.E. and Hager, W.H. (Eds.) *Proceedings of the International Workshop on Hydraulics of Stepped Spillways*, Zürich, Switzerland, Balkema, 69-76.

Matos, J. and Meireles, I. (2014). Hydraulics of stepped weirs and dam spillways: engineering challenges, labyrinths of research. in Chanson, H. and Toombes, L., Hydraulic structures and society - Engineering challenges and extremes, *Proceedings of 5th IAHR International Symposium on Hydraulic Structures*, Brisbane, Australia, 1-30.

Meireles, I. and Matos, J. (2009). Skimming flow in the non-aerated region of stepped spillways over embankment dams. *Journal of Hydraulic Engineering*, 135(8), 685-689.

Meireles, I., Renna, F., Matos, J. and Bombardelli, F.A. (2012). Skimming, nonaerated flow on stepped spillways over roller compacted concrete dams. *Journal of Hydraulic Engineering*, 138(10), 870-877.

Montes, J.S. (1994). Potential flow solution to 2D transition from mild to steep slopes. *Journal of Hydraulic Engineering*, 120(5), 601-621.

Montes, J.S. (1997). Irrotational flow and real fluid effects under planar sluice gates. *Journal of Hydraulic Engineering*, 123(3), 219-232.

Ohtsu, I. and Yasuda, Y. (1997). Characteristics of flow conditions on stepped channels. *Proceedings of 27th IAHR Congress*, San Francisco, USA, 583-588.

Ohtsu, I., Yasuda, Y., and Takahashi, M. (2004). Flow characteristic of skimming flow in stepped channels. *Journal of Hydraulic Engineering*, 130, (9), 860-869.

Ostad Mirza, M. J., Matos, J., Pfister, M., and Schleiss, A. J. (2015a). Air entrainment and pressure development in skimming flow on an abrupt slope change on stepped spillways. *E-proceedings of the 36th IAHR World Congress*, The Hague, the Netherlands, 1-9. URL: http://89.31.100.18/~iahrpapers/87169.pdf

Ostad Mirza, M. J., Pfister, M., Schleiss, A. J., and Matos, J. (2015b). Air entrainment in skimming flow on stepped spillways: the effect of an abrupt slope change. *5th IAHR International Junior Researcher and Engineer Workshop on Hydraulic Structures*, Spa, Belgium [En ligne], URL: http://popups.ulg.ac.be/IJREWHS2014/index.php?id=96

Pegram, G., Officer, A. and Mottram, S. (1999). Hydraulics of skimming flow on modelled stepped spillways. *Journal of Hydraulic Engineering*, ASCE, 125(4), 361-368.

Peterka, A. J. (1953). The effect of entrained air on cavitation pitting. *Proceedings of 5th IAHR Congress*, Minneapolis, 507-518.

Pfister, M. (2009). Effect of control section on stepped spillway flow. *Proceedings of 33rd IAHR Biennial Congress*, Vancouver, Canada, 8 pages.

Pfister, M., Hager, W.H., Minor, H.-E. (2006a). Bottom aeration of stepped spillways. *Journal of Hydraulic Engineering*, 132, (8), 850-853.

Pfister, M., Hager, W.H., Minor, H.-E., (2006b). Stepped chutes: pre-aeration and spray reduction. *International Journal of Multiphase Flow*, 32 (2), 269–284.

Pfister, M. and Hager, W.H. (2011). Self-entrainment of air on stepped spillways. *International Journal of Multiphase Flow* 37(2), 99-107.

Pfister, M., and Chanson, H. (2014). Two-phase air-water flows: scale effects in physical modelling. *Journal of Hydrodynamics*, 26(2), 291-298.

Rajaratnam, N. (1990). Skimming flow in stepped spillways. *Journal of Hydraulic Engineering*, 116, (4), 587-591.

Rice, C. E. and Kadavy, K. C. (1996). Model study of a roller compacted concrete stepped spillway, *Journal of Hydraulic Engineering*, 122, (6), 292-297.

Sánchez-Juny, M., Pomares, J. and Dolz. J. (2000). Pressure field in skimming flow over a stepped spillway. *Proceedings of International Workshop on Hydraulics of Stepped Spillways*, VAW, ETH Zurich, Minor, H.-E., and Hager, W.H., (Eds.). Balkema, Rotterdam, 137-145.

Sánchez-Juny, M., Bladé, E. and Dolz, J. (2007). Pressure on a stepped spillway. *Journal of Hydraulic Research*, 45(4), 505-511.

Sánchez-Juny, M., Bladé, E. and Dolz, J. (2008). Analysis of pressure on a stepped spillway. *Journal of Hydraulic Research*, 46(3), 410-414.

Sánchez-Juny, M., Dolz, J. (2005).Experimental study of transition and skimming flows on stepped spillways in RCC dams: qualitative analysis and pressure measurements. *Journal of Hydraulic Research*, 43(5), 540-548.

Schleiss, A. J. (2009). Discussion of "Turbulence characteristics in skimming flows on stepped spillways" by Carosi, G. and Chanson, H., in *Canadian Journal of Civil Engineering*, 36(4), 677-677.

Sorensen, R. M. (1985). Stepped spillway hydraulic model investigations. *Journal of Hydraulic Engineering, ASCE*, 111, (12), 1461-1472.

Stephenson, D. (1988). Stepped energy dissipators. *Proceedings of IAHR International Symposium on Hydraulics for High Dams*, Madrid, Spain, 1228-1235.

Takahashi, M., and Ohtsu, I. (2012). Aerated flow characteristics of skimming flow over stepped chutes. *Journal of Hydraulic Research*, 50(4), 427-434.

Takahashi, M., Yasuda, Y., Ohtsu, I. (2005). Effect of Reynolds number on characteristics of skimming flows in stepped channels. *Proceedings 31st IAHR Congress*, Seoul, 2880-2889.

Takahashi, M., Yasuda, Y., Ohtsu, I. (2006). Effect of Reynolds number on characteristics of aerated flow in stepped channels. *Ann. Journal of Hydraulic Engineering*, 50(1), 871-876 (in Japanese).

Tennekes, H., Lumley, J. L. (1972). *A first course in turbulence. The MIT Press, Cambridge. Massachusetts and London, England.*

Terrier S., Pfister, M., and Schleiss, A. J. (2015). Comparison of chute aerator effect on stepped and smooth spillways. *E-proceedings of the 36th IAHR World Congress*, The Hague, the Netherlands, 1-5.

Toombes, L. (2002). Experimental study of air-water flow properties on low-gradient stepped cascades. *PhD Thesis*, University of Queensland, Brisbane.

USBR (1965). *Design of small dams. Bureau of Reclamation, US Department of the Interior, Denver CO, USA, 3rd edition.*

Willey, J., Ewing, T., Lesleighter, E., and Dymke, J. (2010). Numerical and physical modeling for a complex stepped spillway. *Journal of Hydropower & Dams*, 3, 103-113.

Wood, I.R. (1985). Air-water flows, *Proceedings of the 21st, IAHR Congress*, Melbourne, Australia, Keynote Address, 18-29.

Wood, I.R. (1991). Free surface air entrainment on spillways, in Wood, I.R. Air entrainment in free-surface flows. *IAHR, Hydraulic Structures Design Manual 4, Hydraulic Design Considerations*, A. A. Balkema, Rotterdam, the Netherlands, 55-84.

Yasuda, Y. & Ohtsu, I. (1999). Flow resistance of skimming flow in stepped channels. *Proceedings of 28th IAHR Congress*, Graz, Austria, in CD.

Zamora, A., Pfister, M., Hager, W. H., and Minor, H.-E. (2008). Hydraulic performance of step aerator. *Journal of Hydraulic Engineering*, 134(2), 127-134.

Zare, H. K. and Doering J. C. (2012a). Effect of rounding edges of stepped spillways on the flow characteristics. *Canadian Journal of Civil Engineering*, 39(2), 140-153.

Zare, H. K. and Doering, J. C. (2012b). Energy dissipation and flow characteristics of baffles and sills on stepped spillways. *Journal of Hydraulic Research*, 50(2), 192-199.

Zarrati, A. M., Jin Yee-Chung, Shanehsaz-zadeh, A., and Ahadi, F. (2004). Potential flow solution for a free surface flow past a sudden slope change. *Canadian Journal of Civil Engineering*, 31, 553-560.

Zhang, J.M., Chen, J.G., Wang, Y. (2012). Experimental study on time-averaged pressure in stepped spillway. *Journal of Hydraulic Research*, 50(2), 236-240.

Acknowledgments

This research work was carried out in the framework of the IST-EPFL Joint Doctoral Initiative. The research was granted by the Fundação para a Ciência e a Tecnologia (FCT), Portugal under grant SFRH/BD/51527/2011, and the Laboratory of Hydraulic Constructions (LCH) of EPFL, Switzerland and was in part funded by the Ministry of Science, Research and Technology of Islamic Republic of Iran.

During the last four years, I have learned a lot from the intellectual environment of EPFL and IST. I am grateful for this opportunity to have the assistance and the friendly support from a large number of people; those had essential influence in my professional and private life aspects.

In my culture we say 'I owe to the person who taught me even a word, everything'. Although it is hard to overstate my gratitude, I wish to express my special appreciation to my supervisors for all their kind trusts and supports. All my gratefulness to Prof. Anton J. Schleiss (EPFL) not only for his tremendous academic support but also for being always very kind and supportive guide to my ideas, which made this work an amazing experience. Similar, special mention and profound gratitude goes to Prof. Jorge Matos (IST), for his great scientific guidance and spending his time to do the data treatment together and extracting the fruitful results. I also have to say that I am indebted to him, not only in professional aspect, but also for the ethical lessons that I learnt from his private life aspect, in particular after my motor bike accident which taught me lessons that I will never forget. Also my especial thanks to Dr. Michael Pfister (EPFL) for his friendly helps and valuable comments. I also would like to thank Dr. Giovanni De Cesare, Prof. Rui Ferreira and Prof. António Pinheiro for their fruitful discussion and comments. My sincerest thanks to all my teachers during my Ph.D, especially to Prof. Jean-Marie Fuerbringer, Dr. Alexis Kalogeropoulos, Prof. Rui Ferreira, Dr. Mário Franca, Prof. Didia Covas, Prof. Antonio Cardoso, Prof. Helena Ramos, Prof. Manuela Portela, Prof. Antonio Pires Silva, and Prof. António Trigo Teixeira.

I wish to express my gratitude to the members of the jury of my PhD defense, Prof. Alain Nussbaumer (EPFL), Prof. Daniel Bung (FH Aachen – University of Applied Sciences), Prof. João Teixeira Borges (IST) and especially Dr. Stephanie André (Stucky SA) that I had

the honour to have her presence and nice comments in my first year candidacy exam as well. All my sincerest thanks to them for accepting to evaluate and discuss my thesis.

I would like also to thank Prof. Jalal Bazargan who changed my life during my Bachelor study and made me interested to study the Hydraulics. I also would like to express my thanks to Prof. Amir Reza Zarrati, who supervised my Master thesis and encouraged me to continue my study to a Ph.D.

When I decided to come to Lausanne, I was not sure about the future, but early later, I found that the future is shining as I found about my nice colleagues there in LCH and IST. Especial thanks to Mrs. Angélique Dublanc (EPFL) and Paula Cunha (IST) who made my life easier during the first moments of my arrival. I also would like to thanks our nice secretaries, Caroline (LCH), Scarlett (LCH), and Dulce (CERIS) for all their nice assistance. During these past years I had a great chance to have very nice colleague-friends who made one of the most memorable periods of my life. First, I would like to thank my dear friend Ana Margarida who was always positive and full of friendly manner and generosity, not only to me, but also to all of her friends, "Muito obrigado Ana"; Milad and Mona, thanks for your all "Big-boss" hints and supports; my cool Spanish friends Sebastian and David; Stéphane, Rafael and Xueqin (Amme) especially for their kind assistance during the experimental measurements; Violaine and Alex "movie director" as a nice office mates; Martin and Michael Müller; Tamara who gave me the chance to be her "slave" in her thesis experiments; Raphael Sprenger who was always amazing for me especially regarding to his abilities to be an acrobat and engineer man at the same time ☺; Sabine who taught me some Lebanese, meshel hal Sabin? Kifik?; José Pedro and Natércia; Ramona, Théodora, Sebastian Schwindt, Fränz, Elena, Davide, Nicolas, Mélanie, Felix, Reyhaneh Sadat, Carmelo, Pedro, Severin, Sara, Paloma, Antonin and Jessica. Also I would like to appreciate all the kind assistance of the workshop colleagues, Michel (the lord of the workshop), Marc-Eric (PanPam), Armin, Cédric, Laurent, David, Younés, and Gabriel.

I would like to thank especially those nice friends that I met at IST, Artur and Pedro especially for the nice moments of Lunch times and consequent fun debates that we had as well as those "revenge basketball tournament" with Artur; Ana Catarina and Ana Filipa, André, Federica and Teresa, Dora "the explorer", Daniel, Mariana "the master of the Word", Nuno, Olga, Ricardo, Ana, João, Moisés, Luis, Rui, Isabel, Ana Clara, Irene Samora, Aisha, Ana Rosa and Inês, thank you all so much.

Although I did not pass these 4 year in Iran, I had a chance to find many Iranian friends that surely I cannot write their names all here, but I thanks all of them :D

Lausanne, April 2016 *Mohammad Javad*

Appendixes

A

Air-water flow measurement with RBI

A.1. Influence of acquisition time

Figures A1 and A2 show the air concentration *C* and velocity *V* profiles respectively obtained on step number +01, +06 and +15 in test run 3. These 3 steps are chosen, as a representative of the areas of slope change, high and low splash zone respectively. Very low scatter and fairly high accordance of all profiles, particularly air concentration, strengthen the conclusion that time acquisition between 20s and 60 seconds does not have major influence on data. Therefore, 25s has been defined for air-water flow measurements in present study.

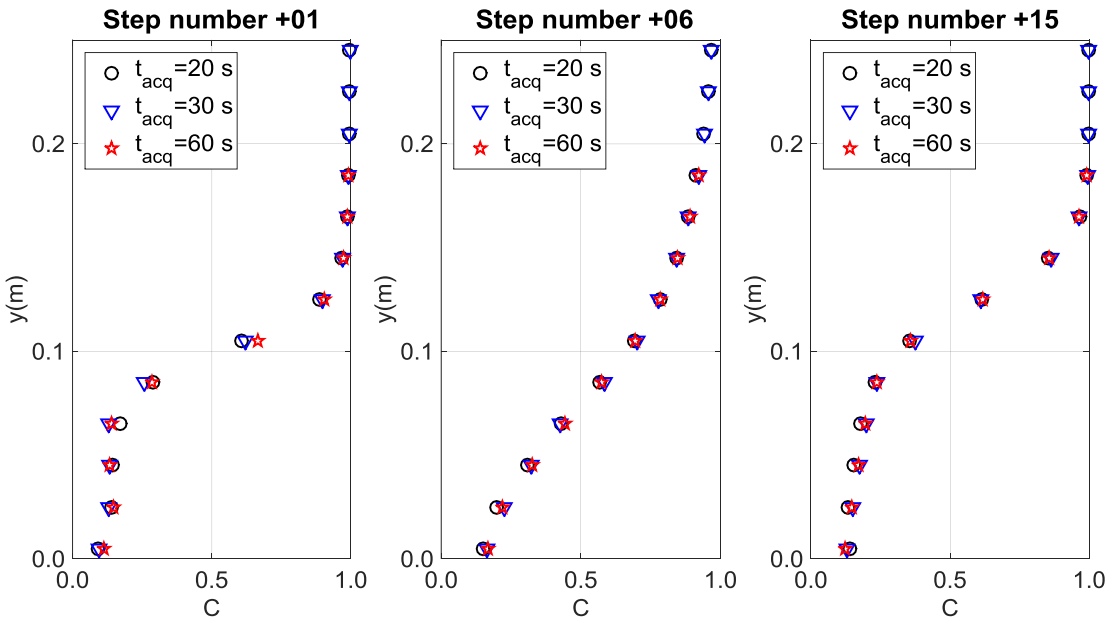

Figure A.1 Influence of the acquisition time t_{acq} on air concentration profiles for different cross-sections of test run number 3, with q_w=0.47, at step numbers +1, +6 and +15 on 18.6º sloping chute.

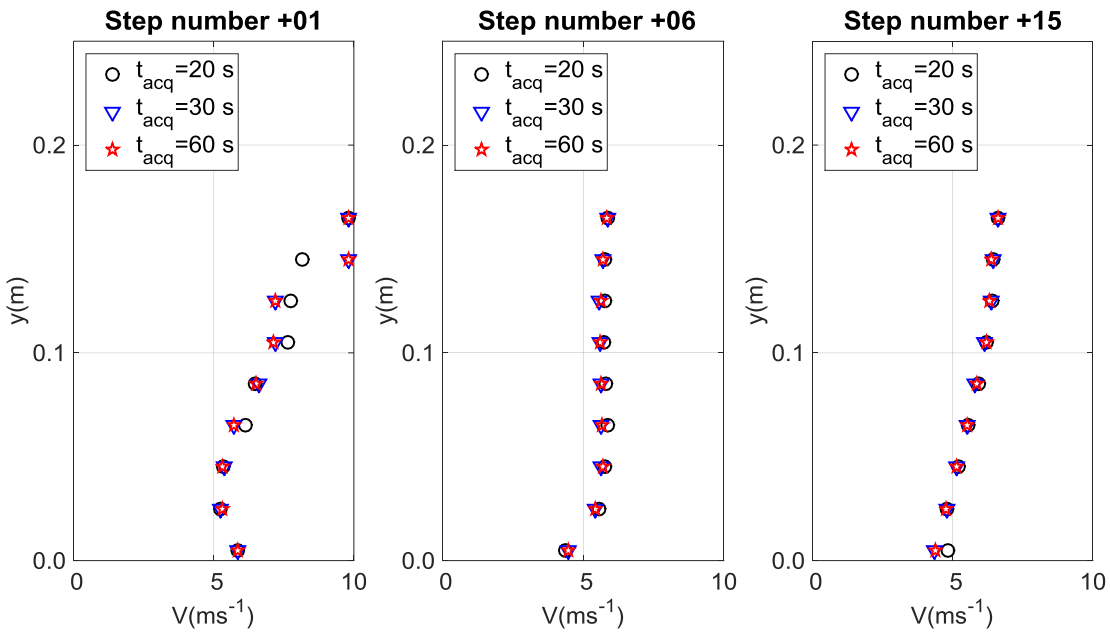

Figure A.2 Influence of the acquisition time t_{acq} on velocity profiles for different cross-sections of test run number 3, with q_w=0.47, at step numbers +1, +6 and +15 on 18.6º sloping chute.

The scatter in the upper region in velocity profiles measured at step number +01, is judged to be caused under the influence of slope change, however it is very negligible.

A.2. Experimental results

This section presents the air concentration, air-phase frequency and velocity results upstream and downstream of the slope change, for the 9 test runs (see Table 3.1). The latter is also available on request at the Laboratory of Hydraulic Constructions of the Ecole Polytechnique Fédérale de Lausanne (LCH-EPFL).

A.2.1 Test run number 1

Table A.1 Air concentration, air-phase frequency and velocity distribution on 50º-18.6º, d_c/h=2.6 (test number 1).

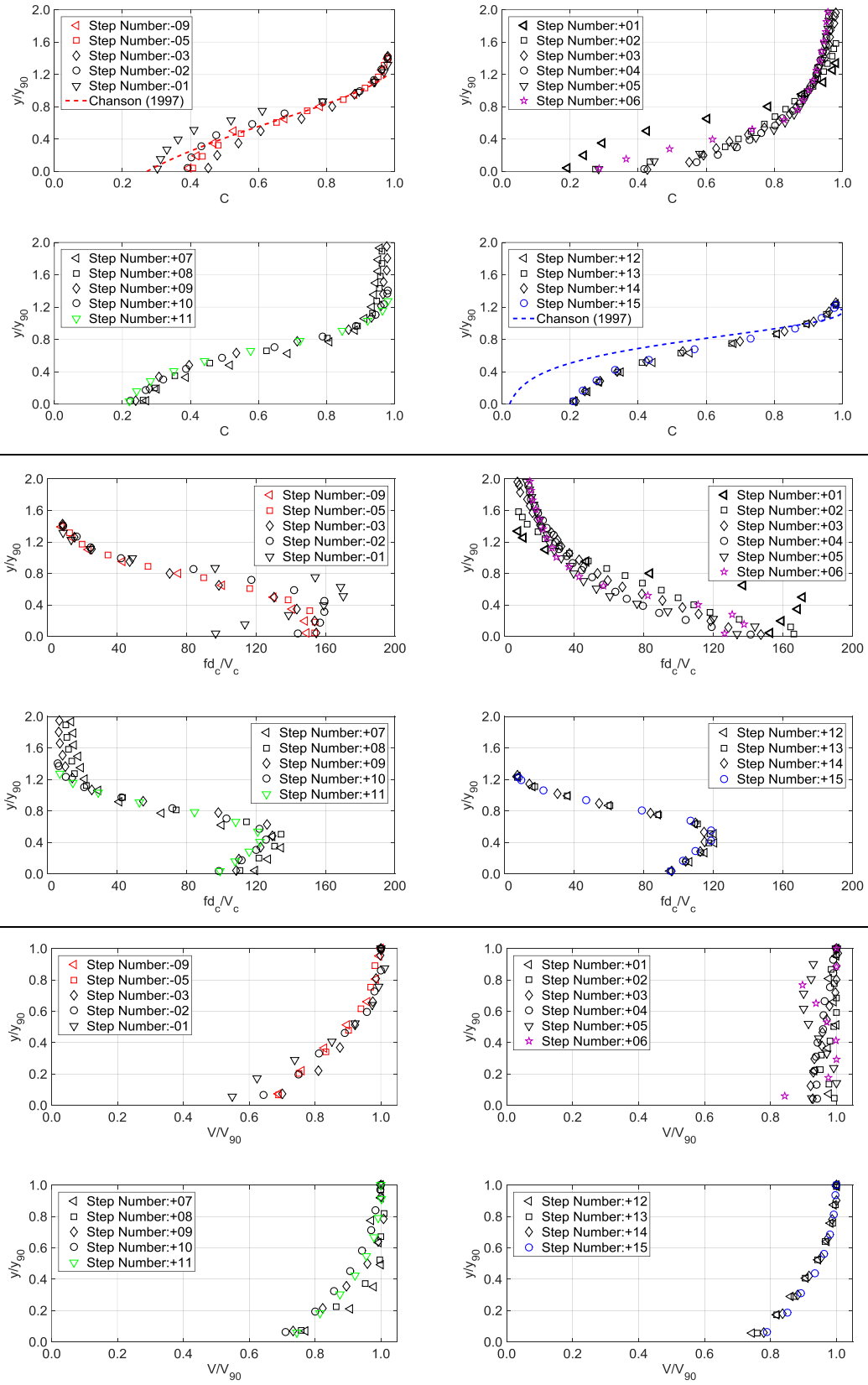

A.2.2. Test run number 2

Table A.2 Air concentration, air-phase frequency and velocity distribution on 50º-18.6º, d_c/h=3.8 (test number 2).

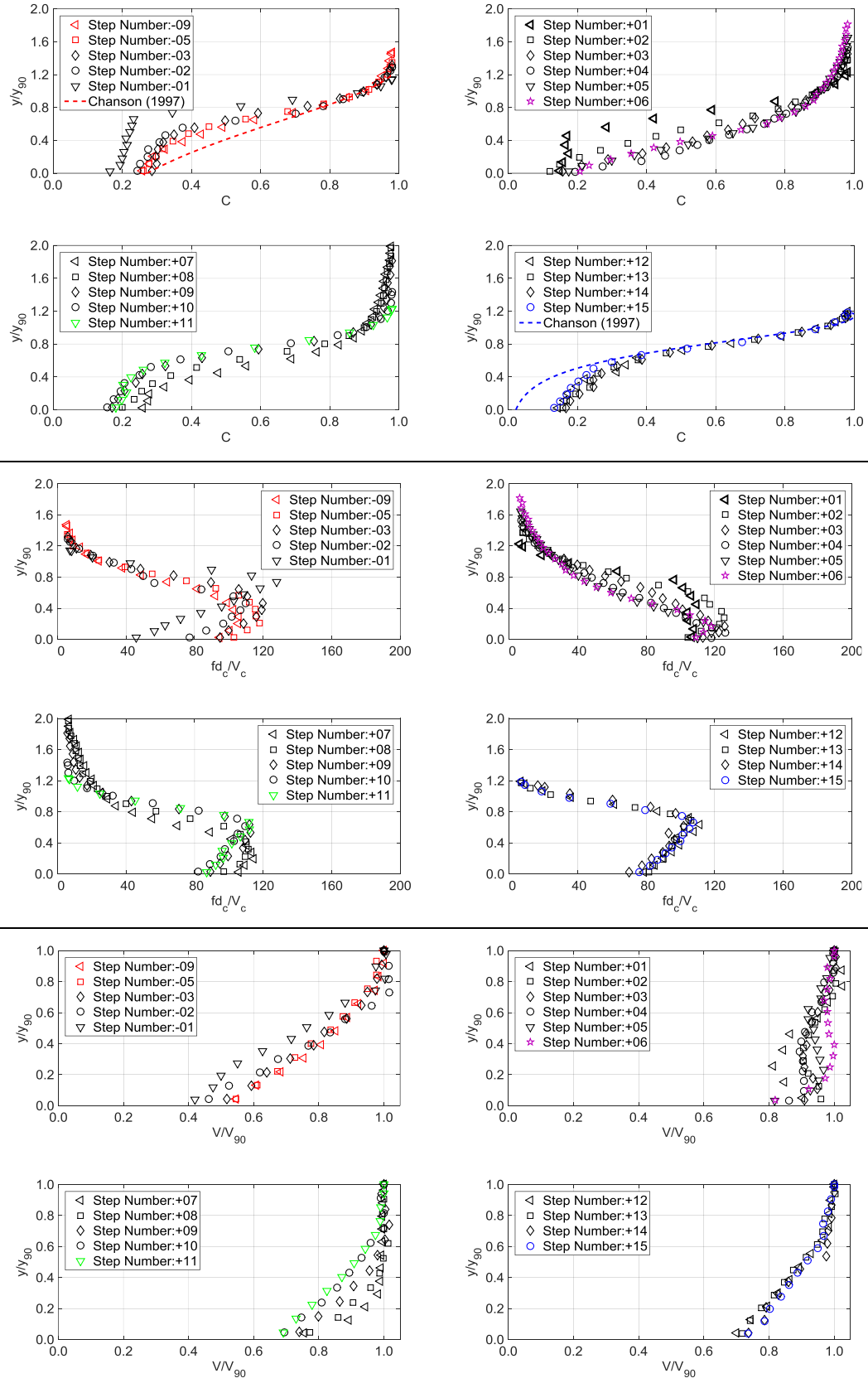

A.2.3. Test run number 3

Table A.3 Air concentration, air-phase frequency and velocity distribution on 50º-18.6º, d_c/h=4.6 (test number 3).

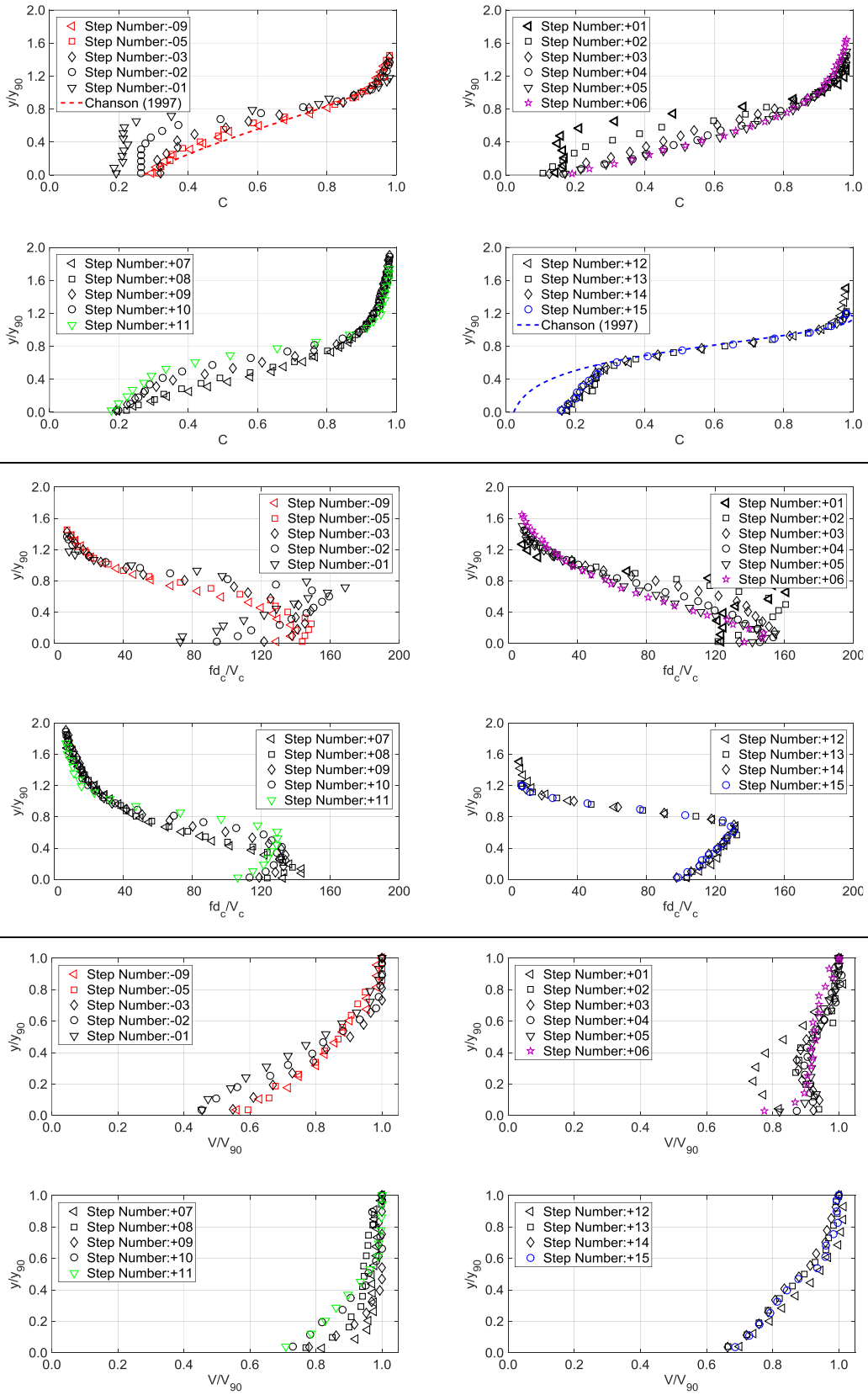

A.2.4. Test run number 4

Table A.4 Air concentration, air-phase frequency and velocity distribution on 50º-18.6º, d_c/h=7.6 (test number 4).

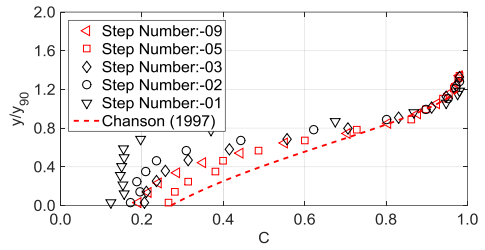

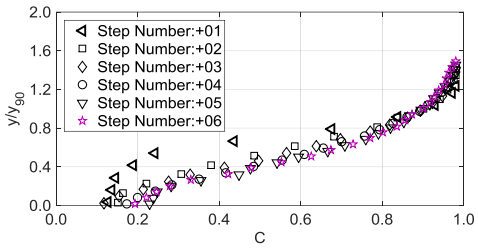

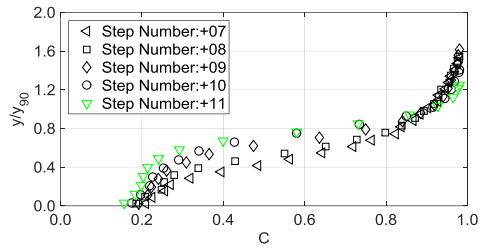

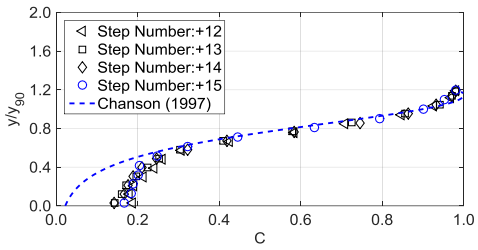

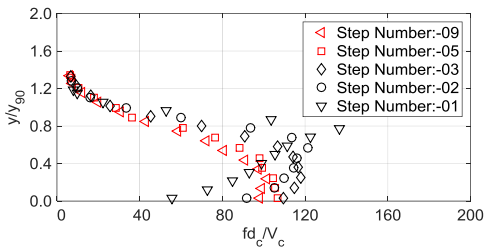

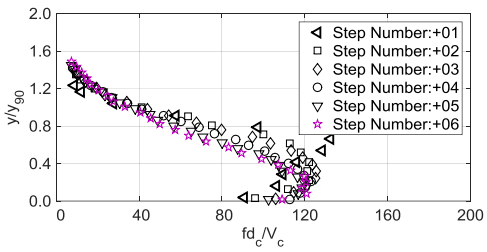

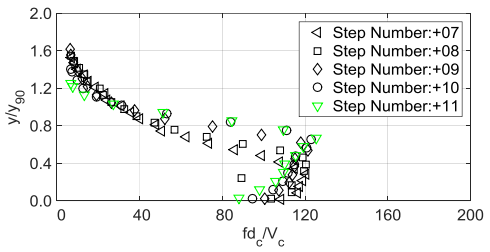

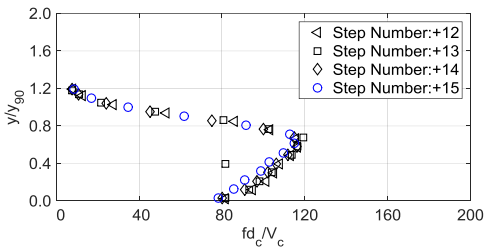

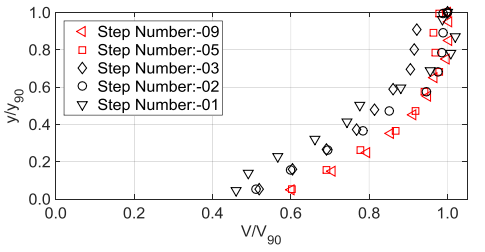

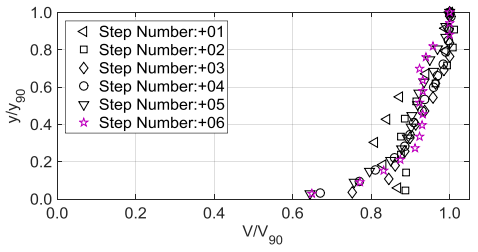

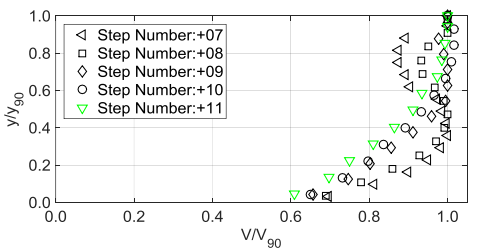

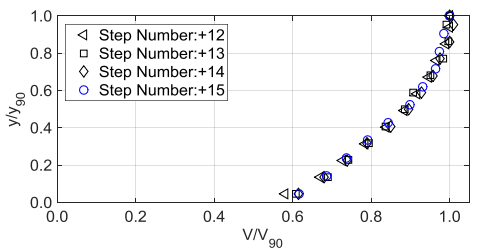

A.2.5. Test run number 5

Table A.5 Air concentration, air-phase frequency and velocity distribution on 50º-18.6º, d_c/h=9.2 (test number 5).

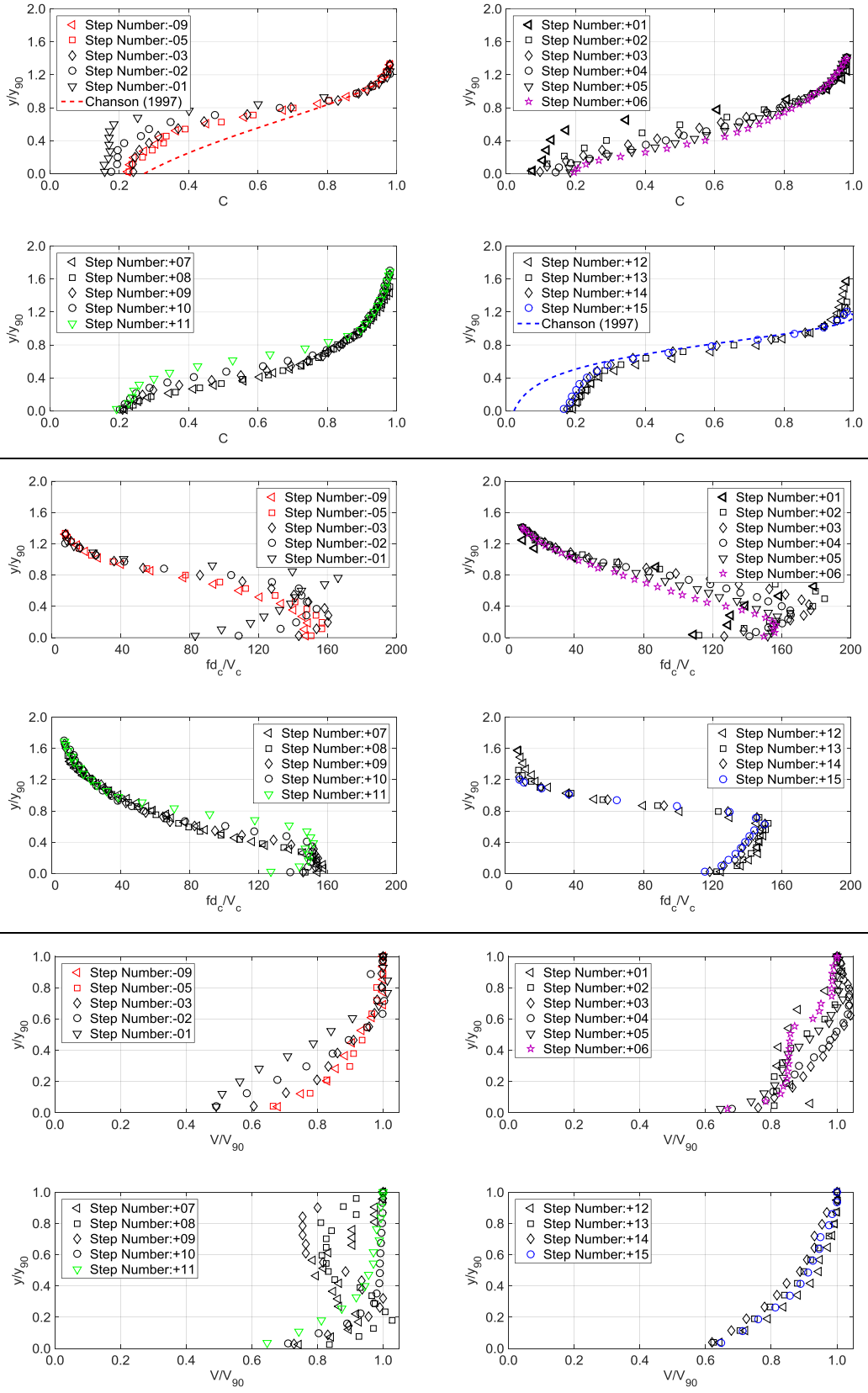

A.2.6. Test run number 6

Table A.6 Air concentration, air-phase frequency and velocity distribution on 50º-30º, d_c/h=2.6 (test number 6).

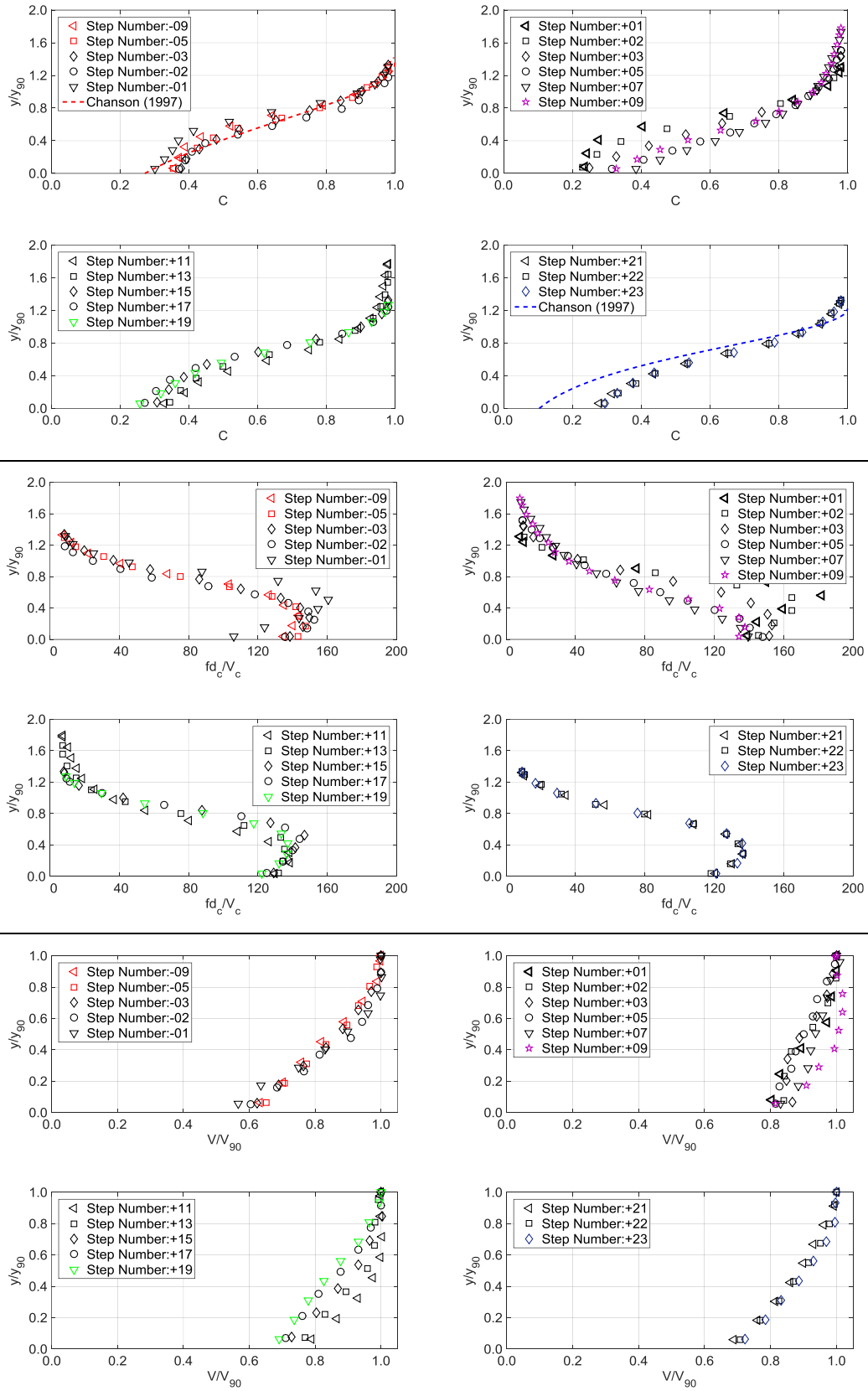

A.2.7. Test run number 7

Table A.7 Air concentration, air-phase frequency and velocity distribution on 50º-30º, d_c/h=3.8 (test number 7).

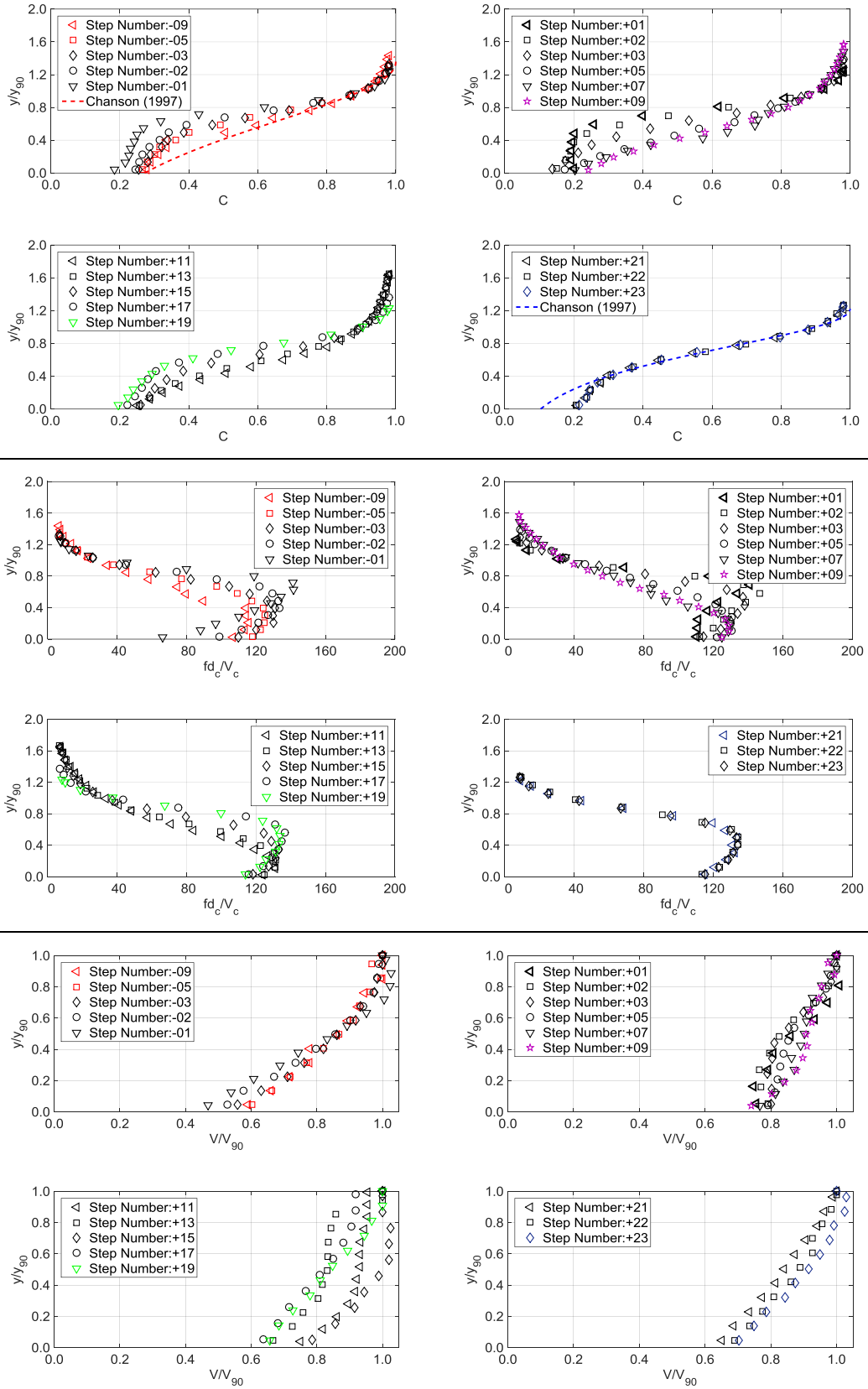

A.2.8. Test run number 8

Table A.8 Air concentration, air-phase frequency and velocity distribution on 50º-30º, d_c/h=4.6 (test number 8).

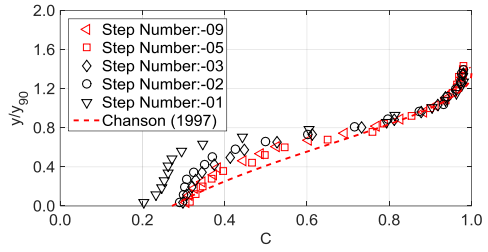

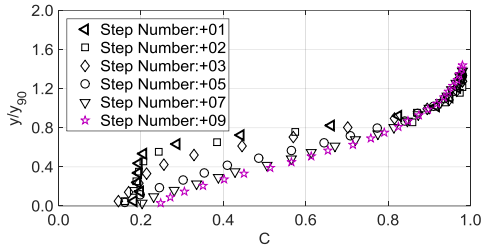

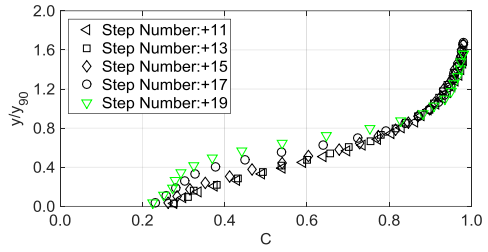

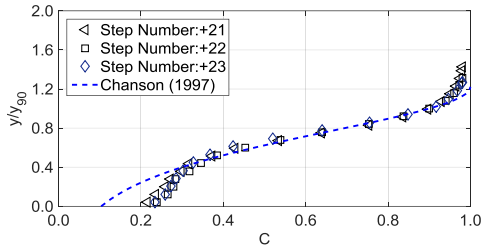

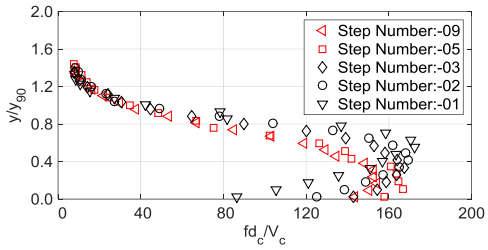

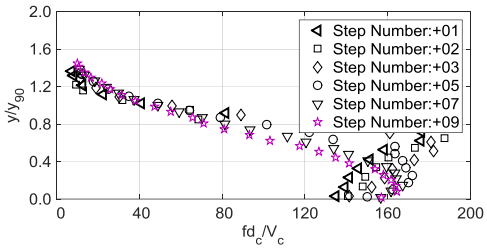

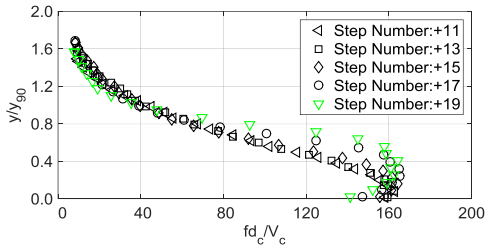

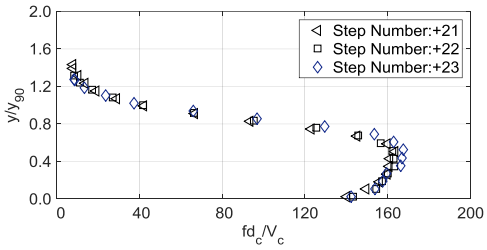

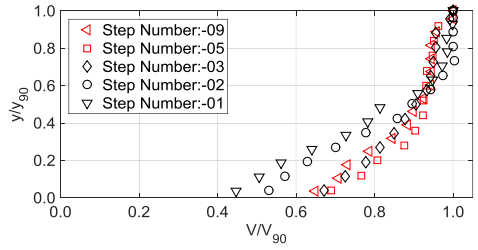

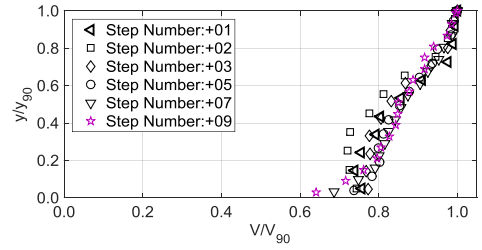

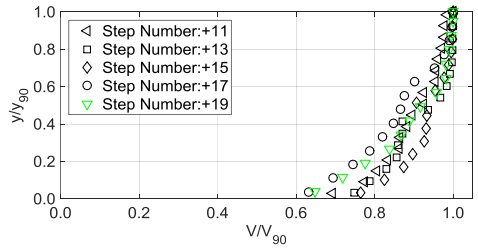

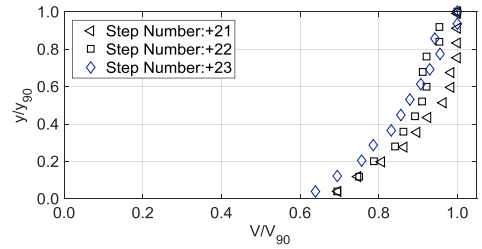

A.2.9. Test run number 9

Table A.9 Air concentration, air-phase frequency and velocity distribution on 50º-30º, d_c/h=9.2 (test number 9).

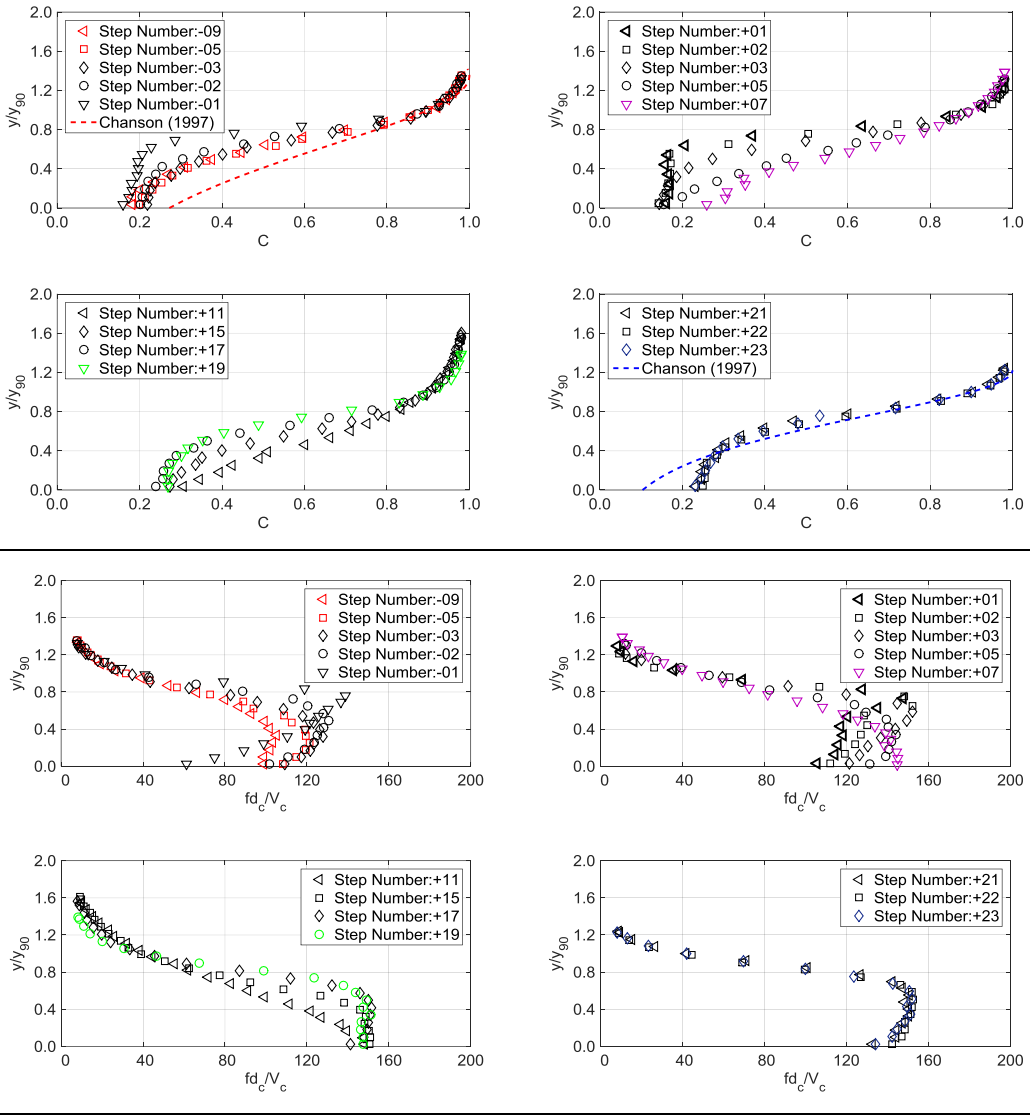

B

Dynamic pressure measurements

B.1. Experimental results

This section presents the time averaged pressures, extreme pressure values, and spectral energy content of the pressure fluctuations results on horizontal and vertical step faces in vicinity and far downstream of the slope change cross-section in four model test runs (number 3 and 6 to 8, see Table 3.1). The latter is also available on request at the Laboratory of Hydraulic Constructions of the Ecole Polytechnique Fédérale de Lausanne (LCH-EPFL).

B.1.1.Test run number 3

Horizontal step faces

Table B.2 Dynamic pressure distribution and PSD on horizontal step faces of 50º-18.6º, d_c/h=4.6 (test number 3).

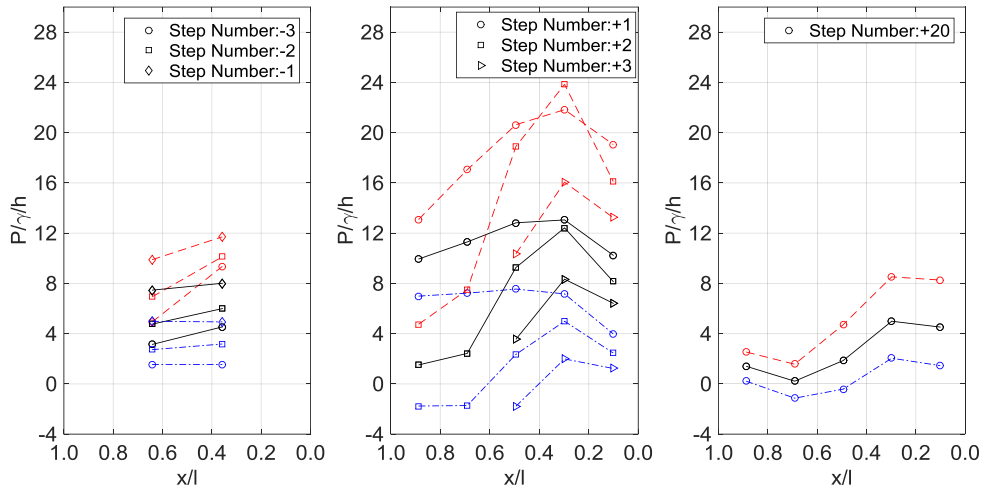

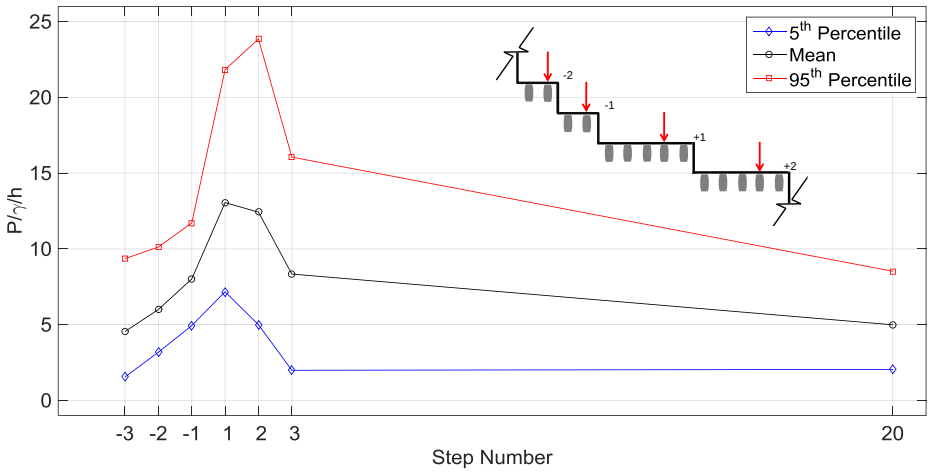

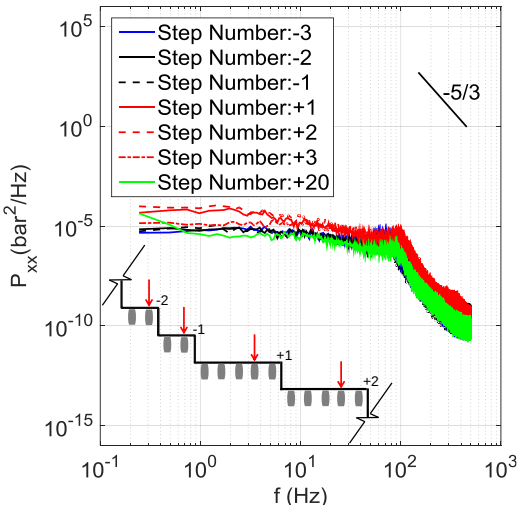

Vertical step faces

Table B.3 Dynamic pressure distribution and PSD on vertical step faces of 50º-18.6º, d_c/h=4.6 (test number 3).

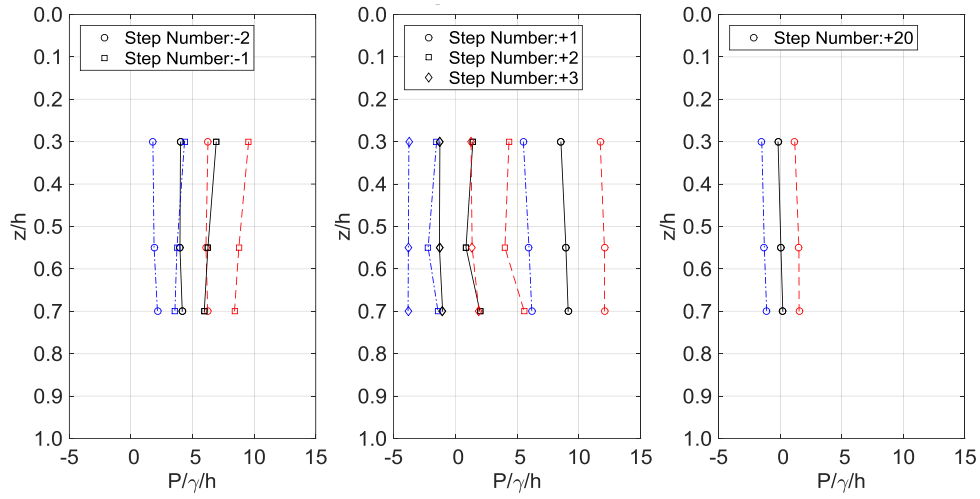

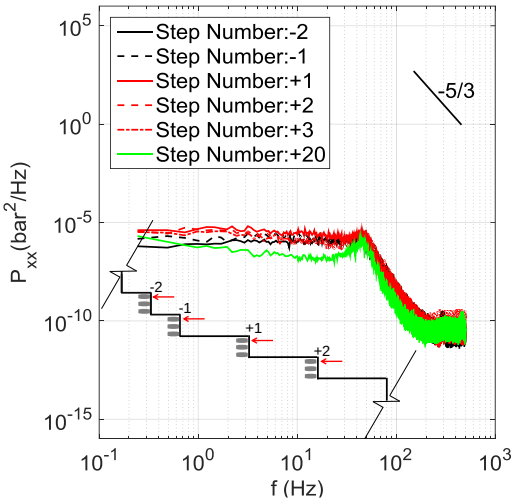

B.1.2.Test run number 6

Horizontal step faces

Table B.4 Dynamic pressure distribution and PSD on horizontal step faces of 50º-18.6º, d_c/h=2.6 (test number 6).

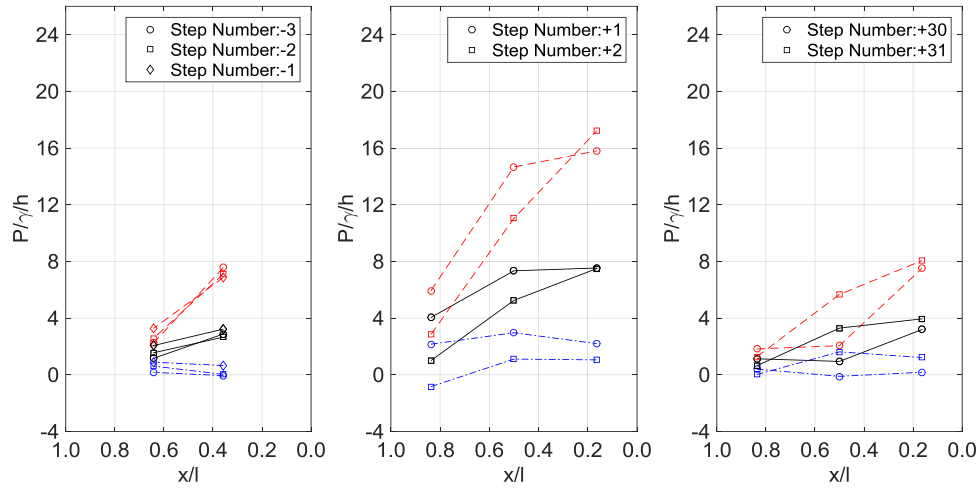

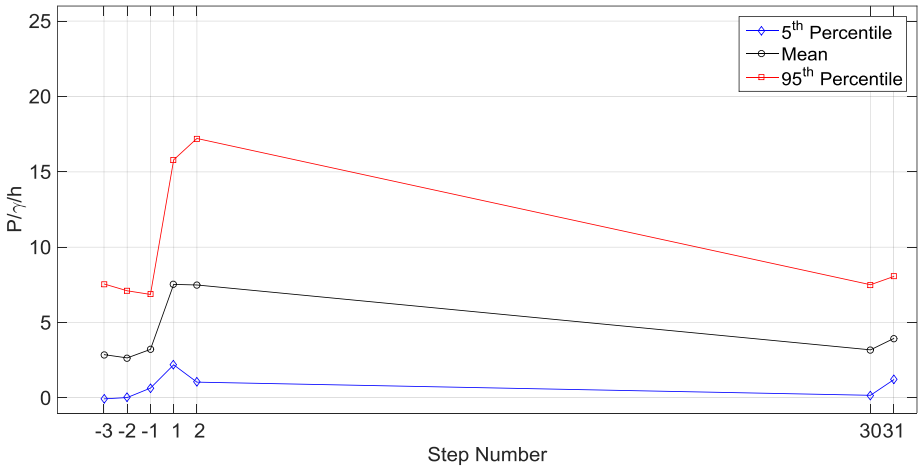

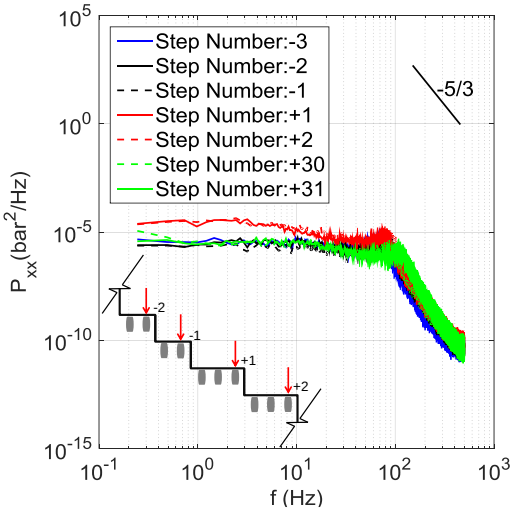

Vertical step faces

Table B.5 Dynamic pressure distribution and PSD on vertical step faces of 50º-30º, d_c/h=2.6 (test number 6).

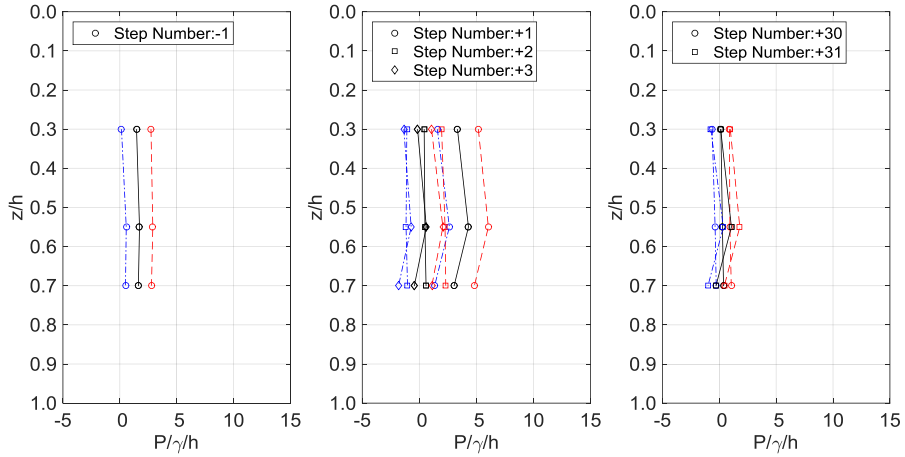

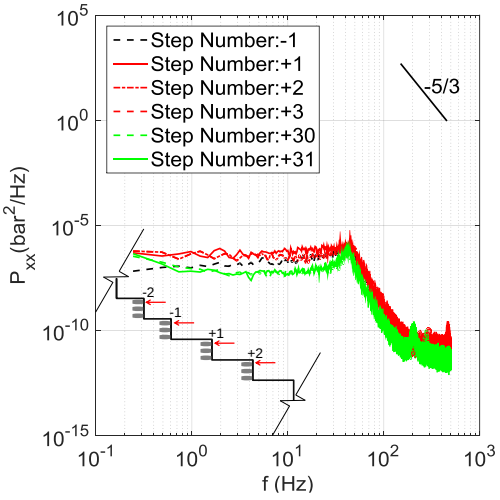

B.1.3.Test run number 7

Horizontal step faces

Table B.6 Dynamic pressure distribution and PSD on horizontal step faces of 50º-18.6º, d_c/h=3.8 (test number 7).

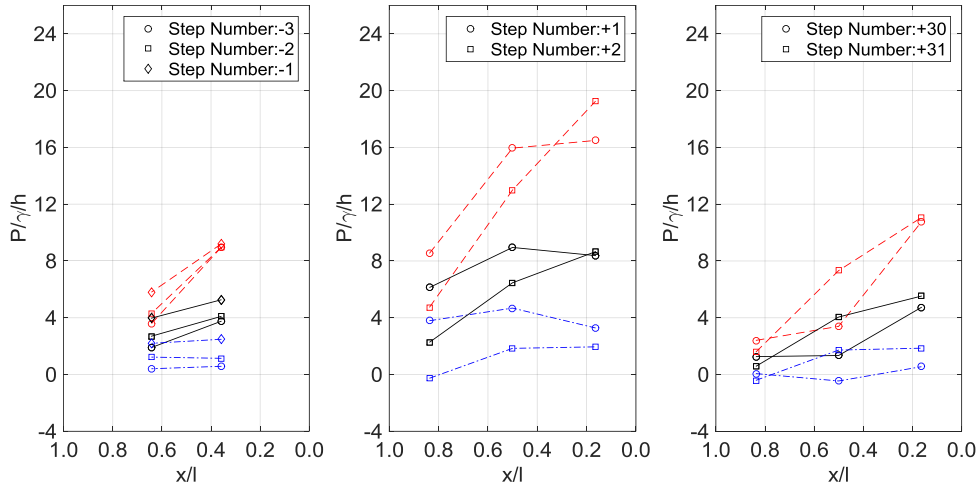

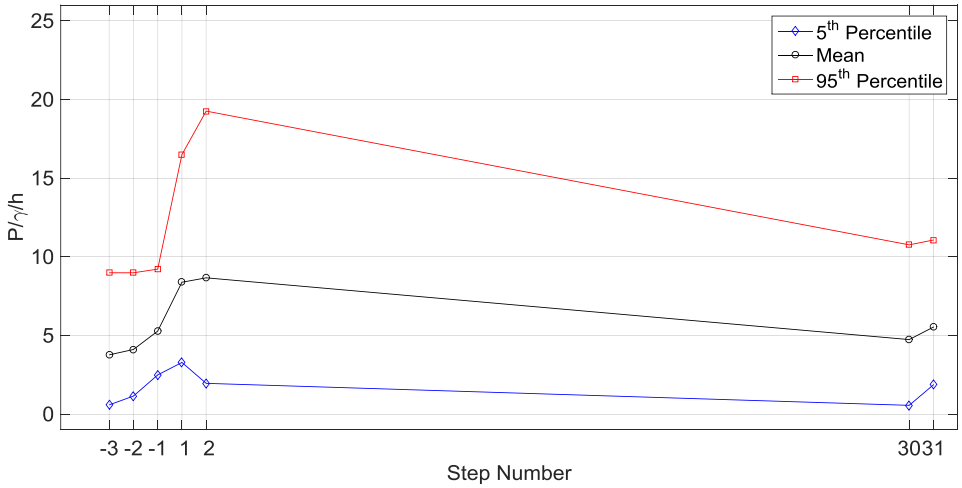

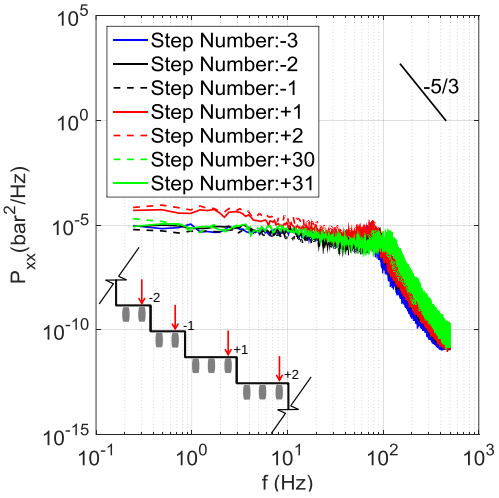

Vertical step faces

Table B.7 Dynamic pressure distribution and PSD on vertical step faces of 50º-30º, d_c/h=3.8 (test number 7).

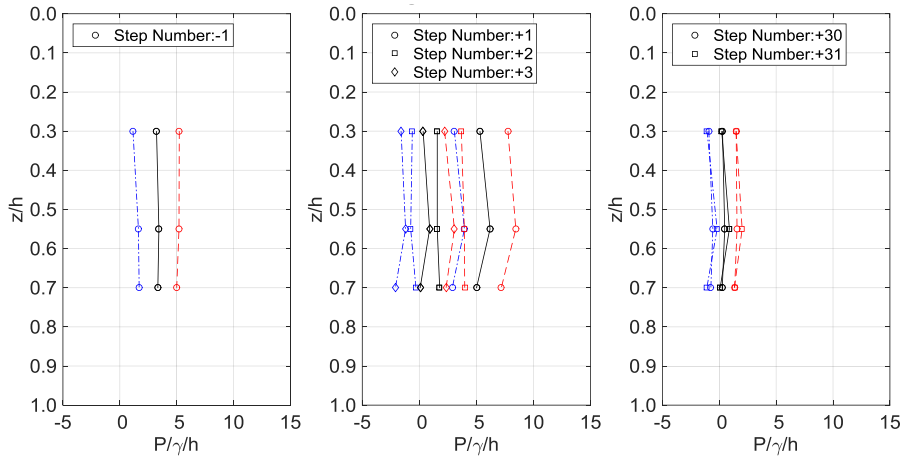

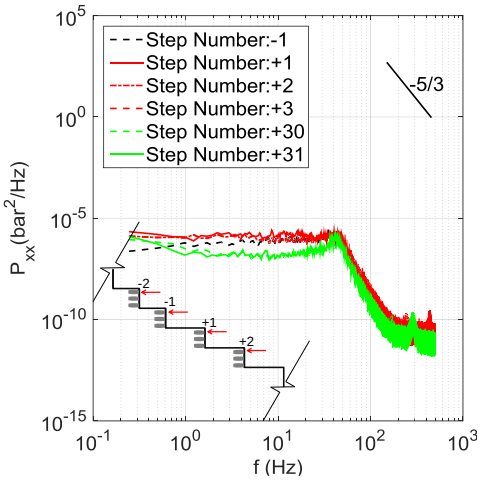

B.1.4.Test run number 8

Horizontal step faces

Table B.8 Dynamic pressure distribution and PSD on horizontal step faces of 50º-30º, d_c/h=4.6 (test number 8).

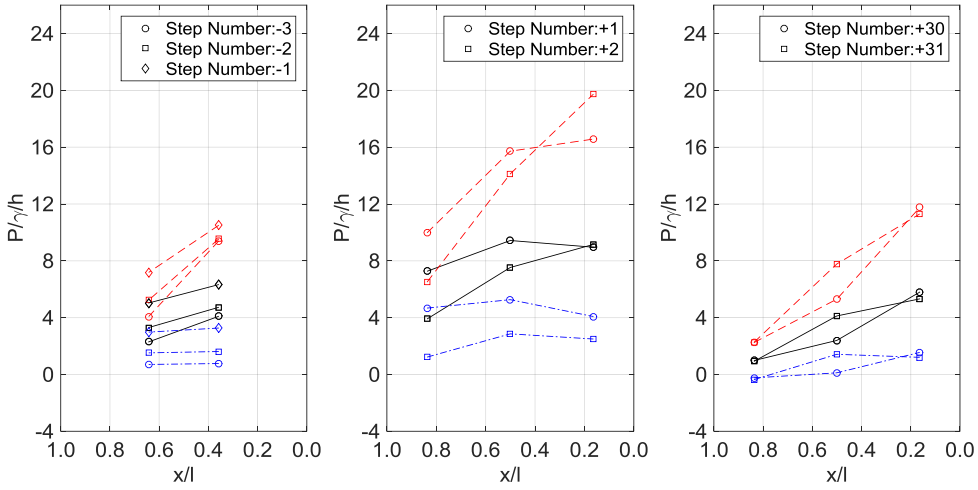

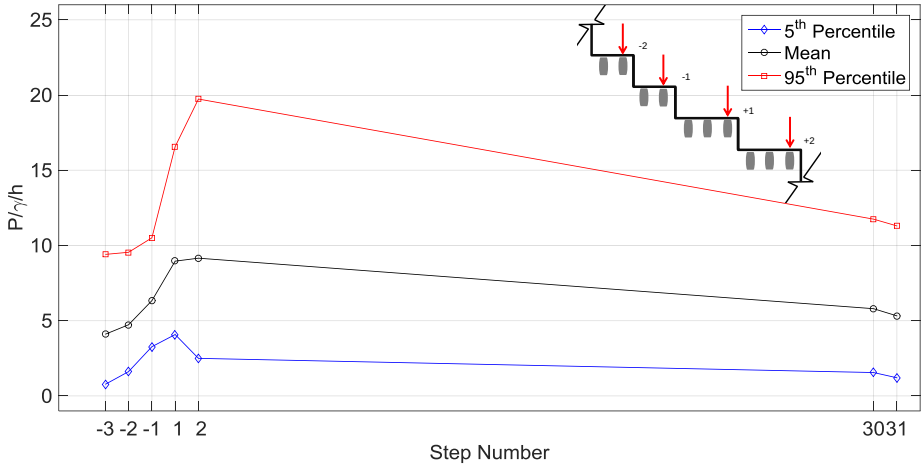

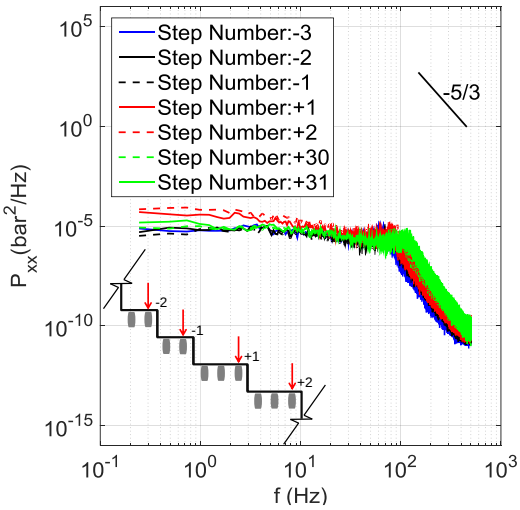

Vertical step faces

Table B.9 Dynamic pressure distribution and PSD on vertical step faces of 50º-18.6º, d_c/h=4.6 (test number 8).

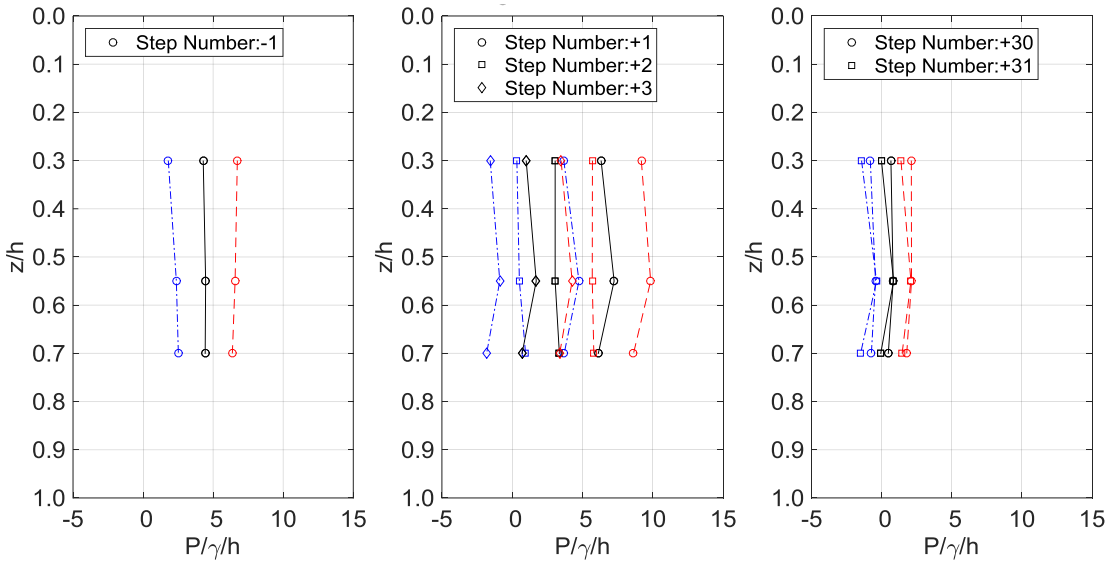

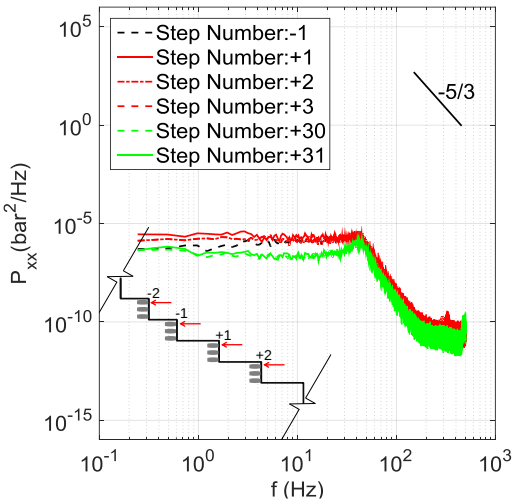

Communications du Laboratoire de Constructions Hydrauliques ISSN 1661-1179
Ecole Polytechnique Fédérale de Lausanne
Editeur: Prof. Dr A. Schleiss

N° 51 2012 W. Gostner
The Hydro-Morphological Index of Diversity:
a planning tool for river restoration projects

N° 52 2012 M. Bieri
Operation of complex hydropower schemes and its impact on the flow regime in the downstream river system under changing scenarios

N° 53 2012 M. Müller
Influence of in- and outflow sequences on flow patterns and suspended sediment behavior in reservoirs

N° 54 2013 V. Dugué
Influencing river morphodynamics by means of a bubble screen: application to open-channel bends

N° 55 2013 E. Person
Impact of hydropeaking on fish and their habitat

N° 56 2013 T. Cohen Liechti
Influence of dam operation on water resources management under different scenarios in the Zambezi River Basin considering environmental objectives and hydropower

N° 57 2014 A. M. da Costa Ricardo
Hydrodynamics of turbulent flows within arrays of circular cylinders

N° 58 2014 T. Ghilardi
Sediment transport and flow conditions in steep rivers with large immobile boulders

N° 59 2014 R. Duarte
Influence of air entrainment on rock scour development and block stability in plunge pools

N° 60 2014 J. P. Matos
Hydraulic-hydrologic model for the Zambezi River using satellite data and artificial intelligence techniques

N° 61 2015 S. Guillén Ludeña
Hydro-morphodynamics of open-channel confluences with low discharge ratio and dominant tributary sediment supply

N° 62 2016 M. Jafarnejad Chaghooshi
Time-dependent failure analysis of large block size riprap as bank protection in mountain rivers

N° 63 2016 S. Terrier
Hydraulic performance of stepped spillway aerators and related downstream flow features

N° 64 2016 M. Ostad Mirza
Experimental study on the influence of abrupt slope changes on flow characteristics over stepped spillways

ISSN 1661-1179

DOI: 10.5075/epfl-lchcomm-64

Prof. Dr A. Schleiss
Laboratoire de constructions hydrauliques - LCH
EPFL, Bât. GC, Station 18, CH-1015 Lausanne
http://lch.epfl.ch
e-mail: secretariat.lch@epfl.ch